

New Fast and Accurate Steady-State Analysis Approach for Design, Optimization, and Simulation of General Power Converter Systems

by

Reza Sadri

A thesis submitted in partial fulfillment of the requirements for the degree of

Master of Science

in

Energy Systems

Department of Electrical and Computer Engineering

University of Alberta

© Reza Sadri, 2022

Abstract

Accurate steady-state analysis of power converters are essential for converter design and optimization. Steady-state responses are also useful for component selection, loss calculation, identification of soft switching operation, and small signal modeling of power converters. Normally, a brute-force simulation is carried out to achieve the steady-state response; however, due to the zero initial conditions assumption, the simulation time in such methods is not efficient and fast. An accurate steady-state response, however, can be obtained if the initial conditions at the beginning of a switching cycle of the converter are accurately known. In this thesis, a non-iterative improved Laplace based theorem and enhanced state vector algorithm are proposed to calculate the steady-state initial conditions of the power converters.

The proposed methods use the system's switching time and state space representation to calculate the system's initial vector. However, assuming the switching times as known inputs is not valid for all types of converters, such as the case of converters with uncontrolled switches or converters operating in discontinuous conduction mode. The proposed method is further modified to address this challenge by using the bisection approach to find the switching time of the converters that feature a monotonic function of the switching time. Then, a Switching Time Estimator (STE) is proposed to remove the monotonic function limitation on the type of converters since it uses a general-purpose simulator to find the uncontrolled events' switching time.

The thesis also discusses the extension of the proposed approaches to AC-DC and DC-AC converters, which are more challenging as multiple frequencies and variable amplitudes are involved. These challenges are overcome by modifying the period that the method will be applied and using a piecewise linear approximation of AC

sources. Furthermore, the thesis discusses the steady-state analysis of the closed loop power converters. To calculate the initial vector of closed loop systems, the proposed Switching Time Estimator (STE) is modified to update the state of the controller.

Several examples are provided in each chapter to demonstrate the speed of the proposed method compared to the existing approaches. In addition, the proposed method uses the calculated initial vector to achieve the steady-state waveforms of each converter, which are then compared to the Power Simulation (PSIM) generated waveforms to show the accuracy of the proposed method.

Acknowledgements

I wish to express my gratitude to my supervisor, Prof. Ali Khajehoddin, for giving me the amazing opportunity of pursuing my master's degree at the prestigious University of Alberta in a vibrant and friendly research group. I would also like to thank him for his guidance, support, encouragement, and insightful feedback.

My appreciation is extended to Prof. Hao Liang, Prof. Venkata Dinavahi, and other committee members for their constructive comments and feedback.

I would also like to thank my fellow graduate students in the uAPEL for their professional and emotional support throughout these years. I especially thank Mr. Mohammad Daryaei for all the insightful and productive discussions.

Last but certainly not least, I wish to express a great debt of gratitude to my wife and my parents for all their invaluable emotional support, encouragement, and devotion. Without their support, none of this would have been possible.

Contents

1	Introduction	1
1.1	Review of Existing Steady-State Calculation Methods	3
1.1.1	Brute-Force Method	4
1.1.2	Newton Raphson	5
1.1.3	Laplace Based Method	7
1.1.4	State Vector Algorithm (SVA)	8
1.2	Objectives	9
1.3	Thesis Outline	10
2	Alternative Steady-State Analysis Methods	12
2.1	Mathematical Modelling of Power Electronic Systems	13
2.1.1	Modelling of Continuous States	13
2.1.2	Definition of Switching Events	15

2.2	Laplace Based Theorem (LBT)	16
2.3	Improved Laplace Based Theorem (ILBT)	19
2.3.1	Improved Laplace Based Theorem (ILBT) for Edge Switch- Network Converters	23
2.3.2	Improved Laplace Based Theorem (ILBT) for Interior Switch- Network Converters	25
2.4	Conventional State Vector Algorithm (SVA)	30
2.5	Proposed Enhanced State Vector Algorithm (SVA)	33
2.5.1	Taylor Series of e^{At}	33
2.5.2	Adaptive Order Selection	35
2.6	Simulation Results	36
2.6.1	Buck Converter	37
2.6.2	Dual Active Bridge Converter	39
2.6.3	Cuk Converter with Parasitic Components	42
2.6.4	Zeta Converter	44
2.6.5	Boost Converter Operating in DCM	47
2.7	Summary	49
3	Steady-State Analysis of Converters with Uncontrolled Switching Events	51

3.1	Determination of Switching Intervals Using Bisection Method	52
3.2	Switching Time Estimator Mechanism Using the General-Purpose Simulator	57
3.3	Simulation Results	60
3.3.1	Buck Converter Operating in DCM	61
3.3.2	Series Resonant Converter (SRC)	63
3.3.3	LLC Converter	66
3.4	Summary	69
4	Steady-State of Closed Loop, DC–AC, and AC–DC Converters	70
4.1	Application of Enhanced SVA to DC–AC and AC–DC Converters	71
4.2	Simulation Results of DC–AC and AC–DC Converters	74
4.2.1	Full Bridge Inverter Connected to the Load	74
4.2.2	Grid Connected Inverter	77
4.3	Study of Closed Loop Converters Using Enhanced SVA	79
4.4	Simulation of Closed Loop Phase-Shifted Full Bridge Converter	82
4.5	Summary	85
5	Summary and Future Work	86
5.1	Summary of Contributions	86

5.2	Suggested Future Work	87
A	Computer Formulation of State Equations	97
A.1	Circuit Identification	98
A.1.1	Network Graph	99
A.1.2	Incidence Matrix	101
A.1.3	Cutset Matrix	103
A.2	Computer Generation of Topological Matrices	105
A.2.1	Finding a Tree	106
A.2.2	Generation of D	107
A.3	State Space Derivation	109

List of Tables

2.1	System parameters of the Buck converter.	38
2.2	The simulation time required to converge to a steady-state in the circuit of Fig. 2.11.	38
2.3	System parameters of the Dual Active Bridge converter.	40
2.4	The simulation time required for different steady-state solvers to find the initial conditions of the Dual Active Bridge.	40
2.5	System parameters of the Cuk converter.	42
2.6	The simulation time required to find the steady-state initial conditions of the Cuk converter.	43
2.7	System parameters of the Zeta converter.	45
2.8	Simulation time of the different steady-state solver for finding the initial vector of the Zeta converter.	47
2.9	System parameters of the Boost converter.	48
2.10	Simulation time required for Boost converter operating in DCM. . . .	48

3.1	System parameters of the Buck converter.	61
3.2	The number of iterations required to converge to a steady-state in the circuit of Fig. 3.8.	62
3.3	System parameters of the SRC.	64
3.4	The number of iterations required for different steady-state solvers to find the initial vector of the SRC.	66
3.5	System parameters of the LLC converter.	67
3.6	The number of iterations required to find the steady-state initial conditions of the LLC converter.	67
4.1	System parameters of the full bridge inverter.	75
4.2	The number of iterations required for different steady-state solvers to find the initial vector of the full bridge inverter.	77
4.3	System parameters of the grid connected inverter.	78
4.4	The number of iterations required to find the steady-state initial conditions of the grid connected inverter.	79
4.5	System parameters of the Phase-shifted full bridge converter	83
4.6	The number of iterations required to converge to a steady-state in the Phase-shifted full bridge converter with PI controller.	84

List of Figures

1.1	Response of a power converter with a zero initial condition, showing its state variable going through a transient before reaching steady state.	2
1.2	Generating the steady-state waveform using brute-force method starting from zero initial conditions.	4
1.3	Generating the steady-state waveform using Newton Raphson with Broyden's update method (PLECS software).	7
1.4	Generating the steady-state waveform using the Laplace based method.	8
2.1	Illustration of a first order switching power converter system with m switching intervals in one switching cycle.	14
2.2	RL circuit with square wave input.	17
2.3	Obtained $v_R(t)$ using LBT.	19
2.4	Flowchart detailing the ILBT method for edge switch-network converters.	24
2.5	Signal $d_i(t)$ during one switching period.	26

2.6	Flowchart of finding the steady-state initial conditions of the interior switch-network using ILBT.	29
2.7	Steady-state operation of a first-order system with three switching intervals.	31
2.8	Algorithm of finding the initial vector of the power converters using the conventional SVA.	32
2.9	Flowchart of the adaptive order selection embedded in the calculation of $\lambda_{i_{approx}}$	34
2.10	Block diagram of the proposed ILBT and Enhanced SVA.	37
2.11	Schematic diagram of the Buck converter.	37
2.12	Steady-state waveforms of the Buck converter: (a) Inductor's current, (b) Output voltage.	39
2.13	Schematic diagram of the Dual Active Bridge converter.	39
2.14	steady-state waveforms of the Dual Active Bridge converter: (a) Current of series inductor, (b) Magnetizing current, (c) Output voltage.	41
2.15	Cuk converter with parasitic capacitance and inductance of the MOS-FET.	42
2.16	Waveforms of the Cuk converter during the steady-state operation: (a) Output voltage, (b) Voltage of c_m , (c) Current of l_m	44
2.17	Circuit configuration of Zeta converter.	45

2.18	Waveforms of the Zeta converter during steady-state operation: (a) Current of L_1 , (b) Current of L_2 , (b) Voltage of C_1 , (c) Output voltage. .	46
2.19	Boost converter operating in DCM.	47
2.20	steady-state waveforms in the Boost converter: (a) Output voltage, (b) Inductor current.	49
3.1	Detecting of diodes' switching events. (a) Turn-OFF event, (b) Turn-ON event.	53
3.2	Flowchart detailing the process of using the bisection method.	55
3.3	Boost converter operating in DCM (duty ration is equal to 0.14 and switching frequency is $100kHz$).	56
3.4	The current of the Boost converter's diode as function of switching time.	56
3.5	The current of the LLC's diode as function of switching time.	57
3.6	Block diagram of the Switching Time Estimator	58
3.7	Configuration of the rate limiter block.	59
3.8	Circuit configuration of the Buck converter operating in DCM.	61
3.9	Steady-state waveforms of the Buck converter operating in the DCM: (a) Inductor's current, (b) Output voltage.	63
3.10	Schematic diagram of the Series resonant converter	64

3.11	Steady-state waveforms of the SRC: (a)The current of the resonant tank's inductor, (b)Voltage of the resonant tank's capacitor, (c) Output Voltage.	65
3.12	Schematic diagram of the LLC converter	66
3.13	Waveforms of the LLC converter during the steady-state operation: (a) Current of the series inductance, (b) Current of the magnetizing inductance, (b) Voltage of the series capacitance, (c)Output voltage.	68
4.1	Illustration of a first order switching power converter with m switching intervals operating in steady-state.	71
4.2	Illustration of a first-order power converter operating in steady-state with m switching interval in each switching period, and the frequency modulation ratio equals m_f	72
4.3	Piecewise constant approximation of an AC source.	72
4.4	Circuit configuration of full bridge inverter connected to the load.	74
4.5	Inductor's current waveform of the full bridge inverter generated by the PSIM software.	75
4.6	Waveforms of the full bridge inverter during the steady-state operation: (a) Output voltage, (b) Inductor current.	76
4.7	Schematic diagram of the grid connected inverter.	77
4.8	Inductor's current during the steady-state operation in the grid connected inverter.	78

4.9	Circuit configuration of closed loop Buck converter.	80
4.10	Block diagram of the modified STE method.	80
4.11	Circuit configuration of the phase-shifted full bridge converter with PI controller	82
4.12	Steady-state waveforms of the Phase-shifted full bridge converter: (a) Inductor's current, (b) Output voltage, (c) Output of the controller (phase shift).	84
A.1	The circuit configuration of the buck converter during each switching interval.	98
A.2	Network and its associated graph.	99
A.3	Sample of graph.	100
A.4	Construction of the cutset matrix for a directed graph.	103
A.5	A typical network.	112

Symbols

η	Error limit
Γ_i	Response of system to the input vector in the i^{th} topology
\mathbf{u}	Input vector
\mathbf{x}_0	State vector at the start of the period
\mathbf{x}_c	The state vector of the control system
\mathbf{x}_i	State vector at the exit from the i^{th} topology
\mathbf{x}_m	State vector at the end of the period
\mathbf{y}	Output vector of the system
\mathcal{J}	Normal tree
\mathcal{L}	Links or cotree
Tr_{th}	Threshold value
Φ_i	State-transition matrix in the i^{th} topology
ε_k	Type k elementary row operation
A_a	Incidence matrix

A_i	State matrix in the i^{th} topology
B_i	Input matrix in the i^{th} topology
D_a	Cutset matrix
e	Maximum relative error
$f(t)$	Periodic input
$p(\cdot)$	Characteristic polynomial
s_j	Eigenvalue of the characteristic matrix
t_{sw}	Switching time
$f(s)$	Laplace transform of the periodic input
U	Laplace transform of the input vector

Chapter 1

Introduction

Power converters' response typically consists of a transient and steady-state interval, as shown in Fig. 1.1. During the transient, the state variables of the converter have different values at the beginning and end of a switching period; however, in the steady-state interval, the state variables have the same values at the beginning and end of the switching period, and the waveform repeats itself. Although the transient behavior of the converter can be used for designing the controller and choosing the rating of the components, the steady-state characteristics of the converter are more valuable because of their use in converter analysis and design. These steady-state characteristics are required for loss calculation, identification of soft switching operations, and small-signal modeling of the power converters [1]-[6].

In this thesis, the focus is on proposing a new approach to find the steady-state response of the power converters. Generally, steady-state waveforms can be found if the initial condition of all the converter states, also known as steady-state initial conditions, are known at the beginning of a switching cycle [7]. However, finding the steady-state initial conditions of the power converters is not a straightforward task

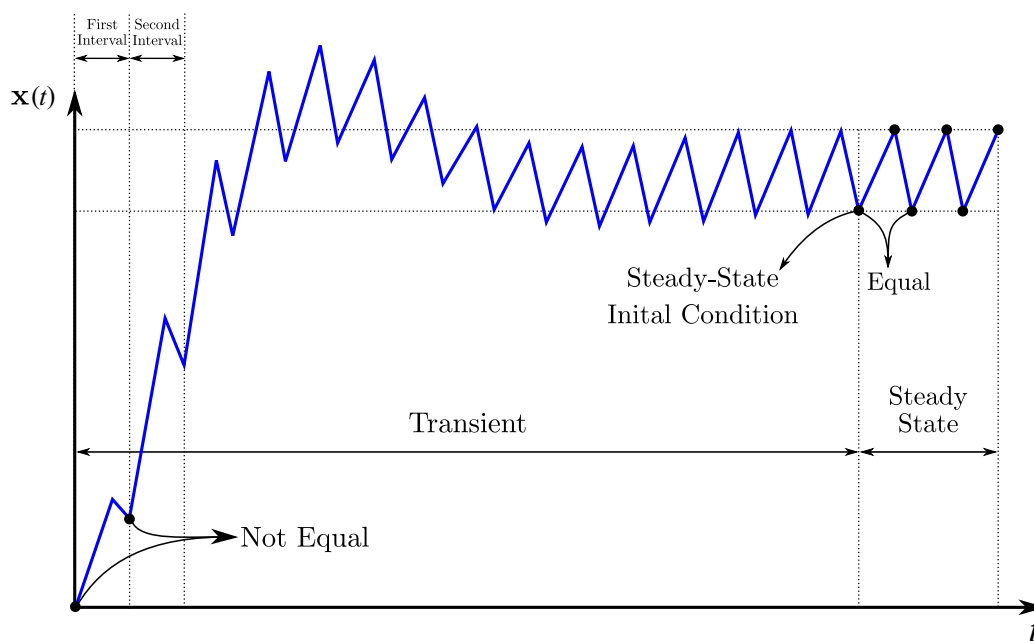


Figure 1.1: Response of a power converter with a zero initial condition, showing its state variable going through a transient before reaching steady state.

because power electronic systems are hybrid systems composed of continuous states (i.e., capacitor voltages and inductor currents) and switching events, which cause the system to become nonlinear and make finding the steady-state initial conditions challenging [8], [9]. In addition, in power converters, continuous states and switching events not only coexist but also deeply interact with each other and co-determine the operating mode of the system. For instance, in power converters with diode, the switching time depends on the systems' states, and the values of the states themselves depend on the diode's switching time, making the steady-state analysis of the system even more complicated.

Normally, simulation software is used to find the steady-state waveforms of the power converter. This software should go through transient before reaching the

steady-state response, which can be time-consuming since the simulation's time step should be chosen much smaller than the switching frequency. Different methods are proposed to avoid this problem by calculating the steady-state initial conditions of the system at the start of the switching interval and then using this initial vector to generate the steady-state waveforms [7]. These methods can be divided into two main groups: 1) the iterative approaches and 2) non-iterative approaches. The iterative approaches can be time consuming to find the steady-state initial vector, and some of these methods, such as the Newton Raohson based approaches, have convergence problems. On the other hand, the non-iterative methods are fast and accurate; however, they normally cannot be generalized for all types of converters. For example, these methods cannot be used for converters with control loops and AC sources. In addition, these methods have limitations for converters with uncontrolled switching events [10], [11].

Considering the challenges that exist in calculating the initial vector of the power converter, an appropriate approach needs to be proposed to calculate the initial conditions of the power converters with uncontrolled switching events, AC sources, and control loops. In addition, the proposed approach should have good speed and accuracy in the calculation of the initial vector.

1.1 Review of Existing Steady-State Calculation Methods

In this section, different existing analysis methods for calculating the steady-state initial conditions have been reviewed to clearly illustrate the advantages and limitations of each method.

1.1.1 Brute-Force Method

The Brute-Force simulation is the most straightforward technique that starts from an arbitrarily initial operating point (typically zero initial conditions) and runs a simulation over small time steps until the system's response passes the transient and the results of the simulation indicate that the system is sufficiently close to the steady-state operation, as shown in Fig. 1.2. This method is usually a very time-consuming simulation, going through hundreds to thousands of switching cycles, depending on how far the initial operating point is separated from the eventual steady-state operating point [12], [13].

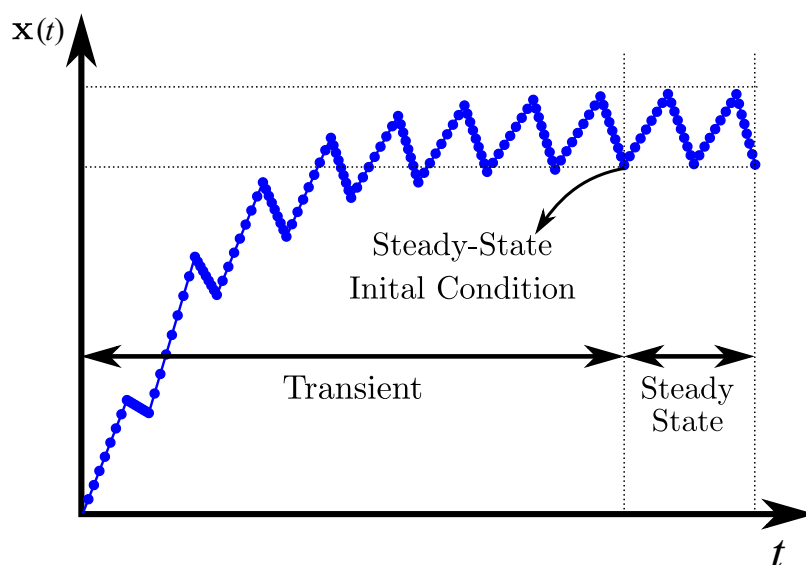


Figure 1.2: Generating the steady-state waveform using brute-force method starting from zero initial conditions.

In the brute-force based methods, the formulation of network equations mainly falls into two categories: 1) the nodal analysis method adopted by PSIM [14], and 2) the state-space approach employed by Simulink [15]. Compared with the nodal analysis method, the state-space approach is more suitable for power electronic system

simulation as the state-space matrices are independent of step size, so a variable-step solver can be used to obtain faster simulation speed [16]. Based on the state-space approach, a discrete state event driven method is recently proposed that uses a variable step and variable order method to further increase the speed of the simulation. However, the method still needs to pass the transient, which can be time consuming [17], [18].

1.1.2 Newton Raphson

In this method, the vector function $F(\mathbf{x}_0)$, which represents the change of the state vector over one switching period, is first defined as follows:

$$F(\mathbf{x}_0) = \mathbf{x}_0 - \mathbf{x}_m \quad (1.1)$$

where \mathbf{x}_0 is the value of the state vector at the start of the period, and \mathbf{x}_m is the value of the state vector at the end of the period. The power converter reaches the steady-state operation when the value of \mathbf{x}_0 and \mathbf{x}_m are equal, resulting in $F(\mathbf{x}_0)$ being equal to the null vector. So, the problem of finding the steady-state solution of the power converter is reduced to finding the appropriate initial condition that leads to :

$$F(\mathbf{x}_0) = 0 \quad (1.2)$$

A wide variety of the Newton Raphson based approaches have been proposed to solve this equation numerically. The main idea is that if the \mathbf{x}_0^j in the j^{th} iteration does not satisfy (1.2), then a correction vector $\Delta\mathbf{x}_0^j$ should be determined so that $F(\mathbf{x}_0^j + \Delta\mathbf{x}_0^j)$ will become equal to zero vector [19]. To calculate the $\Delta\mathbf{x}_0^j$, first, the

Taylor series expansion of the system can be written as follows:

$$\begin{aligned} F(\mathbf{x}_0^j + \Delta\mathbf{x}_0^j) &= F(\mathbf{x}_0^j) + \frac{\partial F(\mathbf{x}_0^j)}{\partial \mathbf{x}_0^{jT}} \Delta\mathbf{x}_0^j + \text{Higher Order Terms} \\ &= F(\mathbf{x}_0^j) + J(\mathbf{x}_0^j) \Delta\mathbf{x}_0^j + \text{Higher Order Terms} \end{aligned} \quad (1.3)$$

where $J(\mathbf{x}_0^j)$ is the Jacobian matrix of the function $F(\mathbf{x}_0^j)$ evaluated at \mathbf{x}_0^j . If the higher-order terms in (1.3) are ignored, the $\Delta\mathbf{x}_0^j$ can be calculated as follows:

$$F(\mathbf{x}_0^j + \Delta\mathbf{x}_0^j) \approx F(\mathbf{x}_0^j) + J(\mathbf{x}_0^j) \Delta\mathbf{x}_0^j = 0 \quad (1.4)$$

giving

$$\Delta\mathbf{x}_0^j = -[J(\mathbf{x}_0^j)]^{-1} F(\mathbf{x}_0^j) \quad (1.5)$$

As shown in the equation (1.5), the calculation of the Jacobian matrix is necessary to find the $\Delta\mathbf{x}_0^j$. Various Newton-based methods differ in how the Jacobian matrix is calculated [20]-[27]. A technique based on the adjoint network approach to calculate the Jacobian matrix is proposed in [20]. However, this approach considered the switching time constant and independent of the states of the system, which is not the case in power converters with uncontrolled switching events. To solve this issue, the switching time sensitivities are considered in the process of finding the Jacobian matrix in [26] and [27]. In addition, a more general approach to calculate the Jacobian matrix is Broyden's update method, which has also been implemented in the PLECS software [28]. In this method, the simulation will run for one period, and then based on the results, the jacobian matrix gets updated, as shown in Fig. 1.3.

This method can be used for closed loop converters and converters with AC sources. In addition, the method can analyze converters with uncontrolled switching events. However, the Jacobian calculation becomes tedious, and convergence is not guaranteed for more-complicated topologies with many energy storage elements or simple topologies with many parasitic elements [29]-[31].

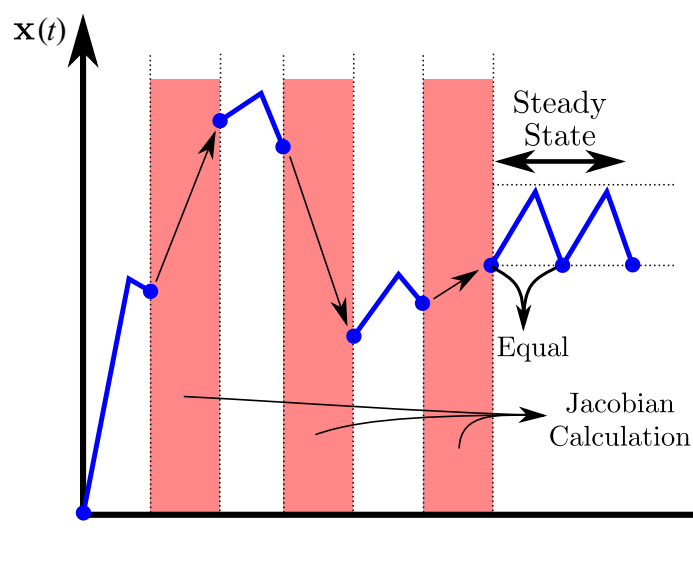


Figure 1.3: Generating the steady-state waveform using Newton Raphson with Broyden's update method (PLECS software).

1.1.3 Laplace Based Method

Laplace based method determines the initial values for the steady-state solution of a constant-coefficient nonhomogeneous ordinary differential equation with periodic and discontinuous input [32]-[34]. It is a non-iterative method based on analysis that can provide the equations to find the steady state initial conditions, which can then be used to achieve the steady state waveforms, as shown in Fig. 1.4.

Although the Laplace based method can find the solution accurately, as a general simulation tool, it has some challenges. First, finding the ordinary differential equation of the system, which the method uses in its formulation, may not be a straightforward step for a complicated topology. Moreover, this method will result in an explicit equation in interior switch-network converters, where the switching action reconfigures the interconnection between the converter's energy storage elements, such as the Boost converter. Such explicit equations should then be solved

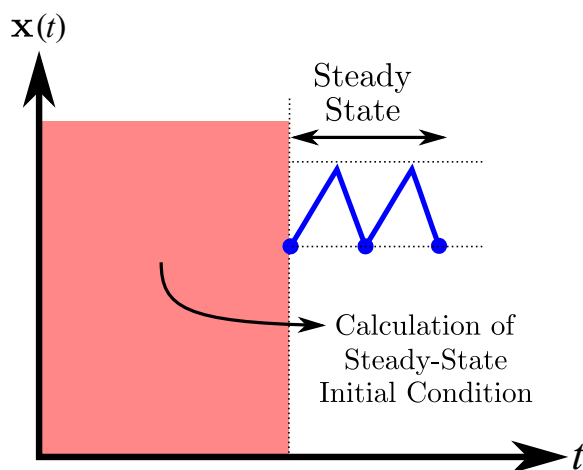


Figure 1.4: Generating the steady-state waveform using the Laplace based method.

numerically, which can be time-consuming. Furthermore, for converters with uncontrolled switching events, the solution is not systematic as more explicit equations are achieved by the method, which should be solved numerically. It is worth noting that the Laplace based method is not developed and studied for converters with the control loop or AC sources.

1.1.4 State Vector Algorithm (SVA)

State Vector Algorithm (SVA) is another non-iterative method to calculate the initial conditions of the power converters [35]-[44]. This method tries to find the steady-state initial conditions by equating the initial state vector and state vector at the end of the period. Although it is an accurate and fast method to calculate the steady-state initial conditions, it can not be used for converters with a singular characteristic matrix such as a Zeta converter because the inverse of the characteristic matrix must be calculated to find the steady-state initial conditions. To solve this problem, Augmented SVA is proposed in [45], where the input are considered as states of the system to calculate

the initial vector without using the inverse of the characteristic matrix. However, both methods require the duration of each switching interval before calculating the initial conditions, which is not the case in converters with passive switching events such as converters operating in DCM. Moreover, these methods can not be used to calculate the initial vector of the converters with AC sources or control loops.

1.2 Objectives

The main objective of this thesis is to find a general approach to calculate the steady-state initial conditions of power converter systems. These initial conditions can then be used to find the steady-state waveforms, which are essential for converter analysis and design. Several methods are investigated, and new approaches are proposed to address existing limitations. Briefly, the main objectives of this thesis are:

1. To propose new approaches to find the initial vector of the power converter system with high accuracy and low computational time. The improved Laplace based theorem (ILBT) and Enhanced SVA are proposed. The ILBT improves the speed of the conventional Laplace based theorem by using the state space representation of the system in its formulation. In addition, ILBT can be expanded to analyze the converters with time variable characteristic matrices such as Boost. Furthermore, Enhanced SVA is proposed to solve the problems of the conventional SVA while increasing speed and accuracy.
2. To analyze the power converters with uncontrolled switching events. The bisection and Switching Time Estimator (STE) methods are proposed to find the switching time of uncontrolled events. The STE method, which uses the general-purpose simulator to find the switching intervals, is proposed to remove

the monotonic function limitation on the bisection approach.

3. To find the initial vector of the AC-DC and DC-AC converters. The Enhanced SVA is modified to be applied to the largest existing period in the circuit and uses the piecewise constant approximation of the AC sources in its calculation process.
4. To calculate the initial conditions of the closed loop power converters. A new approach is proposed to find the steady-state initial conditions of the controller as well as the power converter circuit. This approach uses the modified STE method to update the states of the controller.
5. To verify the accuracy and speed of the proposed methods by comparing results with the steady-state results of the simulation software and with existing approaches.

1.3 Thesis Outline

Chapter 2 of this thesis first discusses how to model the power electronic systems. Then it presents an improved Laplace based theorem (ILBT) along with mathematical proof of the theorem. This method is proposed to solve the problems of calculating the initial conditions in the interior switch-network converters and finding the ODE of the system that the Laplace based theorem (LBT) faced. In addition, an Enhanced SVA is also proposed to solve the problems of the conventional SVA and improve the speed of calculating the initial vector by using the Taylor series and adaptive order selection. Finally, several examples are discussed to show the speed and advantages of the proposed methods over the existing approaches. Moreover, in each example, after finding the steady-state initial conditions, the steady-state waveforms are drawn, and

a comparison with the PSIM generated steady-state waveforms are provided to show the accuracy of the proposed approaches.

In chapter 3, two methods are proposed to find the initial vector of the converters with uncontrolled switching events. The first method can analyze the converter with the monotonic function of the switching time, and it uses the bisection approach and Enhanced SVA to find the uncontrolled events' switching time and initial conditions. The second method is the STE, which does not have the monotonic function constraint and can be applied to a wide range of converters. This method uses the general-purpose simulator to find the uncontrolled events' switching time, and it uses Enhanced SVA to calculate the steady-state initial conditions. Ultimately in several examples, the speed and accuracy of the proposed methods are validated by comparing their results with the steady-state analysis tool of the PLECS. In addition, the steady-state generated waveforms are also gets compared with the PSIM results.

Calculating the steady-state initial conditions of the closed loop circuit, AC-DC, and DC-AC power converters are discussed in chapter 4. First, Enhanced SVA is expanded to AC-DC and DC-AC converters by modifying the period that the method will be applied to and using the piecewise linear approximation of the AC sources. Then, the STE is modified to update the controller's state to analyze the closed loop power converters. Finally, some examples are provided to show the speed and accuracy of the proposed methods compared to the results of the PLECS and PSIM software.

Finally, the thesis is concluded in Chapter 5, and suggestions for the future work of this research are presented.

Chapter 2

Alternative Steady-State Analysis Methods

Many of design specifications in a power electronic system are given in terms of the system's steady-state characteristics, so it is extremely valuable to determine the steady-state waveforms of the power converters. In general, the steady-state waveforms can be found if the initial condition of all the converter states, also known as steady-state initial conditions, are known at the beginning of a switching cycle.

As discussed in section 1.1, various methods have been proposed to find the steady-state initial conditions of the converter; however, these methods have several limitations. In this chapter, two new approaches are proposed to address these limitations and increase the accuracy and speed in finding the steady-state initial conditions of the power converters. The first one is an Improved Laplace Based Theorem (ILBT) that solves the problems of LBT, including calculating the initial conditions in interior switch-network converters and finding the ordinary differential equation (ODE) of the circuit. Although ILBT can be used for many converters and does not

have the situations of the LBT, it cannot be used to analyze the converters whose characteristic matrix has zero eigenvalues, such as the converters operating in DCM mode. In addition, this method suffers from the high number of integrals, which should be calculated separately. Accordingly, an Enhanced State Vector algorithm (SVA) is proposed that overcomes these problems. This method is based on the Conventional SVA and uses the Taylor series and adaptive order selection to increase the speed of the approach and solve the problem of analyzing converters with a singular characteristic matrix that exists in Conventional SVA. The performance of the proposed methods is further investigated by providing several examples and comparing the results with other existing methods. In addition, the accuracy of the generated steady-state waveforms using the Enhanced SVA is shown by comparing the results with the PSIM steady-state results.

2.1 Mathematical Modelling of Power Electronic Systems

To find the steady-state initial conditions of the power converter system, first, it is crucial to accurately model the system. Power electronic systems are hybrid dynamic systems that contain continuous states and discrete events. Continuous states are modeled using the state space representation, while discrete events are defined as the trigger of change in the system configuration.

2.1.1 Modelling of Continuous States

The system is often modeled by m different linear topologies to make the study of continuous states tractable. In the case of a power electronic circuit consisting of n_{sw} switches, there is $2^{n_{sw}}$ different possible combination of these switches, which results in different linear topologies; however, normally only a limited number m of these

linear configurations are physically feasible. These piece-wise linear systems can be modeled using the state space equations:

$$\begin{aligned} \dot{\mathbf{x}}(t) &= A_i \mathbf{x}(t) + B_i \mathbf{u}(t) \\ \mathbf{y}(t) &= C_i \mathbf{x}(t) + D_i \mathbf{u}(t) \end{aligned} \quad 1 \leq i \leq m \quad (2.1)$$

where \mathbf{x} is $n \times 1$ state vector which contains the independent state variables of the system, voltage of the capacitors, and current of the inductors, \mathbf{y} is $p \times 1$ output matrix containing the output of the circuit, and \mathbf{u} is $l \times 1$ the input vector. A , B , C , and D are the system matrices that are determined base on the configuration of the circuit and the component values. The subscript i indicates that the matrix is associated with i^{th} topologies.

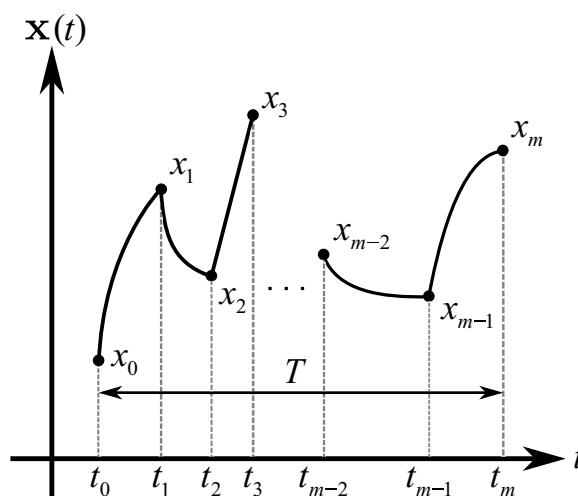


Figure 2.1: Illustration of a first order switching power converter system with m switching intervals in one switching cycle.

The following convention for symbols is adopted to keep track of the state variables' values during one switching cycle. The symbol \mathbf{x}_{i-1} represents the value of the state vector at the start of the i^{th} interval, while the symbol \mathbf{x}_i represents the value

of the state vector at the end of the i^{th} interval. Similarly, the symbols \mathbf{y}_{i-1} and \mathbf{y}_i stand for the value of the output vector at the start and end of the i^{th} interval, respectively. The symbol t_i represents the time duration that the system stays in the i^{th} interval. Without any loss of generality, it is assumed that the system enters the 1st interval at the start of a switching cycle, followed by the 2nd, the 3rd, \dots , and it is in the m^{th} interval right before the end of a switching cycle. The waveform of one transient cycle of a first-order switching system with m different interval is illustrated in Fig. 2.1.

2.1.2 Definition of Switching Events

As mentioned, the discrete events cause the system to exit the i^{th} interval, and the new topology will be formed. These switching actions can be divided into two main groups:

1. **Controlled switching events:** The gating signal determines the switching time of these events, typically including the switching of controllable power semiconductor switches.
2. **Uncontrolled switching events:** The switching time of these events is a function of a certain output variable, say the q^{th} component of the output vector \mathbf{y}_i drops to zero as a signal to change the system topology. For example, when the current through the diode of a voltage step-up (boost) converter drops from a positive value to zero, the converter goes into a new topology in which neither the transistor nor the diode is conducting.

Finding the exact time of these switching events is essential in calculating the steady-state initial condition of the system. So the approach must be able to find the

switching time of the uncontrolled events as well. Two methods will be proposed in the next chapter to address this issue. In this chapter, the assumption is that all the switching intervals are known, and the focus is on finding a fast and accurate approach to calculate the steady-state initial conditions of the power converter systems.

2.2 Laplace Based Theorem (LBT)

Laplace Based Theorem (LBT) was proposed in [34] to predict an accurate steady-state solution of power converters. This approach finds the appropriate steady-state initial condition of the power converter circuit modeled by ordinary differential equations (ODE) with discontinuous and periodic input. The following equation can be written for a power converter modeled by an ODE with periodic input:

$$p(D)x(t) = f(t) \tag{2.2}$$

where, $f(t)$ is a periodic input with period T that can have any finite number of discontinuities, and $x(t)$ is the ODE response. In addition, $D = \frac{d}{dt}$ is the differentiation operator, and $p(\cdot)$ is the characteristic polynomial:

$$p(D) = \sum_{k=0}^n a_k D^k \tag{2.3}$$

The characteristic polynomial has n roots, denoted by s_j . To apply the LBT to these equations, the following steps must be taken.

1. Obtain the ODE of the converter passive components.
2. Find the Laplace transform of the ODE, which results in:

$$p(s)x(s) - g(s) = f(s) \tag{2.4}$$

here $p(s)$ is the characteristic polynomial in the Laplace domain for which the differentiation operator has been changed to Laplace variable s , and $f(s)$ is the Laplace transform of the input function:

$$f(s) = \frac{\int_0^T f(t)e^{-st}dt}{1 - e^{-sT}} \quad (2.5)$$

And $g(s)$ is a function of initial conditions of $x(t)$:

$$g(s) = x_0 a_n s^{n-1} + (x_0 a_{n-1} + x_1 a_n) s^{n-2} + \dots = \sum_{k=0}^{n-1} b_k s^k \quad (2.6)$$
$$x(0) = x_0, \quad x^{(1)}(0) = x_1, \quad \dots \quad x^{(n-1)}(0) = x_{n-1}$$

3. After finding $f(s)$ and $g(s)$, assuming x_0, \dots, x_{n-1} are n unknown initial conditions, form the following n set of equations $g(s_j) = -f(s_j)$ for all roots of $p(s)$, and then solve them to find x_0, \dots, x_{n-1} .
4. Now that the initial conditions at the start of each period at steady-state are known, solve the ODE to find the $x(t)$.

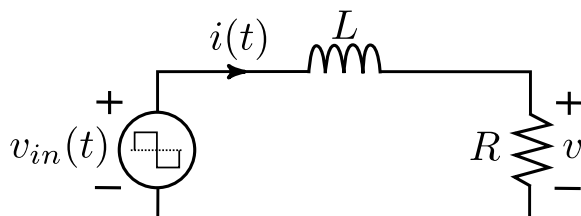


Figure 2.2: RL circuit with square wave input.

To illustrate the procedure of applying the LBT method to power circuits, a simple RL circuit is discussed here. Fig. 2.2 shows the configuration of the circuit with square wave input, which is a periodic and discontinuous function. Although the steady-state waveform of this circuit can not be easily found using the conventional method, the LBT is used to find the response in the following steps.

Step 1: The system ODE is obtained as:

$$\frac{di(t)}{dt} + Ri(t) = v_{in}(t) \quad (2.7)$$

Step 2: Finding the Laplace transform of the ODE results in:

$$(Ls + R)I(s) - LI_0 = V_{in}(s) \quad (2.8)$$

$$V_{in}(s) = \frac{A(1 - e^{-0.5Ts})}{s(1 + e^{-0.5Ts})} \quad (2.9)$$

where A and T are the input's amplitude and period, respectively.

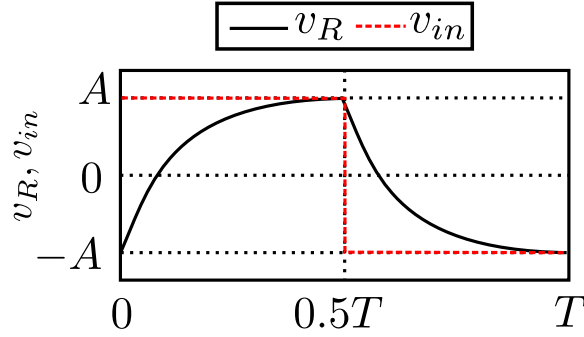
Step 3: The only root of characteristic equation is $s_j = -\frac{R}{L}$ then I_0 is found by solving the $V_{in}(s_j = -R/L) = LI_0$ as:

$$I_0 = \left(\frac{A}{R}\right) \frac{1 - e^{\frac{TR}{2L}}}{1 + e^{\frac{TR}{2L}}} \quad (2.10)$$

Step 4: Now using this initial condition, the ODE can be solved to find the steady-state waveform of the $i(t)$. Fig. 2.3 shows steady-state voltage across R obtained by (2.11).

$$\begin{cases} i(t) = \frac{A}{R} \left(1 - \frac{2e^{\frac{TR}{2L}}}{1+e^{\frac{TR}{2L}}} e^{-\frac{R}{L}t}\right) & 0 \leq t < \frac{T}{2} \\ i(t) = -\frac{A}{R} \left(1 - \frac{2e^{\frac{TR}{2L}}}{1+e^{\frac{TR}{2L}}} e^{-\frac{R}{L}t}\right) & \frac{T}{2} \leq t < T \end{cases} \quad (2.11)$$

Although the LBT is a powerful tool to find the steady-state of the power converters, it can be improved to achieve the followings. First, applying this method to the system's state-space representation can increase the speed of the method, which is not fully studied. In addition, although LBT can be used to find the steady-state initial conditions of the circuit that the switching actions do not change the connection of the storage element (Edge switch-network converters), if the switching actions

Figure 2.3: Obtained $v_R(t)$ using LBT.

change the connection of the storage element (Interior switch-network converters) such as Boost, Cuck, and DAB, the LBT method results in an explicit equation that should be solved using the numerical method.

2.3 Improved Laplace Based Theorem (ILBT)

Improved Laplace Based Theorem (ILBT) is proposed in this section to find the steady-state initial conditions of the power converter systems. This approach uses the state space representation of the power converters in its formulation, and it will be applied to the Edge switch-network converter in the next section. Then, by combining the time domain response of the state space model of the power converters with the formulation of the ILBT, the steady-state initial conditions of the Interior switch-network converters will be calculated.

Improved Laplace Based Theorem. As discussed in section 2.1, the power converter with constant characteristic matrix, can be modeled as:

$$\dot{\mathbf{x}}(t) = \mathbf{A}\mathbf{x}(t) + \mathbf{B}\mathbf{u}(t) \quad (2.12)$$

\mathbf{A} and \mathbf{B} are constant matrices, and $\mathbf{u}(t)$ is the periodic input function. Using the

ILBT, steady-state initial condition of the (2.12) can be found using the following equation:

$$\mathbf{x}(0) = - \left(\sum_{j=1}^n G(s_j) \right)^{-1} \left(\sum_{j=1}^n H(s_j) U(s_j) \right) \quad (2.13)$$

where $U(s_j)$ is the Laplace transform of the input function and s_j is the Eigenvalue of the matrix A , which can be found by solving the equation $Det(sI - A) = 0$. In addition, $G(s)$ and $H(s)$ are a function of A and B :

$$G(s) = adj(sI - A) \quad (2.14)$$

$$H(s) = adj(sI - A) B \quad (2.15)$$

here I is a n dimensional identity matrix.

Proof. To prove the theorem, it is assumed that $\mathbf{x}(t)$ is the steady-state periodic solution, then the necessary initial conditions for this are obtained. $\mathbf{x}_{1p}(t)$ is defined to be the truncated version of $\mathbf{x}(t)$ which is equal to $\mathbf{x}(t)$ for $0 < t < T$ and zero anywhere else. Since $\mathbf{x}(t)$ is the steady-state periodic solution, its Laplace transform can be written as:

$$X(s) = \frac{X_{1p}(s)}{1 - e^{-sT}} \quad (2.16)$$

Based on this equation, the Laplace transform of the $\mathbf{x}_{1p}(t)$ is:

$$X_{1p}(s) = X(s) \times (1 - e^{-sT}) \quad (2.17)$$

The Laplace transform of the $\mathbf{x}(t)$ can also be calculated using the (2.12) as follows:

$$\begin{aligned} X(s) &= (sI - A)^{-1} \mathbf{x}(0) + (sI - A)^{-1} B U(s) \\ &= \frac{1}{\varphi(s)} G(s) \mathbf{x}(0) + \frac{1}{\varphi(s)} G(s) B U(s) \end{aligned} \quad (2.18)$$

where $\varphi(s) = \text{Det}(sI - A)$ and $G(s) = \text{adj}(sI - A)$. If the (2.18) is substituted in (2.17):

$$\begin{aligned} X_{1p}(s) &= \frac{1}{\varphi(s)} G(s) \mathbf{x}(0) \times (1 - e^{-sT}) \\ &\quad + \frac{1}{\varphi(s)} G(s) BU(s) \times (1 - e^{-sT}) \end{aligned} \quad (2.19)$$

By replacing $G(s)B$ with $H(s)$ and $U(s)(1 - e^{-sT})$ with $U_{1p}(s)$, (2.19) can be written as follows:

$$X_{1p}(s) = \frac{1}{\varphi(s)} G(s) \mathbf{x}(0) (1 - e^{-sT}) + \frac{1}{\varphi(s)} H(s) U_{1p}(s) \quad (2.20)$$

$$\begin{aligned} X_{1p}(s) &= \frac{1}{\varphi(s)} G(s) \mathbf{x}(0) - \frac{1}{\varphi(s)} G(s) \mathbf{x}(0) e^{-sT} \\ &\quad + \frac{1}{\varphi(s)} H(s) U_{1p}(s) \end{aligned} \quad (2.21)$$

Taking inverse Laplace from both sides results in:

$$\begin{aligned} X_{1p}(t) &= L^{-1} \left(\frac{1}{\varphi(s)} G(s) \mathbf{x}(0) \right) - L^{-1} \left(\frac{1}{\varphi(s)} G(s) \mathbf{x}(0) e^{-sT} \right) \\ &\quad + L^{-1} \left(\frac{1}{\varphi(s)} H(s) U_{1p}(s) \right) \end{aligned} \quad (2.22)$$

Consider s_j are roots of the characteristic equation $\varphi(s) = 0$, using the Heaviside expansion theorem followings are obtained.

$$L^{-1} \left(\frac{1}{\varphi(s)} G(s) \mathbf{x}(0) \right) = \sum_{j=1}^n e^{s_j t} \frac{1}{\varphi'(s_j)} G(s_j) \mathbf{x}(0) \quad (2.23)$$

$$L^{-1} \left(\frac{1}{\varphi(s)} H(s) \right) = \sum_{j=1}^n e^{s_j t} \frac{1}{\varphi'(s_j)} H(s_j) = \mathbf{q}(t) \quad (2.24)$$

$$\begin{aligned}
 L^{-1} \left(\frac{1}{\varphi(s)} H(s) U_{1p}(s) \right) &= \mathbf{q}(t) * \mathbf{u}_{1p}(t) = \int_0^t \mathbf{u}_{1p}(\tau) \mathbf{q}(t - \tau) d\tau \\
 &= \int_0^t \mathbf{u}_{1p}(\tau) \sum_{j=1}^n \frac{e^{s_j(t-\tau)}}{\varphi'(s_j)} H(s_j) d\tau
 \end{aligned} \tag{2.25}$$

If (2.25) and (2.23) are substituted in (2.22):

$$\begin{aligned}
 \mathbf{x}_{1p}(t) &= \sum_{j=1}^n e^{s_j t} \frac{1}{\varphi'(s_j)} G(s_j) \mathbf{x}(0) - \sum_{j=1}^n e^{s_j(t-T)} \frac{1}{\varphi'(s_j)} G(s_j) \mathbf{x}(0) \\
 &\quad + \int_0^t \mathbf{u}_{1p}(\tau) \sum_{j=1}^n \frac{e^{s_j(t-\tau)}}{\varphi'(s_j)} H(s_j) d\tau
 \end{aligned} \tag{2.26}$$

For $t > T$, $\mathbf{u}_{1p}(\tau) = 0$ that results in:

$$\begin{aligned}
 \int_0^t \mathbf{u}_{1p}(\tau) \sum_{j=1}^n \frac{e^{s_j(t-\tau)}}{\varphi'(s_j)} H(s_j) d\tau &= \int_0^T \mathbf{u}_{1p}(\tau) \sum_{j=1}^n \frac{e^{s_j(t-\tau)}}{\varphi'(s_j)} H(s_j) d\tau \\
 &= \sum_{j=1}^n \frac{e^{s_j t}}{\varphi'(s_j)} H(s_j) \int_0^T \mathbf{u}_{1p}(\tau) e^{-s_j \tau} d\tau
 \end{aligned} \tag{2.27}$$

Therefore $\mathbf{x}_{1p}(t)$ for $t > T$ is:

$$\begin{aligned}
 \mathbf{x}_{1p}(t) &= \sum_{j=1}^n e^{s_j t} \frac{1}{\varphi'(s_j)} G(s_j) \mathbf{x}(0) - \sum_{j=1}^n e^{s_j(t-T)} \frac{1}{\varphi'(s_j)} G(s_j) \mathbf{x}(0) \\
 &\quad + \sum_{j=1}^n \frac{e^{s_j t}}{\varphi'(s_j)} H(s_j) \int_0^T \mathbf{u}_{1p}(\tau) e^{-s_j \tau} d\tau
 \end{aligned} \tag{2.28}$$

Combining all terms of the (2.28) results in the following equation for the $\mathbf{x}_{1p}(t)$:

$$\begin{aligned}
 \mathbf{x}_{1p}(t) &= \sum_{j=1}^n \frac{e^{s_j t}}{\varphi'(s_j)} (G(s_j) \mathbf{x}(0) (1 - e^{-s_j T}) \\
 &\quad + H(s_j) \int_0^T \mathbf{u}_{1p}(\tau) e^{-s_j \tau} d\tau)
 \end{aligned} \tag{2.29}$$

As it can be seen for $t > T$, $\mathbf{x}_{1p}(t)$ is the summation of some exponential terms. Since $e^{s_j t}$ are linearly independent functions then $\mathbf{x}_{1p}(t)$ is zero for $t > T$ if and only if all the coefficients of the exponential terms are equal to zero:

$$G(s_j) \mathbf{x}(0) (1 - e^{-s_j T}) + H(s_j) \int_0^T \mathbf{u}_{1p}(\tau) e^{-s_j \tau} d\tau = 0 \quad (2.30)$$

$$G(s_j) \mathbf{x}(0) = -H(s_j) \frac{\int_0^T \mathbf{u}_{1p}(\tau) e^{-s_j \tau} d\tau}{(1 - e^{-s_j T})} \quad (2.31)$$

$$G(s_j) \mathbf{x}(0) = -H(s_j) U(s_j) \quad (2.32)$$

The (2.33) contains n equation which are linearly dependent, $Det(G(s_j)) = 0$. To find n independent equation from this set of equations, summation of the equations for $j = 1, \dots, n$ is used, which results in:

$$\sum_{j=1}^n G(s_j) \mathbf{x}(0) = - \sum_{j=1}^n H(s_j) U(s_j) \quad (2.33)$$

So based on this equation, the steady-state initial conditions of the system can be calculated as follows:

$$\mathbf{x}(0) = - \left(\sum_{j=1}^n G(s_j) \right)^{-1} \left(\sum_{j=1}^n H(s_j) U(s_j) \right) \quad (2.34)$$

2.3.1 Improved Laplace Based Theorem (ILBT) for Edge Switch-Network Converters

In the Edge switch-network converters, the switching action of the converter's switches does not reconfigure the interconnection between its energy storage elements, so the

system characteristic matrix is constant, and the system can be modeled as shown in (2.12). Therefore the step to find the initial conditions of the Edge switch-network converters can be summarized as follow (Fig. 2.4):

1. Find the Eigenvalue of the characteristic polynomial matrix (A).
2. Calculate the $G(s_j)$ and $H(s_j)$ using (2.14) and (2.15).
3. Find the system's initial condition from equation (2.13).

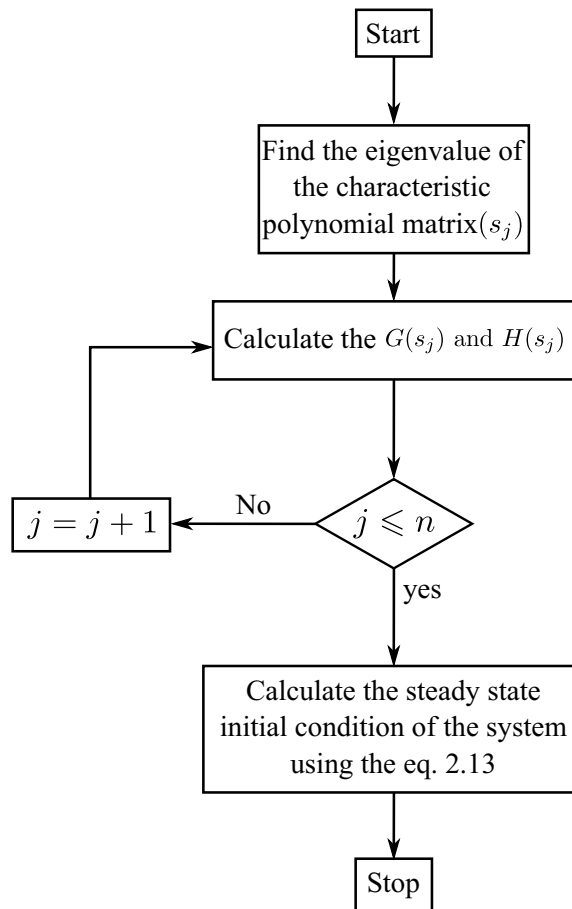


Figure 2.4: Flowchart detailing the ILBT method for edge switch-network converters.

2.3.2 Improved Laplace Based Theorem (ILBT) for Interior Switch-Network Converters

In the previous section proposed ILBT was used for converters modeled by state space representation and constant characteristic matrix (Edge switch-network converters). However, in the Interior switch-network converters such as boost and Zeta, the characteristic matrix is time-varying, and the converters can be modeled by piece-wise linear state space representation as:

$$\dot{\mathbf{x}}(t) = A_i \mathbf{x}(t) + B_i \mathbf{u}(t) \quad 1 \leq i \leq m \quad (2.35)$$

This model consists of m equations that can be combined and written in the following form:

$$\dot{\mathbf{x}}(t) = A(t) \mathbf{x}(t) + B(t) \mathbf{u}(t) \quad (2.36)$$

$$A(t) = A_m + \bar{A}_1 d_1(t) + \bar{A}_2 d_2(t) + \cdots + \bar{A}_{m-1} d_{m-1}(t) \quad (2.37)$$

$$B(t) = B_m + \bar{B}_1 d_1(t) + \bar{B}_2 d_2(t) + \cdots + \bar{B}_{m-1} d_{m-1}(t) \quad (2.38)$$

where the $d_i(t)$ for $i = 1, \dots, m - 1$ is a periodic step function that is equal to one during the i^{th} switching interval and zero anywhere else in each switching period (T) as shown in Fig. 2.5. Matrices \bar{A}_i and \bar{B}_i are chosen in such a way that by adding A_m and B_m , the value of A_i and B_i are obtained during the i^{th} interval:

$$\begin{aligned} \bar{A}_i &= A_i - A_m \\ \bar{B}_i &= B_i - B_m \end{aligned} \quad (2.39)$$

If (2.37) is substituted in (2.36):

$$\begin{aligned} \dot{\mathbf{x}}(t) &= A_m \mathbf{x}(t) + I(\bar{A}_1 d_1(t) \mathbf{x}(t) + \bar{A}_2 d_2(t) \mathbf{x}(t) + \cdots \\ &+ \bar{A}_{m-1} d_{m-1}(t) \mathbf{x}(t) + B(t) \mathbf{u}(t)) = A_m \mathbf{x}(t) + I \mathbf{u}_{new}(t) \end{aligned} \quad (2.40)$$

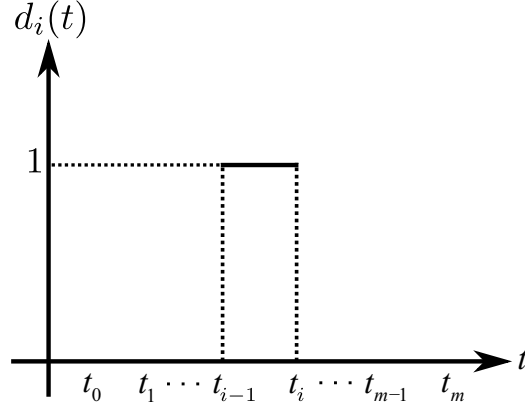


Figure 2.5: Signal $d_i(t)$ during one switching period.

In (2.40), the time-varying parts are considered as input of the system, and the characteristic matrix is constant, so the ILBT can be applied to this system. Using (2.13), the steady-state initial conditions of this system can be calculated as:

$$\mathbf{x}(0) = -\left(\sum_{j=1}^n G(s_j)\right)^{-1} \left(\sum_{j=1}^n H(s_j) U_{new}(s_j)\right) \quad (2.41)$$

$$G(s) = \text{adj}(sI - A_m) \quad H(s) = G(s)I = G(s)$$

Here $H(s)$ and $G(s)$ are equal because B is an identity matrix, moreover s_j are the eigenvalues of the A_m . Now the steady-state initial conditions can be found if the Laplace transpose of $\mathbf{u}_{new}(t)$ can be calculated. Laplace transform of $\mathbf{u}_{new}(t)$ can be written as:

$$U_{new}(s) = \bar{A}_1 L\{d_1(t)\mathbf{x}(t)\} + \bar{A}_2 L\{d_2(t)\mathbf{x}(t)\} + \cdots + \bar{A}_{m-1} L\{d_{m-1}(t)\mathbf{x}(t)\} + L\{B(t)\mathbf{u}(t)\} \quad (2.42)$$

The last term in (2.42) can easily be calculated because both $B(t)$ and $\mathbf{u}(t)$ are known, so the main problem in calculating this equation is finding the Laplace of $d_i(t)\mathbf{x}(t)$ due to the dependency on the states of the system. Since $d_i(t)\mathbf{x}(t)$ is a periodic function its Laplace transform can be written as:

$$L\{d_i(t)\mathbf{x}(t)\} = \frac{1}{1 - e^{-Ts}} \int_0^T e^{-st} d_i(t)\mathbf{x}(t) dt \quad (2.43)$$

In one switching period, $d_i(t)$ is one for $t_{i-1} < t < t_i$ and zero anywhere else, so this equation can be further simplify as:

$$L \{d_i(t)\mathbf{x}(t)\} = \frac{1}{1 - e^{-Ts}} \int_{t_{i-1}}^{t_i} e^{-st} \mathbf{x}_i(t) dt \quad (2.44)$$

In (2.44), $\mathbf{x}_i(t)$ is equal to $\mathbf{x}(t)$ for $t_{i-1} < t < t_i$, and during this interval the system can be represented by the following linear equation:

$$\dot{\mathbf{x}}_i(t) = (A_m + \bar{A}_i) \mathbf{x}_i(t) + (B_m + \bar{B}_i) \mathbf{u}(t) \quad (2.45)$$

The analytical expression for the state vector $\mathbf{x}_i(t)$ in (2.45) can be determined using the following equation:

$$\mathbf{x}_i(t) = e^{(t-t_{i-1})(A_m + \bar{A}_i)} \mathbf{x}(t_{i-1}) + \int_{t_{i-1}}^t e^{(t-\tau)(A_m + \bar{A}_i)} (B_m + \bar{B}_i) \mathbf{u}(\tau) d\tau \quad (2.46)$$

By substituting (2.46) in (2.44), the Laplace transform of $d_i(t)\mathbf{x}(t)$ could be written as:

$$L \{d_i(t)\mathbf{x}(t)\} = \frac{1}{1 - e^{-Ts}} \left\{ \int_{t_{i-1}}^{t_i} e^{-st} e^{(t-t_{i-1})(A_m + \bar{A}_i)} \mathbf{x}(t_{i-1}) dt + \int_{t_{i-1}}^{t_i} \int_{t_{i-1}}^t e^{(t-\tau)(A_m + \bar{A}_i)} (B_m + \bar{B}_i) \mathbf{u}(\tau) d\tau dt \right\} \quad (2.47)$$

The only unknown variable in (2.47) is the initial value $\mathbf{x}(t_{i-1})$ that can be calculated recursively based on the steady-state initial conditions of the system using the

following equation:

$$\begin{aligned} \mathbf{x}(t_{i-1}) &= e^{(t_{i-1}-t_{i-2})(A_m+A_{i-1})}\mathbf{x}(t_{i-2}) \\ &+ \int_{t_{i-2}}^{t_{i-1}} e^{(t_{i-1}-\tau)(A_m+A_{i-1})} (B_m + \bar{B}_{i-1}) \mathbf{u}(\tau) d\tau \end{aligned} \quad (2.48)$$

After finding the unknown variable in (2.47) using (2.48), the steady-state initial condition of the system can be found. The steps to find the initial conditions of the Interior switch-network converters can be summarized as follow (Fig. 2.6):

1. Find the Eigenvalue of the characteristic polynomial matrix (A_m).
2. Calculate the $\sum_{j=1}^n G(s_j)$.
3. Using (2.48), find the $\mathbf{x}(t_{i-1})$ based on $\mathbf{x}(0)$ for $i = 1, \dots, m - 1$.
4. Calculate the $U_{new}(s_j)$ for $j = 1, \dots, n$ using (2.42) and(2.47)
5. Find the steady-state initial condition of the system using (2.41)

The Improved Laplace Based Theorem (ILBT) can calculate the steady-state initial conditions of the Interior switch-network converters without using the numerical methods and uses state space representation in its formulation, which can increase the speed of the method. Using ILBT, for a power converter with m switching intervals and n independent states, $m \times (3n + 1)$ integrals should be calculated. Another assumption is that ILBT requires the characteristic matrix not to have zero eigenvalue because $\sum_{j=1}^n G(s_j)$ will be non-invertible. Therefore, ILBT cannot be used for converters that operate in discontinuous conduction mode(DCM) or converters with complex topologies. A new approach based on the State Vector Algorithm (SVA) is proposed in the following sections, which does not have these limitations.

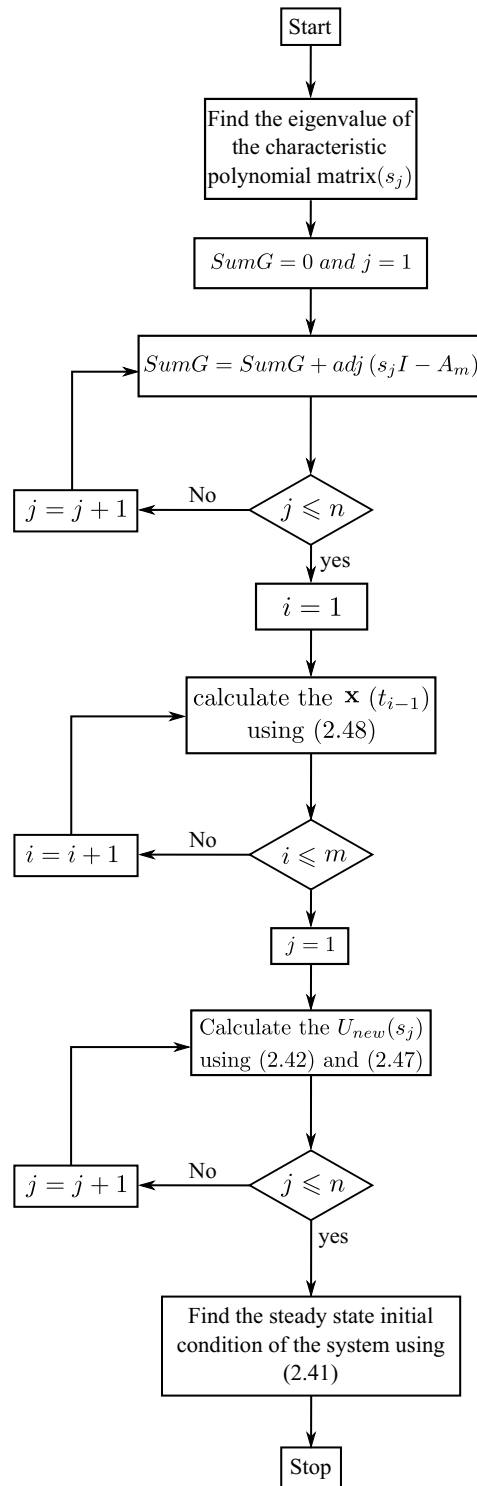


Figure 2.6: Flowchart of finding the steady-state initial conditions of the interior switch-network using ILBT.

2.4 Conventional State Vector Algorithm (SVA)

Conventional SVA was first proposed in [45], which is a non-iterative method that tries to calculate the steady-state initial vector of (2.1) by finding the value of the state vector at the end of the period (\mathbf{x}_m) based on the initial vector (\mathbf{x}_0) and equating them. For this purpose, finding $\mathbf{x}(t)$, which is the state trajectory of the system during i^{th} interval, is the first step in the method. The $\mathbf{x}(t)$ in each switching interval is the solution of the (2.1), which is shown here:

$$\mathbf{x}(t) = e^{A_i(t-t_{i-1})}\mathbf{x}(t_{i-1}) + \int_{t_{i-1}}^t e^{A_i(t-\tau)}B_i\mathbf{u}d\tau \quad \begin{array}{l} 1 \leq i \leq m \\ t_i \leq t < t_{i-1} \end{array} \quad (2.49)$$

where t_{i-1} and $\mathbf{x}(t_{i-1})$ are the time and state vector at the start of the i^{th} interval, respectively. After finding the state trajectory of the system during i^{th} interval, the value of the state vector at $t = t_i$ can be expressed as:

$$\mathbf{x}(t_i) = \Phi_i\mathbf{x}(t_{i-1}) + \Gamma_i \quad (2.50)$$

$$\Phi_i = e^{A_i d_i T} \quad (2.51)$$

$$\Gamma_i = \int_{t_{i-1}}^{t_i} e^{A_i(t_i-\tau)}B_i\mathbf{u}d\tau = A_i^{-1}(e^{A_i d_i T} - I)B_i\mathbf{u} \quad (2.52)$$

In (2.50), $\mathbf{x}(t_i)$ is expressed based on $\mathbf{x}(t_{i-1})$, so the value of the state vector at the end of the period (\mathbf{x}_m) can be calculated recursively based on the initial vector (\mathbf{x}_0).

$$\mathbf{x}_m = \Phi_m\Phi_{m-1}\cdots\Phi_1\mathbf{x}_0 + \Phi_m\Phi_{m-1}\cdots\Phi_2\Gamma_1 + \cdots + \Phi_m\Gamma_{m-1} + \Gamma_m \quad (2.53)$$

During the steady-state operation, the power converter is periodic with period T that implies (\mathbf{x}_m) and (\mathbf{x}_0) are equal when the system reaches the steady-state. Fig. 2.7

shows a steady-state operation of a first-order system with three different topologies. Therefore, equating \mathbf{x}_m with \mathbf{x}_0 and solving the recursive equation results in the following equation:

$$\mathbf{x}_0 = (I - \Phi_m \Phi_{m-1} \cdots \Phi_1)^{-1} (\Phi_m \Phi_{m-1} \cdots \Phi_2 \Gamma_1 + \cdots + \Phi_m \Gamma_{m-1} + \Gamma_m) \quad (2.54)$$

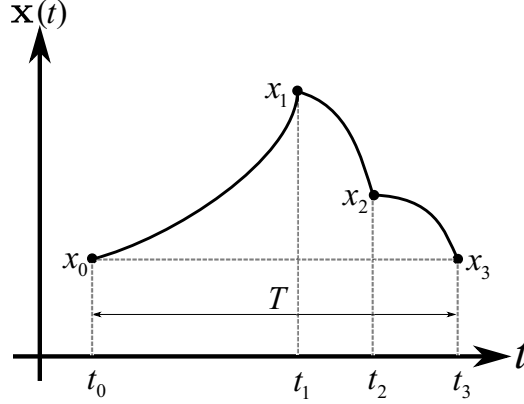


Figure 2.7: Steady-state operation of a first-order system with three switching intervals.

The steps to find the steady-state initial condition of the power converter system using the conventional SVA can be summarized as follow (Fig. 2.8):

1. Find Φ_i and Γ_i using (2.51) and (2.52).
2. Calculate the steady-state initial condition using (2.54).

The SVA does not need any integral calculation in the process of finding the steady-state initial condition of the power converter. However, it faces the following problems:

- When the characteristic matrix A_i of the circuit is singular (such as Boost converter), Γ_i cannot be computed using (2.52) as the inverse matrix (A_i^{-1}) is required.

- The matrix exponential calculations may become computationally burdensome.
- Equation (2.54) contains $2m$ terms (m for Φ_i and m for Γ_i) that must be calculated separately, which can be time-consuming.

To solve the aforementioned shortcomings in the calculation of steady-state condition, a new approach based on the State Vector Algorithm (SVA) is proposed in the next section, which is faster than conventional SVA and can be applied to a wide range of converters.

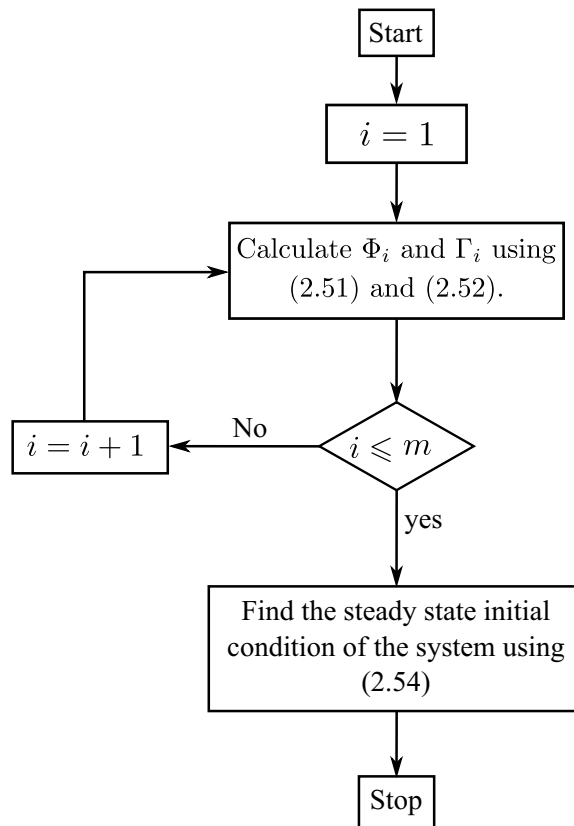


Figure 2.8: Algorithm of finding the initial vector of the power converters using the conventional SVA.

2.5 Proposed Enhanced State Vector Algorithm (SVA)

Here, a new method based on the state vector algorithm is proposed, which uses the Taylor series of e^{At} to solve the problem of converters with a non-invertible characteristic matrix such as the Boost converter. In addition, the number of terms that should be calculated separately is reduced by using the Taylor series. Moreover, this method uses an adaptive order selection to reduce the calculation time of the matrix exponential and further increase the speed of calculating the steady-state initial conditions.

2.5.1 Taylor Series of e^{At}

The exponential of the matrix A, denoted by e^{At} , is the $n \times n$ matrix. The Taylor series of this function can be written as:

$$e^{At} = I + \sum_{n=1}^{\infty} \frac{A^n t^n}{n!} \quad (2.55)$$

If the Taylor series of e^{At} is substituted in (2.54), Γ_i and Φ_i can be written as:

$$\Phi_i = \left[I + \sum_{n=1}^{\infty} \frac{A_i^n (t_i - t_{i-1})^n}{n!} \right] \quad (2.56)$$

$$\Gamma_i = \left[\sum_{n=1}^{\infty} \frac{A_i^{n-1} (t_i - t_{i-1})^n}{n!} \right] B_i U \quad (2.57)$$

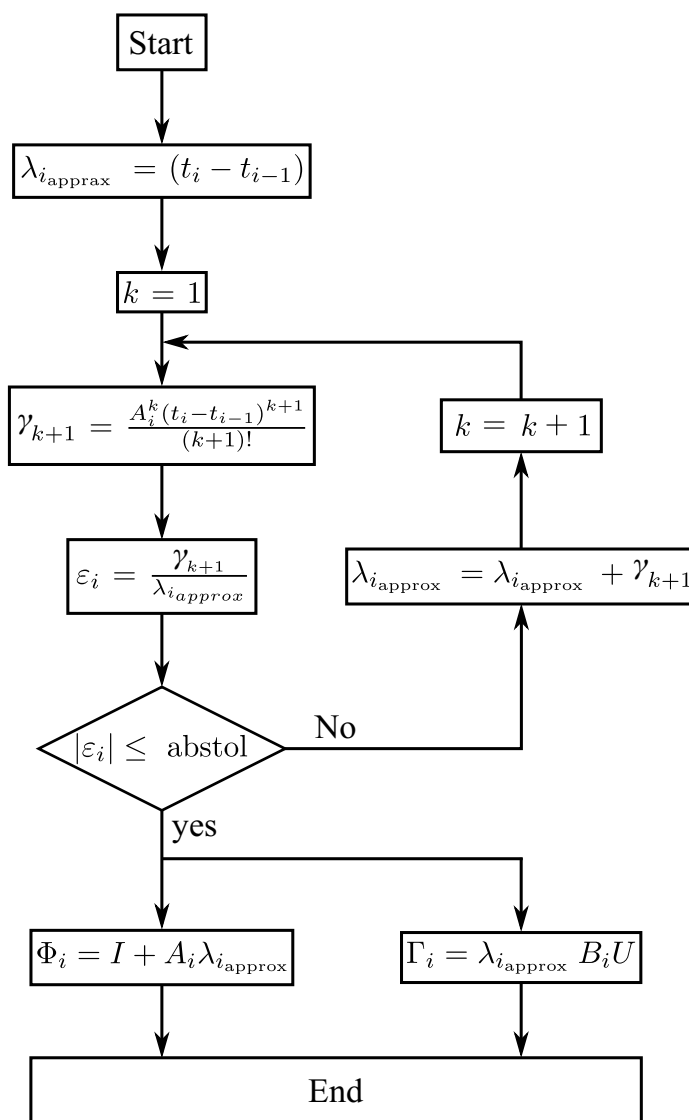


Figure 2.9: Flowchart of the adaptive order selection embedded in the calculation of $\lambda_{i,approx}$.

Equations (2.56) and (2.57) does not have the problem of singular A_i , because instead of integrating $e^{A_i(t_i-\tau)}$, which results in A_i^{-1} , Taylor series' terms are integrated that are integrable polynomial terms. In addition, Φ_i and Γ_i have a common term that can be reused in the calculation process to reduce the number of terms that must

be calculated separately in equation (2.54) and improve the speed of the algorithm. Therefore, first λ_i is determined, and then using this value, Φ_i and Γ_i can be calculated as follows:

$$\lambda_i = \sum_{n=1}^{\infty} \frac{A_i^{n-1}(t_i - t_{i-1})^n}{n!} \quad (2.58)$$

$$\Phi_i = [I + A_i \lambda_i] \quad (2.59)$$

$$\Gamma_i = \lambda_i B_i U \quad (2.60)$$

The proposed Enhanced SVA requires an infinite sum in equation (2.58). The following section discusses how to efficiently calculate this infinite sum while maintaining accuracy.

2.5.2 Adaptive Order Selection

Generally, in the calculation of λ_i , the Taylor series will be truncated at the term of k^{th} order, and $\lambda_{i_{approx}}$ is defined as:

$$\lambda_i \approx \lambda_{i_{approx}} = \sum_{n=1}^k \frac{A_i^{n-1}(t_i - t_{i-1})^n}{n!} \quad (2.61)$$

The choice of k is important because if a small number is selected, accuracy will be lost, and if a large number is selected, the calculation will become time-consuming. In addition, the choice of k depends on the circuit configuration, and to maintain accuracy, it must increase as the complexity of the circuit increases. Therefore, to choose an appropriate k , the rate of change is defined as:

$$\begin{aligned} \varepsilon_i &= \frac{\lambda_i - \lambda_{i_{approx}}}{\lambda_{i_{approx}}} = \frac{\frac{A_i^k(t_i - t_{i-1})^{k+1}}{k+1!} + O(k+2)}{\lambda_{i_{approx}}} \\ &\approx \frac{\frac{A_i^k(t_i - t_{i-1})^{k+1}}{k+1!}}{\lambda_{i_{approx}}} = \frac{\gamma_{k+1}}{\lambda_{i_{approx}}} \end{aligned} \quad (2.62)$$

In this equation, the difference between λ_i and $\lambda_{i_{approx}}$ is equal to the sum of the terms of order higher than k , which is approximated by $(k + 1)^{th}$ term. Now, k should be chosen as the smallest possible number that makes the rate of change in equation (2.62) less than the absolute tolerance (*abstol*).

Based on (2.62), an adaptive order selection totally embedded in the calculation of Φ_i and Γ_i can be proposed, as shown in Fig. 2.9. First, the initial value of the $\lambda_{i_{approx}}$ is set to $t_i - t_{i-1}$. Then the $(k + 1)^{th}$ term of the Taylor series (γ_{k+1}) is determined and used to calculate the rate of change. If the rate of change is greater than absolute tolerance, γ_{k+1} is used to find a new $\lambda_{i_{approx}}$. Otherwise, $\lambda_{i_{approx}}$ is used to determine Φ_i and Γ_i . This method has the advantage of the reusability of the increments for both adaptive order selection and calculation of $\lambda_{i_{approx}}$. Therefore, no extra computational costs have to be entailed to choose an appropriate k .

2.6 Simulation Results

In this section, several examples are provided to show the speed and accuracy of the proposed ILBT and Enhanced SVA methods in finding the steady-state initial conditions of the power converter systems. The proposed ILBT and Enhanced SVA methods are implemented in the Script of PSIM, and Fig. 2.10 shows the block diagram of these methods. The first block has the task of constructing the steady-state representation of the power converter circuit from the incident matrix and circuit parameter. The detail of automatic generation of the system matrices A_k, B_k, C_k, D_k is discussed in Appendix A. After that, the steady-state initial conditions will be calculated using these matrices and the switching times of the power switches. Finally, (2.49) is used to draw the steady-state waveforms of the converters, which are then compared to the generated waveforms of the PSIM software to show the accuracy of these methods. In addition, the results of ILBT and Enhanced SVA methods are

compared with LBT and conventional SVA to show the advantages of the proposed approaches.

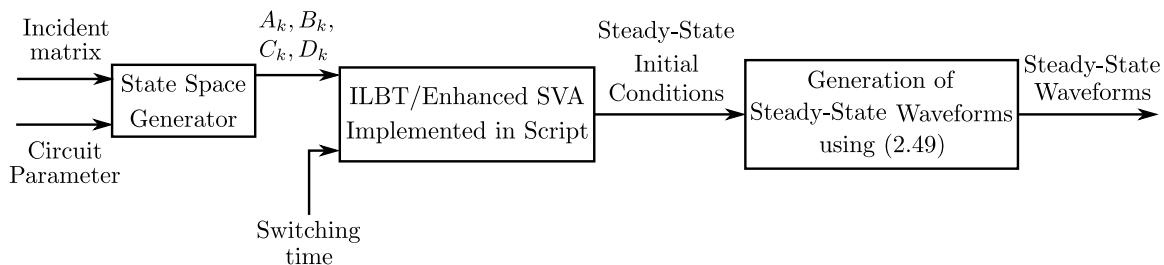


Figure 2.10: Block diagram of the proposed ILBT and Enhanced SVA.

2.6.1 Buck Converter

Buck converter in Fig. 2.11 is considered as the first example. In this circuit, the parameters are chosen as shown in Table 2.1:

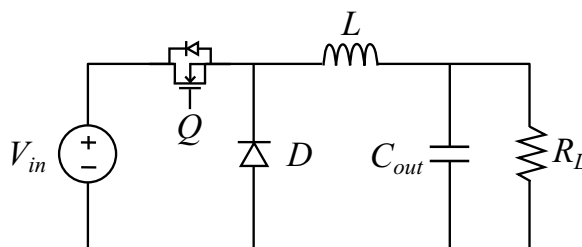


Figure 2.11: Schematic diagram of the Buck converter.

The simulation time of different methods to calculate the steady-state initial vector of this converter is shown in Table 2.2. These results show that by using the state space representation of the system, ILBT can calculate the steady-state initial vector faster than LBT. In addition, the Enhanced SVA reduces the simulation time by around three orders of magnitude compared to the Conventional SVA due to the fast calculation of the exponential function of the matrix and the reduction of the terms needed for this method.

Table 2.1: System parameters of the Buck converter.

	Parameter	Value
Input voltage	V_{in}	24v
Filter inductance	L	40 μ H
Output capacitance	C_{out}	22 μ F
Load resistance	R_L	5 Ω
Switching frequency	f_s	100kHz
Duty cycle	D	0.73

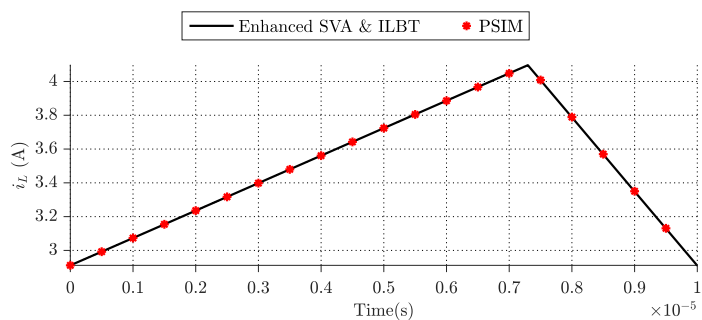
Table 2.2: The simulation time required to converge to a steady-state in the circuit of Fig. 2.11.

Method	Simulation time (ms)
LBT	18.043
ILBT	10.043
Conventional SVA	4.747
Enhanced SVA	1.772

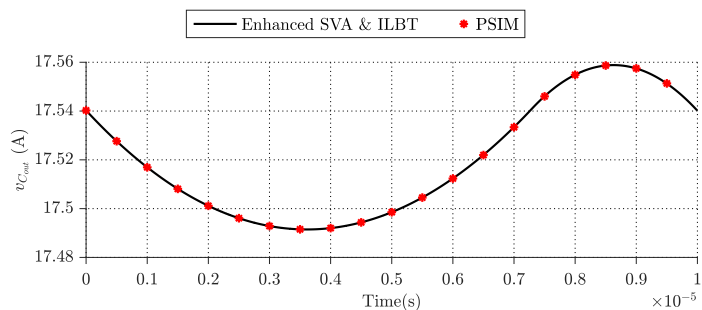
The ILBT and Enhanced SVA calculate the following vector as the initial vector of the converter:

$$\begin{bmatrix} I_L(0) \\ V_{C_{out}}(0) \end{bmatrix} = \begin{bmatrix} 2.91158 \\ 17.54026 \end{bmatrix} \quad (2.63)$$

To show the accuracy of the ILBT and Enhanced SVA results, after finding the initial vector of the buck converter, these methods use (2.49) to draw the steady-state waveform of the converter. Fig 2.12 compares the results of the methods with PSIM, which shows a complete match between the results.



(a)



(b)

Figure 2.12: Steady-state waveforms of the Buck converter: (a) Inductor’s current, (b) Output voltage.

2.6.2 Dual Active Bridge Converter

As an example of a converter system with variable characteristic polynomial, Dual Active Bridge(DAB), as shown in Fig. 2.13, is studied. In this circuit, due to the switching action of the converter, the connection of the storage elements will change, which results in a variable characteristic matrix.

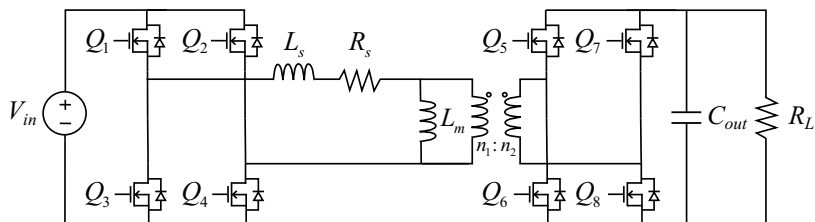


Figure 2.13: Schematic diagram of the Dual Active Bridge converter.

In addition, the magnetizing inductance of the transformer is also added to show the accuracy of the proposed ILBT and Enhanced SVA methods in finding the steady-state initial condition. The value of this magnetizing inductance and other circuit parameters are shown in Table 2.3.

Table 2.3: System parameters of the Dual Active Bridge converter.

	Parameter	Value
Input voltage	V_{in}	35v
Series inductance	L_s	90 μ H
Series resistance	R_s	2 Ω
Magnetizing inductance	L_m	3mH
Transformer turn ratio	$n_1 : n_2$	1
Output capacitance	C_{out}	33 μ F
Load resistance	R_L	1k Ω
Switching frequency	f_s	200kHz

Table 2.4: The simulation time required for different steady-state solvers to find the initial conditions of the Dual Active Bridge.

Method	Simulation time (ms)
LBT	–
ILBT	104.7988
Conventional SVA	30.5203
Enhanced SVA	6.3643

The computation time required for the different algorithms is shown in Table 2.4. The LBT simulation time is not reported due to its problem in solving the circuit with the variable characteristic polynomial as discussed in section 2.2. In addition,

the results show that the Enhanced SVA outperforms other methods and can find steady-state initial vector faster than other methods. To show the accuracy of the proposed methods, the steady-state waveforms generated using (2.49) are compared to PSIM results in Fig. 2.14.

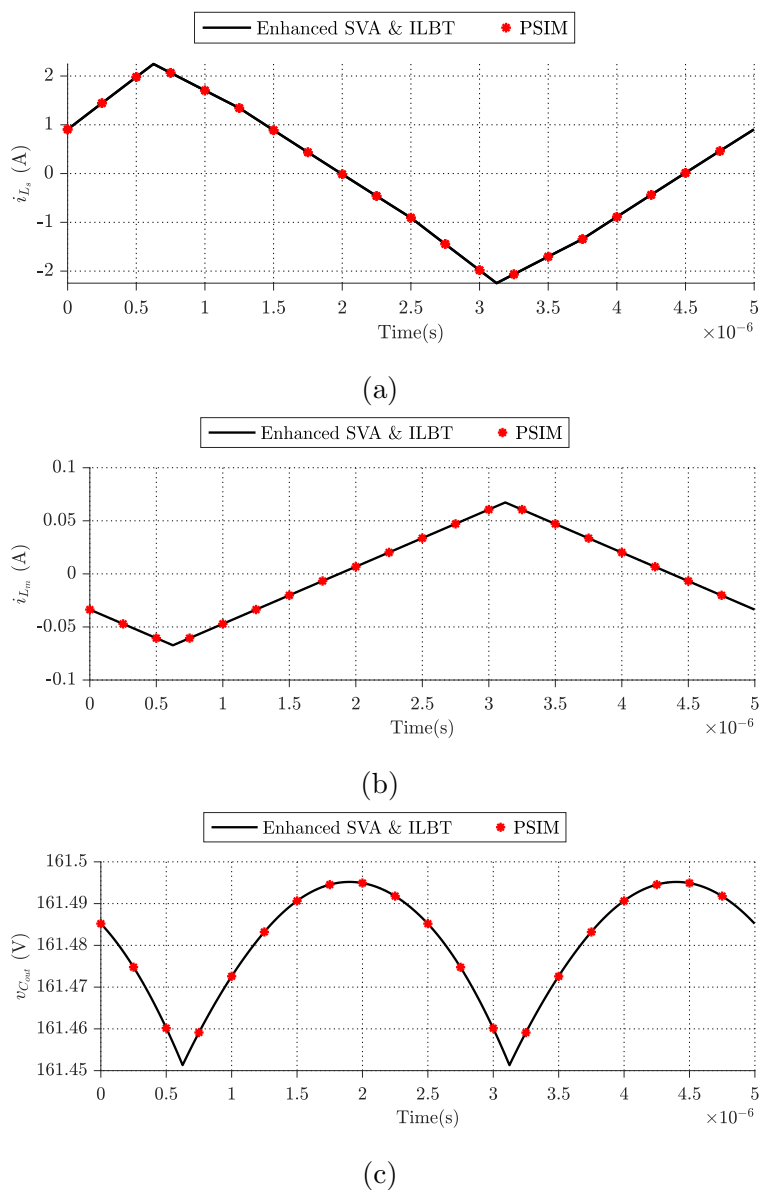


Figure 2.14: steady-state waveforms of the Dual Active Bridge converter: (a) Current of series inductor, (b) Magnetizing current, (c) Output voltage.

2.6.3 Cuk Converter with Parasitic Components

Fig. 2.15 shows a Cuk converter with MOSFET parasitic components. This example is provided to show the capability of the ILBT and Enhanced SVA methods in analyzing the circuit with complicated behavior such as the ringing effect.

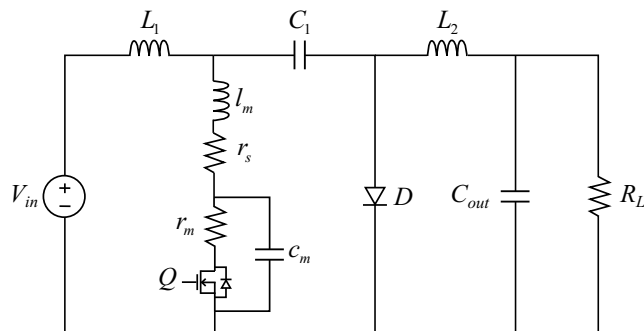


Figure 2.15: Cuk converter with parasitic capacitance and inductance of the MOSFET.

Table 2.5: System parameters of the Cuk converter.

	Parameter	Value
Input voltage	V_{in}	100v
Input inductance	L_1	780 μ H
Output inductance	L_2	540 μ H
Parasitic inductance	l_m	0.2nH
Parasitic resistance	r_s	10m Ω
MOSFET resistance	r_m	2.5m Ω
Input capacitance	C_1	47 μ F
Output capacitance	C_2	54 μ F
Drain to source capacitance	c_m	180pF
Load resistance	R_L	83 Ω
Duty cycle	D	0.73
Switching frequency	f_s	100kHz

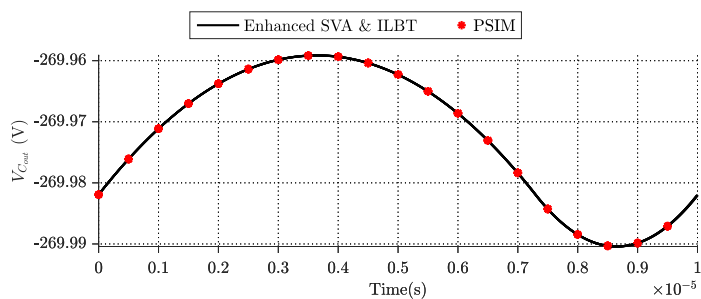
The parameters of this Cuk converter are listed in Table 2.5, and the steady-state initial condition of this converter, using the proposed methods, is found as follows:

$$\begin{bmatrix} I_{L_1}(0) \\ I_{L_2}(0) \\ I_{L_m}(0) \\ V_{C_1}(0) \\ V_{C_{out}}(0) \\ V_{C_m}(0) \end{bmatrix} = \begin{bmatrix} 8.3520 \\ -2.5773 \\ 3.198e^{-5} \\ 370.2112 \\ -269.981 \\ 370.2112 \end{bmatrix} \quad (2.64)$$

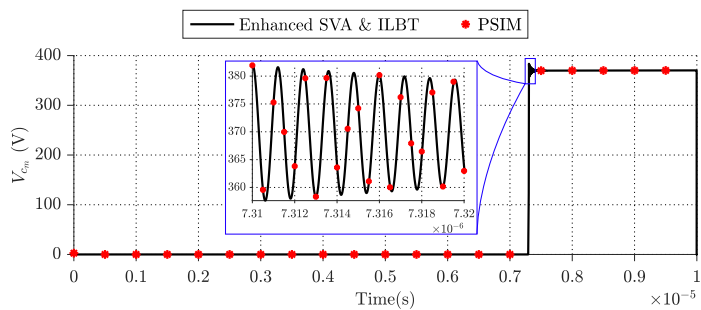
Table 2.6: The simulation time required to find the steady-state initial conditions of the Cuk converter.

Method	Simulation time (<i>ms</i>)
LBT	—
ILBT	87.1445
Conventional SVA	22.7578
Enhanced SVA	4.7456

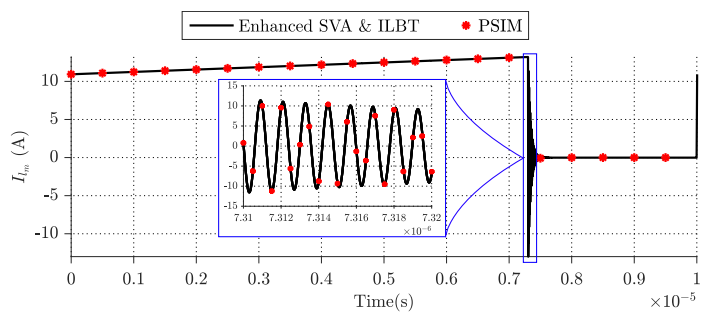
Table 2.6 shows the performance of the different methods. In this case, the Enhanced SVA converged faster than the conventional SVA algorithm and ILBT. In this circuit, due to the variable characteristic matrix, LBT cannot converge to the solution. Moreover, the proposed ILBT and Enhanced SVA, after finding the initial vector, can use (2.49) to draw the inductor current (I_{l_m}), capacitor voltage (V_{c_m}), and the output voltage ($V_{C_{out}}$) waveform. To show the accuracy of the proposed methods, the waveforms are compared with the results produced by PSIM software, as shown in Fig. 2.16.



(a)



(b)



(c)

Figure 2.16: Waveforms of the Cuk converter during the steady-state operation: (a) Output voltage, (b) Voltage of c_m , (c) Current of l_m .

2.6.4 Zeta Converter

As mentioned in section 2.4, conventional SVA cannot find the initial vector of the converters with a singular characteristic matrix; however, the proposed Enhanced SVA solved this problem by using the Taylor series. In addition, this method has

better computational speed than the conventional SVA. A Zeta converter, as shown in Fig. 2.17, is provided here to show the capability of the proposed ILBT and Enhanced SVA in handling the converter with the singular characteristic matrix. The converter parameters are listed in Table 2.7.

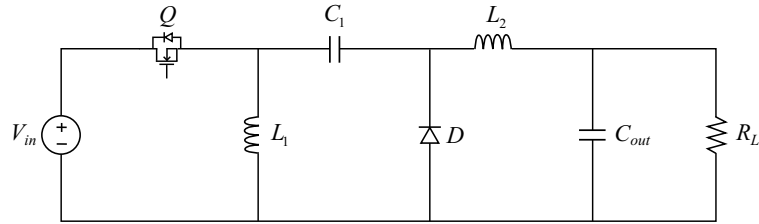


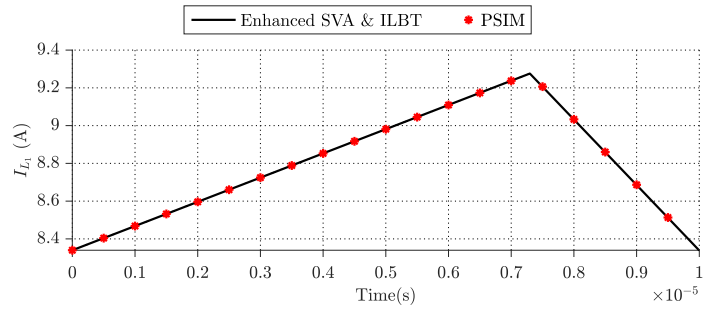
Figure 2.17: Circuit configuration of Zeta converter.

Table 2.7: System parameters of the Zeta converter.

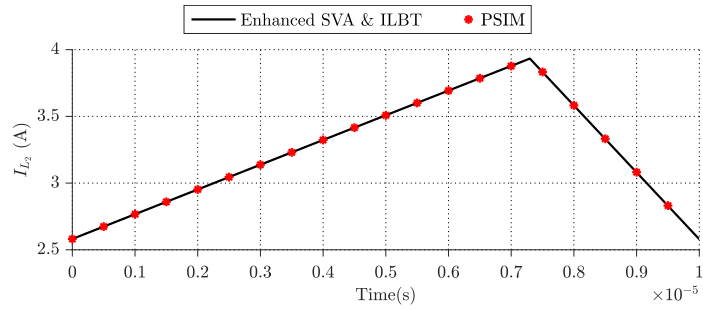
	Parameter	Value
Input voltage	V_{in}	100v
Input inductance	L_1	780 μ H
Output inductance	L_2	540 μ H
Input capacitance	C_1	47 μ F
Output capacitance	C_{out}	54 μ F
Load resistance	R_L	83 Ω
Duty cycle	D	0.73
Switching frequency	f_s	100kHz

Using the proposed ILBT and Enhanced SVA, the steady-state initial conditions of this converter are calculated as follows:

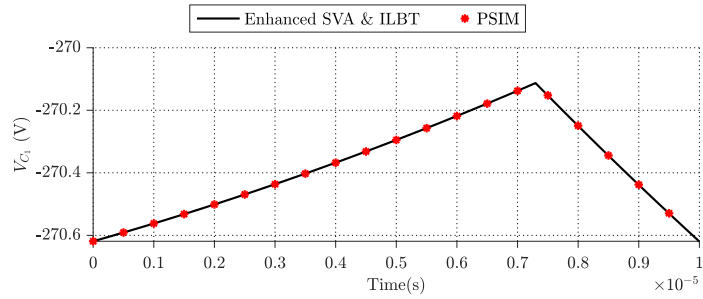
$$\begin{bmatrix} I_{L_1}(0) \\ I_{L_2}(0) \\ V_{C_1}(0) \\ V_{C_{out}}(0) \end{bmatrix} = \begin{bmatrix} 8.33987 \\ 2.58118 \\ -270.61888 \\ 270.38945 \end{bmatrix} \quad (2.65)$$



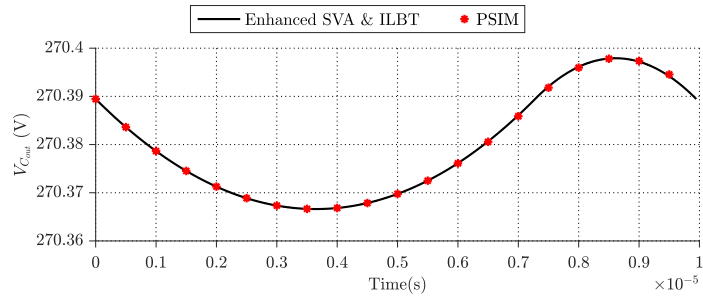
(a)



(b)



(c)



(d)

Figure 2.18: Waveforms of the Zeta converter during steady-state operation:
 (a) Current of L_1 , (b) Current of L_2 , (b) Voltage of C_1 , (c) Output voltage.

Table 2.8 shows the performance of the different methods. In this case, the Enhanced SVA converged faster compared to the ILBT. In addition, the conventional SVA solver cannot find this circuit's steady-state initial vector due to the singularity of the characteristic matrix. Furthermore, LBT has a problem finding this circuit's steady-state initial condition because the characteristic matrix is time-variable. To show the accuracy of the ILBT and Enhanced SVA, the steady-state waveforms of the converter are generated based on the calculated initial conditions, and the waveforms are compared with the PSIM results in Fig. 2.18.

Table 2.8: Simulation time of the different steady-state solver for finding the initial vector of the Zeta converter.

Method	Simulation time (<i>ms</i>)
LBT	–
ILBT	60.978
Conventional SVA	–
Enhanced SVA	4.492

2.6.5 Boost Converter Operating in DCM

Fig. 2.19 illustrates the overall circuit of the Boost converter operating in discontinuous conduction mode. The circuit parameters of this Boost converter are listed in Table 2.9. This example shows that none of the other methods can calculate the system's steady-state initial conditions except for Enhanced SVA.

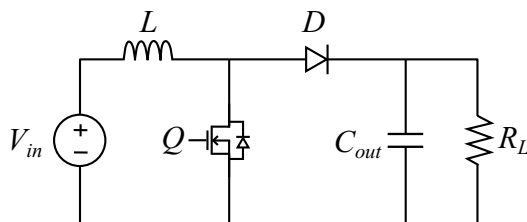


Figure 2.19: Boost converter operating in DCM.

Table 2.9: System parameters of the Boost converter.

	Parameter	Value
Input voltage	V_{in}	46v
Inductance	L	5 μ H
Output capacitance	C_{out}	13 μ F
Load resistance	R_L	15 Ω
Duty cycle	D	0.14
Switching frequency	f_s	100kHz

Table 2.10 shows the simulation time for the Enhanced SVA. However, the simulation time for other methods is not reported because the steady-state initial conditions of the system cannot be calculated due to the converter's singular A_i and variable characteristic matrix. The Enhanced SVA calculates the initial condition of the circuit as follows:

$$\begin{bmatrix} I_L(0) \\ V_{C_{out}}(0) \end{bmatrix} = \begin{bmatrix} 3.1819e^{-5} \\ 56.4357 \end{bmatrix} \quad (2.66)$$

Table 2.10: Simulation time required for Boost converter operating in DCM.

Method	Simulation time (ms)
LBT	—
ILBT	—
Conventional SVA	—
Enhanced SVA	2.961

Finally, after finding the boost converter's initial vector, the circuit's steady-state waveforms are plotted using (2.49). The comparison of these waveforms with the

PSIM generated results is shown in Fig. 2.20.

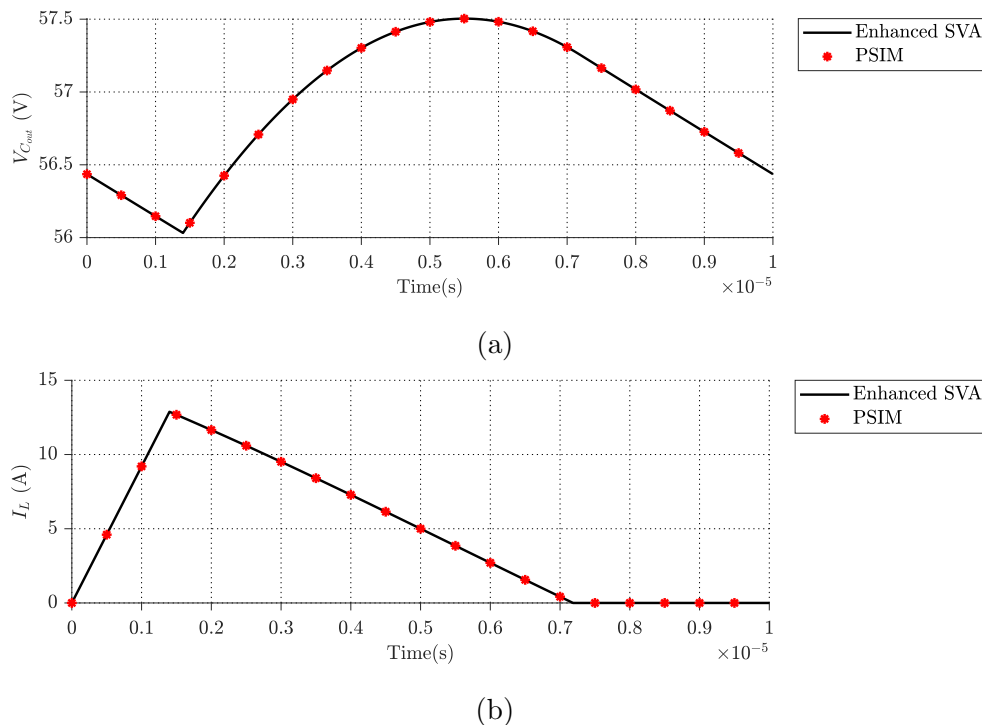


Figure 2.20: steady-state waveforms in the Boost converter: (a) Output voltage, (b) Inductor current.

2.7 Summary

This chapter proposed two new methods to find the steady-state initial conditions of the power converter systems. The first method was the improved Laplace based theorem (ILBT), which solved the problem of finding the differential equation of the system associated with LBT. In addition, ILBT can be used to analyze the converter with a variable characteristic matrix like Boost, Cuck, and DAB. Then the Enhanced state vector algorithm (SVA) was proposed, which used the Taylor series

and adaptive order selection to solve the problems associated with conventional SVA, such as the inability to analyze the converters with a singular characteristic matrix. Finally, several examples were provided to show the speed and capability of the proposed ILBT and Enhanced SVA. Moreover, to show the accuracy of the methods, steady-state waveforms of each converter are generated after calculating the initial conditions, and a comparison of these waveforms with generated waveforms of the PSIM is provided.

Chapter 3

Steady-State Analysis of Converters with Uncontrolled Switching Events

In the previous chapter, two new methods were proposed to calculate the steady-state initial conditions of the power converters. The first method was ILBT, which uses a time-consuming integration process, and it faced the issue in the converters that their characteristic matrix has zero eigenvalues. To overcome these challenges, the Enhanced SVA was proposed. Although the proposed Enhanced SVA has good speed and accuracy, the switching intervals of the converters were considered known variables, which is not the case in converters with uncontrolled switching events such as resonant converters.

To apply the Enhanced SVA to converters with uncontrolled switching events, the occurrence time of these switching events should be found. Then the switching intervals of the converter can be calculated, which are required to calculate the

steady-state initial conditions of the converter. This chapter proposes two methods to find the switching time of uncontrolled events. Firstly, an iterative method based on bisection is proposed to find the switching time of the converters with the monotonic function of switching time. Although this method is fast and simple to implement, using it for converters with more than one unknown switching time can be complicated, and convergence is not guaranteed. Moreover, it cannot be used for converters with the non-monotonic function of switching time, such as the resonant LLC converter. Accordingly, Switching Time Estimator (STE) mechanism using the general-purpose simulator tool is proposed that overcomes the problems associated with the bisection method. The feasibility of the proposed methods is shown by providing several examples and comparing the results with PSIM results. Furthermore, the results of the PLECS steady-state analysis tool are provided in the simulation section to show the superiority of the proposed method.

3.1 Determination of Switching Intervals Using Bisection Method

As mentioned, in all of the approaches discussed in the previous chapter, the assumption was that the duration of each switching interval is a known variable and can be used directly in the calculation of the steady-state initial conditions, which is not the case in the converter with uncontrolled switching events. So, a general approach for calculating the steady-state initial conditions must be able to find the switching time of the uncontrolled event.

Unlike controlled switching events that the switching time was determined based on the gating signal of the switches; the switching time of the uncontrolled events is

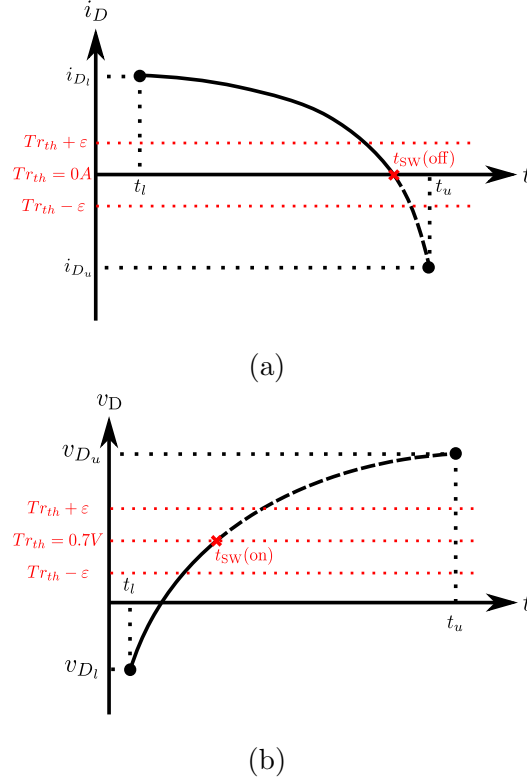


Figure 3.1: Detecting of diodes' switching events. (a) Turn-OFF event, (b) Turn-ON event.

a function of the states of the system, which means these uncontrolled events happen when a trigger variable crosses a corresponding threshold (Tr_{th}). For example, as illustrated in Fig. 3.1a, for the turn-off event of a diode, the trigger variable should be defined as the device current $i_D(t)$ and the corresponding threshold condition value will be $Tr_{th} = 0$ A, since an on-state diode will only be turned off when its device current drops to 0 A. Likewise, for the turn-on event of a diode, as presented in Fig. 3.1b, the trigger variable should be defined as the device voltage $v_D(t)$ and the corresponding threshold condition value will be $Tr_{th} = 0.7$ V. The trigger equations can be written as follow:

$$Tr_{th} = (\mathbf{x}_t)_q \Rightarrow Tr_{th} = (C_t)_q \mathbf{x}(t_{sw}) + (D_t)_q \mathbf{u} \quad (3.1)$$

where $(D_t)_q$ and $(C_t)_q$ represent the q^{th} row of D_t and C_t , respectively. The trigger vector \mathbf{y}_t is a set of p_t output variables obtained for detecting uncontrolled events. The index q changes for each uncontrolled switching event since the exit from each topology is typically associated with a different trigger variable.

$\mathbf{x}(t_{sw})$ in the trigger equation is function of value of states at the start of switching interval (\mathbf{x}_{i-1}) and switching time (t_{sw}), as shown in (3.2). In addition, as discussed in the previous chapter, (\mathbf{x}_{i-1}) is a function of the initial condition of the system (\mathbf{x}_0), which is a function of switching time (t_{sw}) itself. So (3.1) is a function of t_{sw} , and the switching time (t_{sw}) can be found from this equation.

$$\mathbf{x}(t_{sw}) = e^{A_i(t_{sw}-t_{i-1})}\mathbf{x}(t_{i-1}) + \int_{t_{i-1}}^{t_{sw}} e^{A_i(t_{sw}-\tau)}B_i\mathbf{u}d\tau \quad (3.2)$$

Now the problem of finding the switching time is transformed into finding a root of a function, which can be solved using different techniques. The choice of the algorithm depends on the characteristic of the circuit. For instance, a bisection method is suited to find the switching time in the converters with the monotonic function of t_{sw} because this search algorithm halves the search interval in each iteration resulting in a significant computational advantage. Furthermore, the greater the required accuracy, the better the bisection search performs relative to an exhaustive search.

To find the switching time (t_{sw}) using the bisection method, the first step is to determine the absolute lower and upper bounds based on physical insights into the converter's operation, and consider the initial guess of the switching time as an average of lower and upper bounds. Then in the next step, using the Enhanced SVA approach, the initial conditions of the converter for the initial guess, upper and lower bound of the switching time are calculated. Then, $\mathbf{x}(t_{sw})$ is calculated using these initial conditions, which can be used to calculate the value of the equation (3.1). In the last step, the initial guess for the switching time will be updated based on the

previous step's results. The search terminates when a solution is found such that the error in the calculation of (3.1) becomes less than a pre-determined error bound (ε). A flowchart of the steps involved in the proposed approach is shown in Fig. 3.2.

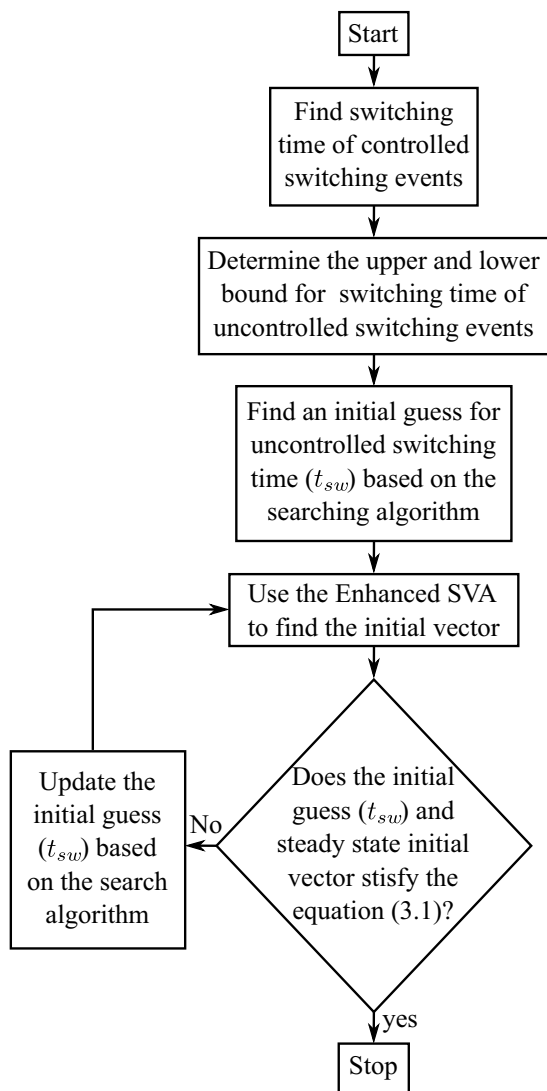


Figure 3.2: Flowchart detailing the process of using the bisection method.

Although this method is fast and can easily be implemented, it faces two main drawbacks. First of all, so far, the number of unknown switching times (t_{sw}) in the power converter circuit was one, which is not the case in all of the power convert-

ers. If the number of unknown switching times is more than one, then using the bisection approach can be complicated, and convergence is not guaranteed. In addition, the bisection approach can only be applied to the power converters with a monotonic function of t_{sw} . For instance, in the Boost converter operating in DCM mode (Fig. 3.3), the current of the diode is a monotonic function of the switching time (t_{sw}), and the acceptable switching time is when the current of the diode crosses zero as shown in the Fig. 3.4.

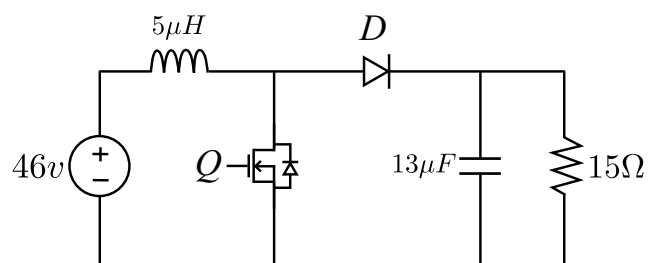


Figure 3.3: Boost converter operating in DCM (duty ration is equal to 0.14 and switching frequency is $100kHz$).

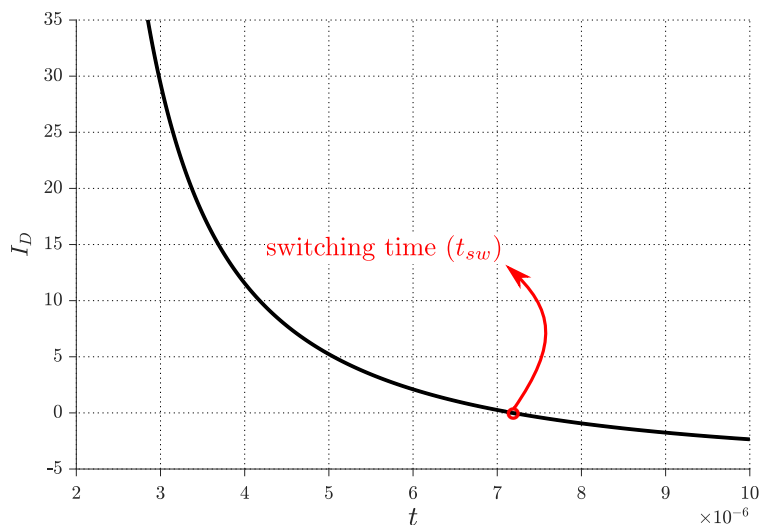


Figure 3.4: The current of the Boost converter's diode as function of switching time.

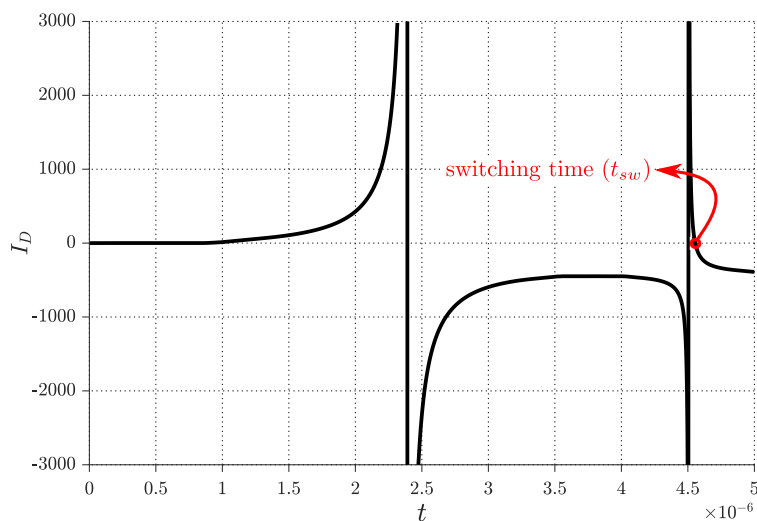


Figure 3.5: The current of the LLC's diode as function of switching time.

However, in the LLC converter of Fig. 3.12, the diode's current is a non-monotonic function of switching time (t_{sw}), which means its first derivative change sign in the range of lower and upper bounds of switching time. As can be seen from Fig. 3.5, in this converter, the diode's current based on the switching time (t_{sw}) has more than one root, but only one of these roots is the acceptable operating point of the system, which is specified using a red circle. These converters cause a problem for the bisection method in the process of finding the switching time, so there is a need for a more general approach that can be easily implemented in the Enhanced SVA approach and solve the issues mentioned above.

3.2 Switching Time Estimator Mechanism Using the General-Purpose Simulator

This section proposes a new method to address the issues that the bisection method faced in finding the switching time of uncontrolled events in the power converters.

This new approach uses a general-purpose simulator such as PSIM in combination with Enhanced SVA to find the system's steady-state initial condition. First, an initial guess for the switching times (t_{sw}) is obtained by running the General-purpose simulator for one switching period starting with the zero initial conditions, and the switching intervals are calculated using the results of the general-purpose simulator. Then, Enhanced SVA uses these switching intervals to calculate the steady-state initial conditions of the circuit associated with the reported initial guess of the switching times. Again simulation will be run using the new initial conditions, and the same procedure will be continued until the convergence to the steady-state initial conditions happens. Here, the Enhanced SVA has been implemented in the Script of PSIM software, and the PSIM engine itself is used as a general-purpose simulator, as shown in Fig. 3.6.

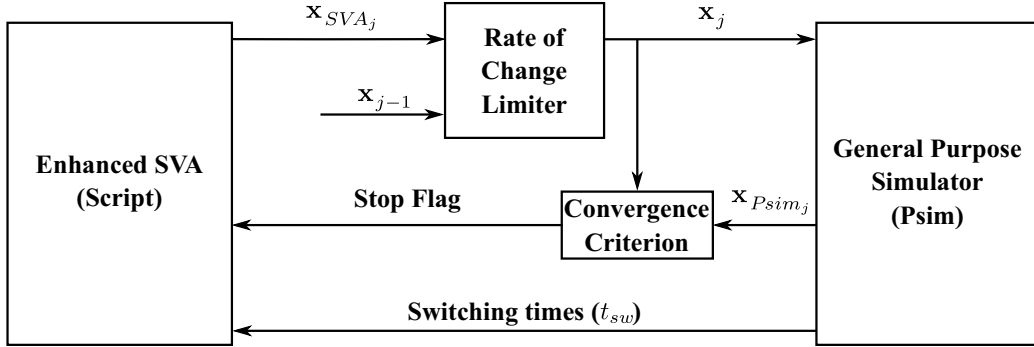


Figure 3.6: Block diagram of the Switching Time Estimator

To indicate when the convergence happens and the iteration should stop, a relative error will be defined as follows:

$$e_l = \frac{|\mathbf{x}_{Psim_j}[l] - \mathbf{x}_j[l]|}{\text{Max}\{|\mathbf{x}_j[l]|, x_{\min}\}} \quad l = 1, \dots, n \quad (3.3)$$

where \mathbf{x}_{Psim_j} is the value of the state variables at the end of the switching period in the j^{th} iteration generated by the general-purpose simulator. Moreover, x_{\min} is a

small constant used to suppress large relative errors in the state variables that are close to zero. Now the convergence criterion is based on the requirement that the maximum relative error e in the state variables should be smaller than a prescribed limit η . The maximum relative error e and the convergence criterion are defined as:

$$e = \text{Max}(e_l) \quad l = 1, \dots, n \quad (3.4)$$

$$e < \eta \quad (3.5)$$

where η is the specified error limit. Once the convergence criterion is satisfied, the general-purpose simulator can be used to generate the steady-state waveforms or to extract other features of the steady-state solution.

As shown in Fig. 3.6, the new initial condition calculated using the Enhanced SVA approach will pass a rate limiter block. This is mainly due to the start of the simulation from zero initial conditions, which can cause large variations in the state variables at the start of the simulation. This large variation can cause a convergence problem in the method, so the rate limiter, as shown in Fig. 3.7, is added to the system to solve this issue.

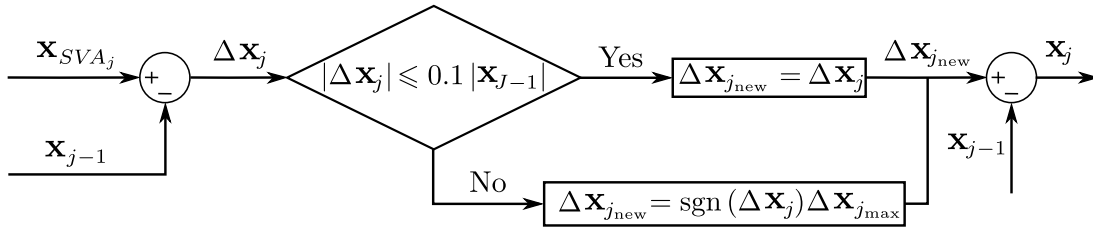


Figure 3.7: Configuration of the rate limiter block.

In the rate limiter block, first, the change in the initial state vector ($\Delta \mathbf{x}_j$) of the system is calculated by differentiating the results of the Enhanced SVA method

($\mathbf{x}_{SV A_j}$) and the initial vector of the previous iteration (\mathbf{x}_{j-1}). Then, if the change in the initial state vector is less than 10% of the initial vector of the previous iteration (\mathbf{x}_{j-1}), the change is acceptable, and this value will be used to find the new initial condition of the system (\mathbf{x}_j). Otherwise, the change in the initial state vector is limited to the maximum rate of limit ($\Delta\mathbf{x}_{j_{\max}}$), which is defined by:

$$\Delta\mathbf{x}_{j_{\max}} = 0.1 \times \text{Max} \{ |\mathbf{x}_{j-1}|, |\mathbf{x}_{SV A_j} - \mathbf{x}_{j-1}| \} \quad (3.6)$$

This approach does not have the issues that the bisection method was facing in finding the switching times and can be used for different types of converters. In addition, using a general-purpose simulator such as PSIM for finding the switching intervals results in an accurate calculation of the switching times of uncontrolled events. In the next section, several examples show the accuracy and speed of the proposed method.

3.3 Simulation Results

Several examples are discussed in this section to show the proposed methods' capability in finding the power converters' steady-state initial conditions with uncontrolled switching events. The STE method and bisection approach are applied to each circuit to calculate the steady-state initial conditions, and then the results are compared. Moreover, to show the advantages of the proposed methods, results are compared to the PLECS steady-state analysis tool, which uses the Newton Raphson with Broyden's update method. Finally, after finding the steady-state initial conditions of the power circuit using the STE method, the general-purpose simulator will run for one more switching period to generate the steady-state waveforms. These results are then compared to the steady-state waveforms generated by the PSIM software to show the

accuracy of this method.

3.3.1 Buck Converter Operating in DCM

In the first example, a simple buck converter operating in DCM will be studied, as shown in Fig. 3.8. The circuit's parameters are chosen as shown in Table 3.1.

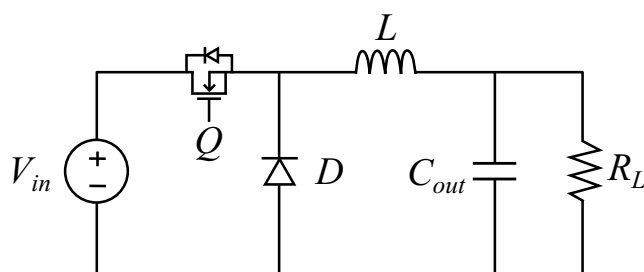


Figure 3.8: Circuit configuration of the Buck converter operating in DCM.

Table 3.1: System parameters of the Buck converter.

	Parameter	Value
Input voltage	V_{in}	24v
Filter inductance	L	20 μ H
Output capacitance	C_{out}	22 μ F
Load resistance	R_L	20 Ω
Switching frequency	f_s	100kHz
Duty cycle	D	0.6

The number of iterations required to find the steady-state initial vector of this converter using bisection, STE method, and PLECS are shown in Table 3.2. These

results indicate that all of the approaches can converge to the steady-state initial conditions of the system. The PLECS has a better performance than the other methods in this example, which is mainly due to the usage of the Newton Raphson in the steady-state analysis tool. Although using Newton Raphson increases the speed of PLECS in finding the steady-state characteristic of the simple topologies, it causes a convergence problem in complicated systems such as the LLC and series resonant converter.

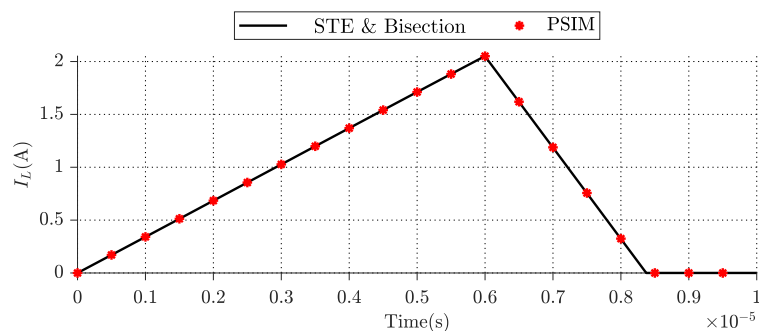
Table 3.2: The number of iterations required to converge to a steady-state in the circuit of Fig. 3.8.

Method	Iteration
PLECS (NR)	10
Bisection method	19
STE method	33

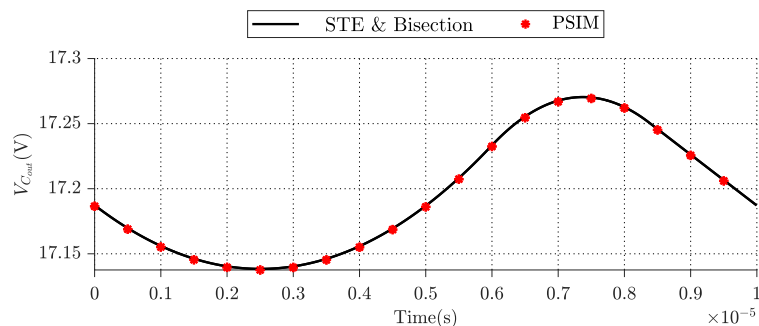
The STE and Bisection methods calculate the initial vector of the converter as follows:

$$\begin{bmatrix} I_L(0) \\ V_{C_{out}}(0) \end{bmatrix} = \begin{bmatrix} -0.000107718 \\ 17.1865 \end{bmatrix} \quad (3.7)$$

After finding this initial vector, the general-purpose simulator can draw the steady-state waveforms of the converter. To show the accuracy of the STE and Bisection methods, these results are then compared to the PSIM generated waveforms in Fig. 3.9.



(a)



(b)

Figure 3.9: Steady-state waveforms of the Buck converter operating in the DCM: (a) Inductor's current, (b) Output voltage.

3.3.2 Series Resonant Converter (SRC)

To show the speed and accuracy of the STE method over the bisection and PLECS software, a Series resonant converter is studied here. The simulation of this circuit using existing software can be time-consuming due to its complicated behavior. In addition, steady-state solvers typically face a problem in calculating this circuit's steady-state characteristics, making it a good benchmark for the proposed method. The overall circuit of the SRC is illustrated in Fig. 3.10.

The parameters of this series resonant converter are listed in Table 3.3, and the steady-state initial condition of this converter, using the STE and Bisection methods,

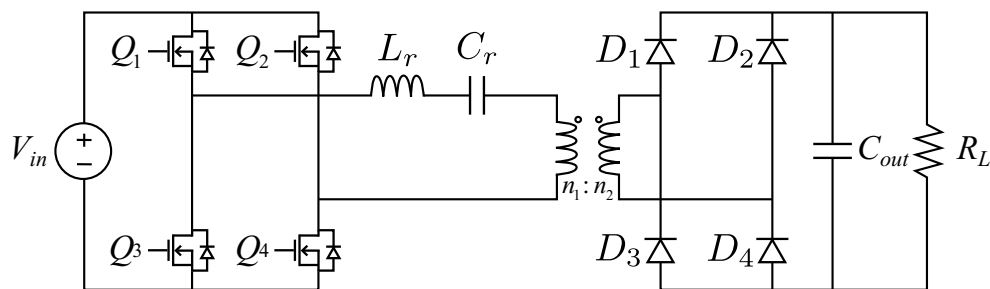


Figure 3.10: Schematic diagram of the Series resonant converter

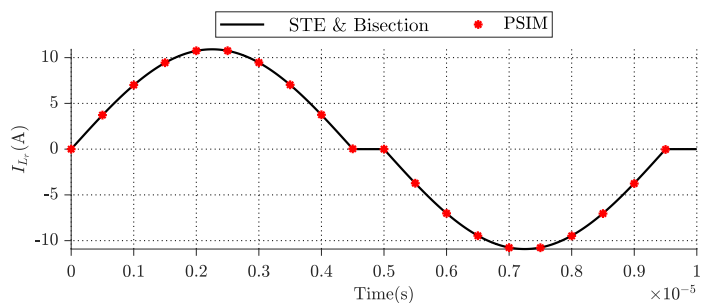
is calculated as follows:

$$\begin{bmatrix} I_{L_r}(0) \\ V_{C_r}(0) \\ V_{C_{out}}(0) \end{bmatrix} = \begin{bmatrix} -8.3412e-06 \\ -16.6293 \\ 99.9498 \end{bmatrix} \quad (3.8)$$

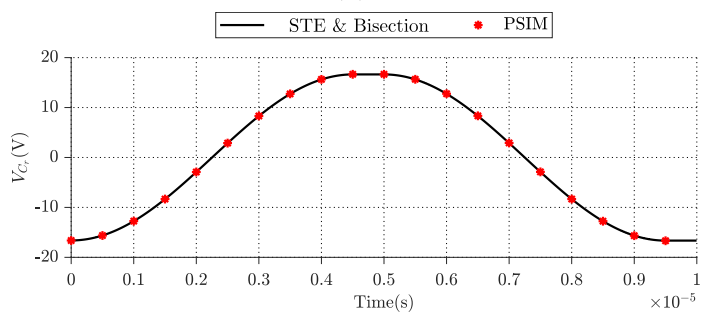
Table 3.3: System parameters of the SRC.

	Parameter	Value
Input voltage	V_{in}	100v
Inductance of resonant tank	L_r	2.2 μ H
Capacitance of resonant tank	C_r	0.94 μ F
Transformer turn ratio	$n_1 : n_2$	1
Output capacitance	C_{out}	200 μ F
Load resistance	R_L	16 Ω
Switching frequency	f_s	100kHz

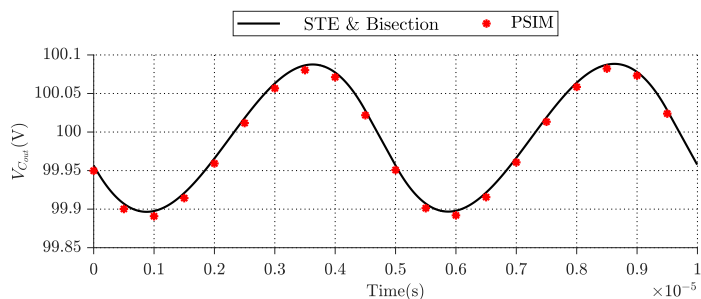
The number of iterations required to find the steady-state characteristics of the circuits using different methods is reported in Table 3.4. Based on these results, the STE method is faster than other methods in finding the steady-state initial condition. In addition, the PLECS steady-state analysis tool cannot converge to the converter's steady-state solution because it uses the Newton Raphson in its calculation, which



(a)



(b)



(c)

Figure 3.11: Steady-state waveforms of the SRC: (a) The current of the resonant tank's inductor, (b) Voltage of the resonant tank's capacitor, (c) Output Voltage.

has well-documented issues with convergence in complex circuits. Finally, the proposed STE and Bisection methods can draw the steady-state waveforms by running the general-purpose simulator for one switching period starting with the steady-state initial conditions. To show the accuracy of the proposed methods, the waveforms are compared with the results generated by PSIM software, as shown in Fig. 3.11.

Table 3.4: The number of iterations required for different steady-state solvers to find the initial vector of the SRC.

Method	Iteration
PLECS (NR)	–
Bisection method	21
STE method	17

3.3.3 LLC Converter

In this section, the LLC converter is studied to show the advantages of the STE method and how the other methods fail to find the steady-state initial conditions of the circuit. Fig. 3.12 illustrates the overall circuit configuration of this power converter, and the system parameters are listed in Table 3.5.

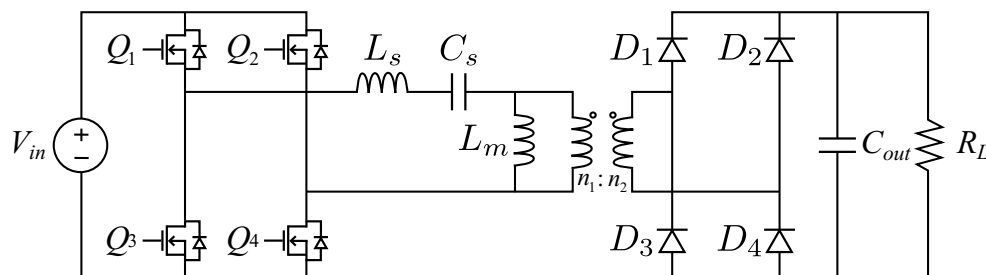


Figure 3.12: Schematic diagram of the LLC converter

The proposed STE method calculates the initial conditions of the circuit as follows:

$$\begin{bmatrix} I_{L_s}(0) \\ I_{L_m}(0) \\ V_{C_s}(0) \\ V_{C_{out}}(0) \end{bmatrix} = \begin{bmatrix} -2.02548 \\ -16.7723 \\ -2.02547 \\ 100.479 \end{bmatrix} \quad (3.9)$$

Table 3.5: System parameters of the LLC converter.

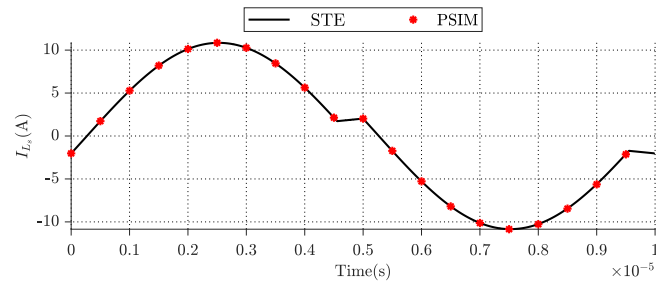
	Parameter	Value
Input voltage	V_{in}	100v
Series inductance	L_s	2.2 μ H
Series capacitance	C_s	0.94 μ F
Magnetizing inductance	L_m	122 μ H
Output capacitance	C_{out}	200 μ F
Load resistance	R_L	16 Ω
Switching frequency	f_s	100kHz

After finding these initial conditions of the LLC converter, the steady-state waveforms of the circuit are plotted using the general-purpose simulator. The drawn waveforms are compared with the PSIM generated results in Fig. 3.13 to show the accuracy of this approach.

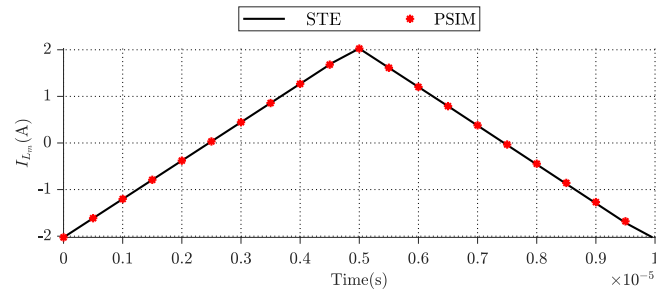
Table 3.6: The number of iterations required to find the steady-state initial conditions of the LLC converter.

Method	Iteration
PLECS (NR)	–
Bisection method	–
STE method	97

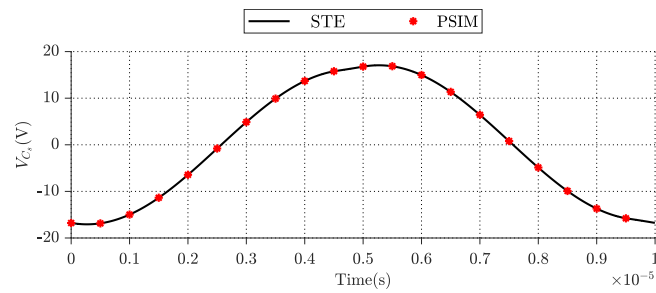
The number of iterations required for different methods is shown in Table 3.6. As can be seen, only the STE method can find the steady-state initial conditions of the system. The steady-state analysis tool of PLECS cannot find the initial vector due to the usage of the Newton Raphson, which has the convergence problem in circuits with complicated topology. Moreover, as mentioned before, the bisection method cannot be used for the LLC converter because the diode's current is a non-monotonic function of the switching time, as shown in Fig. 3.5.



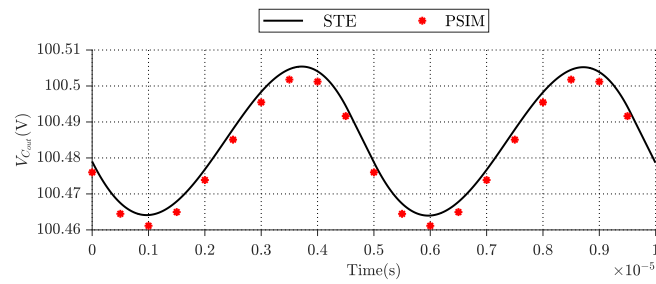
(a)



(b)



(c)



(d)

Figure 3.13: Waveforms of the LLC converter during the steady-state operation: (a) Current of the series inductance, (b) Current of the magnetizing inductance, (b) Voltage of the series capacitance, (c) Output voltage.

3.4 Summary

In this chapter, two methods were proposed to find the switching time (t_{sw}) of uncontrolled events in power converters. The first method is bisection which is a computationally efficient and accurate approach, but it is limited to the converters with the monotonic function of the switching time, which causes a problem in circuits with complex behavior such as LLC converter. The proposed STE method solves this issue by using a general-purpose simulator for finding the switching intervals. This approach has the advantage of good accuracy in calculating the switching time because of using the general-purpose simulator. Finally, several examples are provided to compare the computational speed of the proposed STE method with other methods. Moreover, to show the accuracy of this method, after finding the steady-state initial conditions, the general-purpose simulator is used to draw the steady-state waveforms, which are then compared to the PSIM generated waveforms.

Chapter 4

Steady-State of Closed Loop, DC–AC, and AC–DC Converters

In previous chapters, new approaches have been proposed to find the steady-state initial conditions of the power converters with controlled and uncontrolled switching events. These steady-state initial conditions can then be used to generate the steady-state waveforms of the circuit, which are necessary for the analysis and design of power converters. Although the methods proposed in the previous chapters have good speed and accuracy, only the converters operating in an open loop mood were studied using these methods. In addition, all of the methods proposed in the previous chapters were applied to DC-DC converters, and no DC–AC or AC–DC converter has been studied.

This chapter first, it will be explained how to find the steady-state initial condition of the DC–AC and AC–DC Converters using the Enhanced SVA. The approach is implemented in the script of PSIM, which is used to generate the steady-state waveforms of the converters. In the second part of the chapter, the closed loop system is studied. To apply the Enhanced SVA to closed loop systems, a STE method

proposed in the previous chapter is modified to update the states of the controller in each iteration. Finally, the performance of the proposed methods is further investigated by providing several examples.

4.1 Application of Enhanced SVA to DC-AC and AC-DC Converters

The proposed Enhanced SVA in the previous chapters can find the steady-state initial conditions of the power converters with good speed and accuracy, but it was only applied to DC-DC converters. This subsection expands this method to DC-AC and AC-DC Converters.

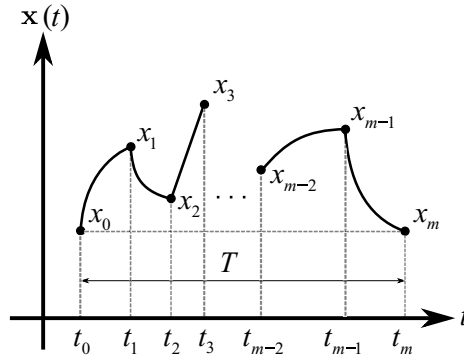


Figure 4.1: Illustration of a first order switching power converter with m switching intervals operating in steady-state.

As described in section 2.5, the Enhanced SVA calculates power converter system's steady-state initial conditions by finding the states' value at the end of the switching period (\mathbf{x}_m) based on the system's initial condition (\mathbf{x}_0). Then, by assuming that the system is operating in a steady-state, it finds the initial conditions by equating the \mathbf{x}_m and \mathbf{x}_0 (Fig. 4.1). The formulation of the method is repeated here for convenience:

$$\mathbf{x}_m = \Phi_m \Phi_{m-1} \cdots \Phi_1 \mathbf{x}_0 + \Phi_m \Phi_{m-1} \cdots \Phi_2 \Gamma_1 + \cdots + \Phi_m \Gamma_{m-1} + \Gamma_m \quad (4.1)$$

$$\mathbf{x}_0 = [I - \Phi_m \Phi_{m-1} \cdots \Phi_1]^{-1} [\Phi_m \Phi_{m-1} \cdots \Phi_2 \Gamma_1 + \cdots + \Phi_m \Gamma_{m-1} + \Gamma_m] \quad (4.2)$$

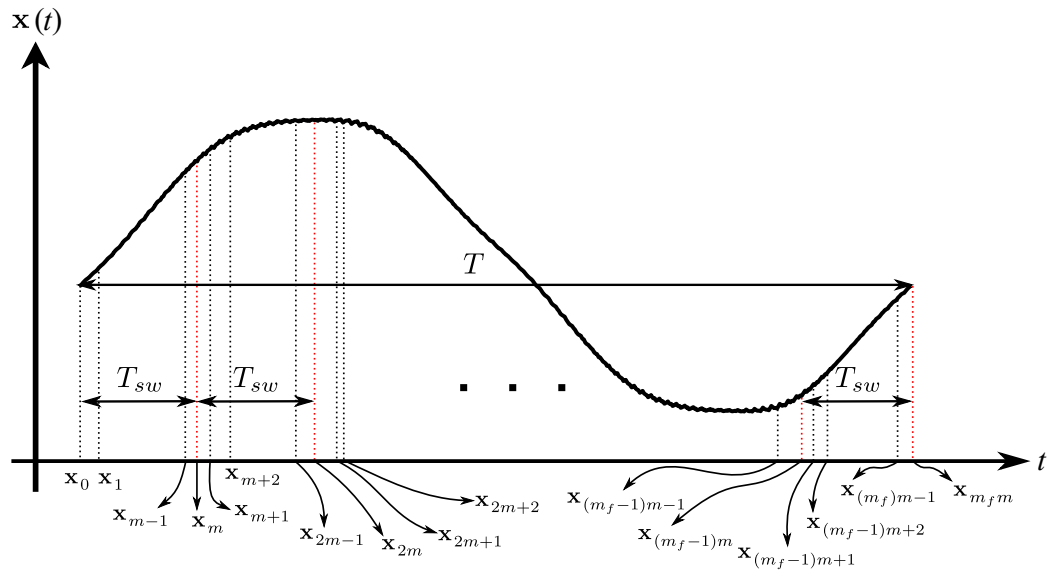


Figure 4.2: Illustration of a first-order power converter operating in steady-state with m switching interval in each switching period, and the frequency modulation ratio equals m_f .

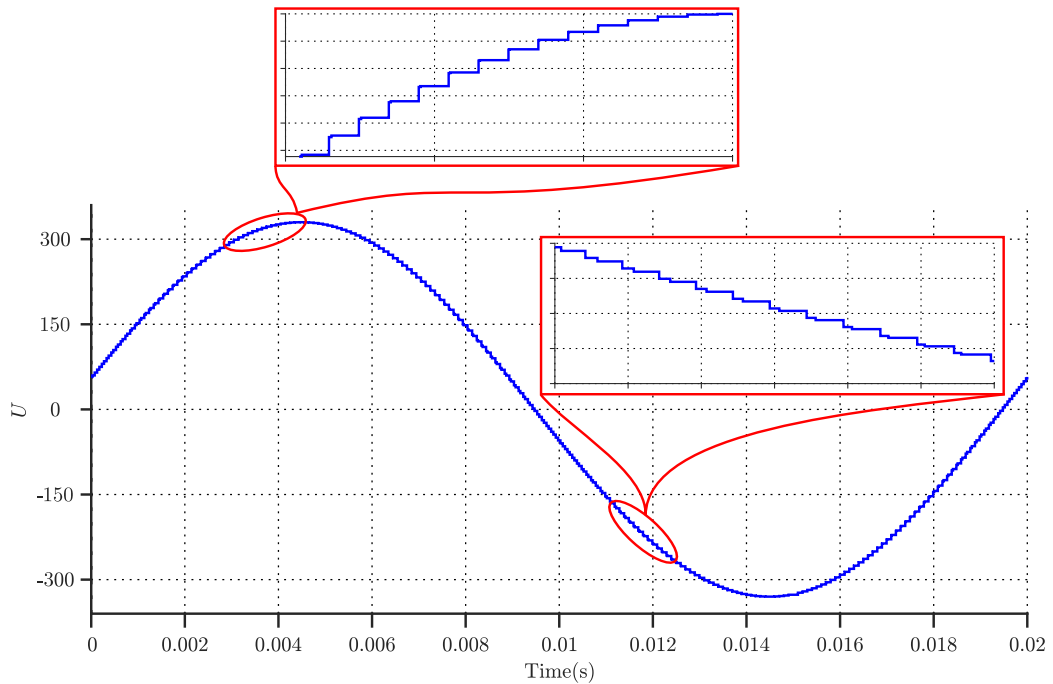


Figure 4.3: Piecewise constant approximation of an AC source.

This method can be used when the period of the states' waveform is equal to the switching period, which usually happens in the DC-DC converters. However, when the converter is connected to AC sources or outputs AC signal, the steady-state waveforms are periodic, with a period equal to a more slowly varying signal. For instance, Fig. 4.2 shows the power converter that its steady-state waveforms are periodic with a period higher than the switching period. Suppose the Enhanced SVA is applied to the first switching period of this system. In that case, the calculated steady-state initial conditions are wrong because the assumption of the equality of \mathbf{x}_m and \mathbf{x}_0 is not correct anymore. To solve this issue, the period should be considered as the largest existing period in the circuit, which is T in this example. Generally, if the circuit consists of m switching intervals in each switching period (T_{sw}), and the frequency modulation ratio is equal to m_f , the steady-state initial conditions of the system using the Enhanced SVA can be calculated as follows:

$$\begin{aligned} \mathbf{x}_0 = & [I - \Phi_{m_fm} \Phi_{m_fm-1} \times \cdots \times \Phi_{(m_f-1)m+1} \Phi_{(m_f-1)m} \Phi_{(m_f-1)m-1} \times \cdots \\ & \times \Phi_2 \Phi_1]^{-1} [\Phi_{m_fm} \Phi_{m_fm-1} \times \cdots \times \Phi_{(m_f-1)m+1} \Phi_{(m_f-1)m} \Phi_{(m_f-1)m-1} \\ & \times \cdots \times \Phi_2 \Gamma_1 + \cdots + \Phi_{m_fm} \Gamma_{m_fm-1} + \Gamma_{m_fm}] \end{aligned} \quad (4.3)$$

where

$$\Phi_i = [I + A_i \lambda_i] \quad (4.4)$$

$$\Gamma_i = \lambda_i B_i U \quad (4.5)$$

$$\lambda_i = \sum_{n=1}^k \frac{A_i^{n-1} (t_i - t_{i-1})^n}{n!} \quad (4.6)$$

In the calculation of Γ_i using (4.5), the input vector (\mathbf{u}) was considered to only have DC sources, such as the full bridge inverter connected to load. However, this is not the case in converters with AC sources such as grid-connected inverters. To solve this problem, the value of the AC sources can be considered as a constant input source during each switching interval where its value is equal to the value of

AC sources in the middle of the switching interval. For instance, Fig. 4.3 shows the piecewise constant approximation of the AC sources used in the Enhanced SVA. In this signal, the intervals are not equal because each interval's duration depends on the circuit's switching time.

4.2 Simulation Results of DC-AC and AC-DC Converters

In this section, two examples are provided to show the increase in the speed of convergence towards the steady-state solution of the AC-DC and DC-AC power converter using the Enhanced SVA method. Each example is also studied by the steady-state analysis tool of the PLECS software, and the results are compared to the proposed approach for showing the method's speed. Furthermore, to show the accuracy of the proposed method, after finding the initial conditions, the waveforms of the system will be drawn using the general-purpose simulator, and the results will be compared to the generated steady-state waveforms of the PSIM software.

4.2.1 Full Bridge Inverter Connected to the Load

As an example of a DC-AC converter, the full bridge inverter connected to the load is studied. The system configuration is shown in Fig. 4.4, and the parameters of this circuit are listed in Table 4.1.

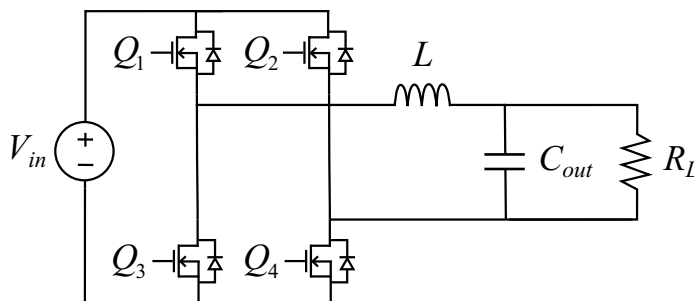


Figure 4.4: Circuit configuration of full bridge inverter connected to the load.

Table 4.1: System parameters of the full bridge inverter.

	Parameter	Value
Input voltage	V_{in}	110v
Inductance	L	0.3mH
Output capacitance	C_{out}	1mF
Load resistance	R_L	16k Ω
Switching frequency	f_s	10kHz
Frequency of modulation signal	f_m	50Hz

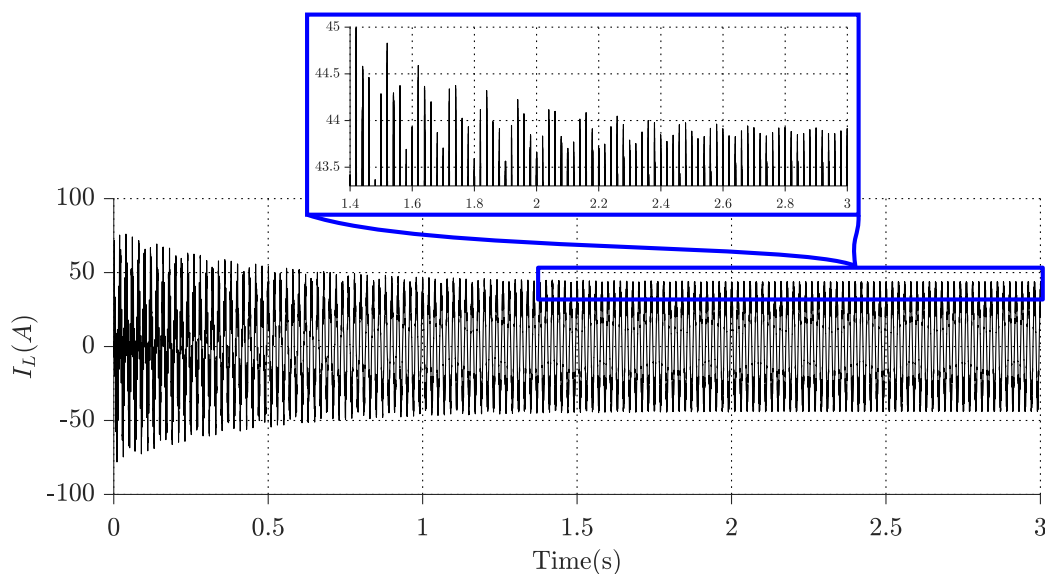


Figure 4.5: Inductor's current waveform of the full bridge inverter generated by the PSIM software.

The simulation of this type of converter can be time-consuming using the existing method since the switching time should be chosen small compared to the output signal period. Fig. 4.5 shows the transient of the inductor's current that the PSIM software calculated before finding the steady-state. The PSIM needs to simulate more than

100 grid cycles before reaching the steady-state, which is time-consuming. However, the proposed approach can find the steady-state initial conditions in one iteration, and the results are as follows:

$$\begin{bmatrix} I_L(0) \\ V_{C_{out}}(0) \end{bmatrix} = \begin{bmatrix} 35.6001 \\ -0.1154 \end{bmatrix} \quad (4.7)$$

After finding the initial conditions of the power converter, steady-state waveforms are drawn by simulating the circuit for one period using the general-purpose simulator. The comparison of the results with the PSIM generated waveforms is shown in Fig. 4.6 to show the method's accuracy.

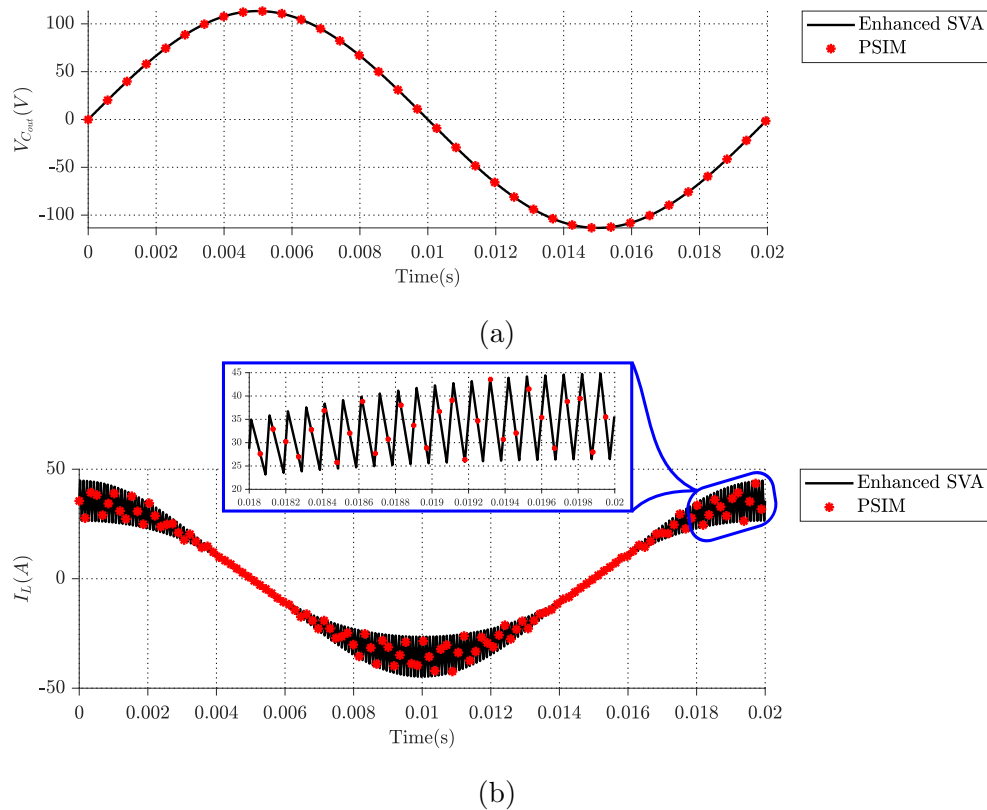


Figure 4.6: Waveforms of the full bridge inverter during the steady-state operation: (a) Output voltage, (b) Inductor current.

Finally, the PLECS's steady-state analysis tool is used to find the initial vector of this power converter. Table. 4.2 compares the results of finding a steady-state solution using the PLECS software and Enhanced SVA method. Using the Enhanced SVA, the number of simulation runs is reduced to one compared to the PLECS software, which needs eleven iterations.

Table 4.2: The number of iterations required for different steady-state solvers to find the initial vector of the full bridge inverter.

Method	Iteration
PLECS (NR)	11
Enhanced SVA	1

4.2.2 Grid Connected Inverter

Fig. 4.7 shows a full bridge inverter connected to the grid. This example shows the application of the Enhanced SVA in circuits with AC sources. The parameters of this circuit are listed in Table 4.3.

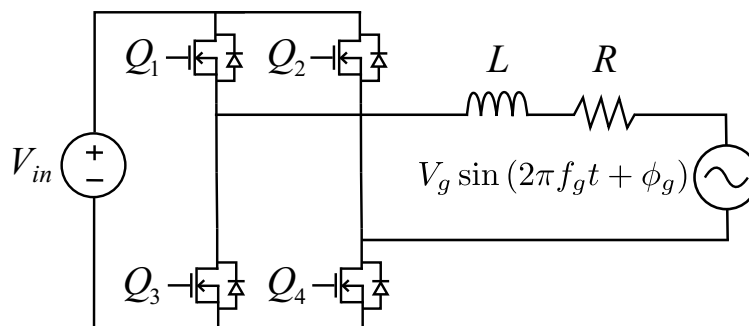


Figure 4.7: Schematic diagram of the grid connected inverter.

To show the method's accuracy, calculated initial conditions by the proposed method are used to generate the steady-state waveform, and the comparison with

PSIM generated waveform is shown in Fig. 4.8. Although the piecewise constant approximation is used in the calculation of the initial conditions using the Enhanced SVA, the result perfectly matches the PSIM generated waveform.

Table 4.3: System parameters of the grid connected inverter.

	Parameter	Value
Input voltage	V_{in}	400v
Inductance	L	2mH
Resistance	R	4 Ω
Frequency of AC source	f_g	50Hz
Amplitude of AC source	V_g	320v
Phase of AC source	ϕ_g	$\pi/18$
Switching frequency	f_s	10kHz
Amplitude modulation ratio	m_a	0.8

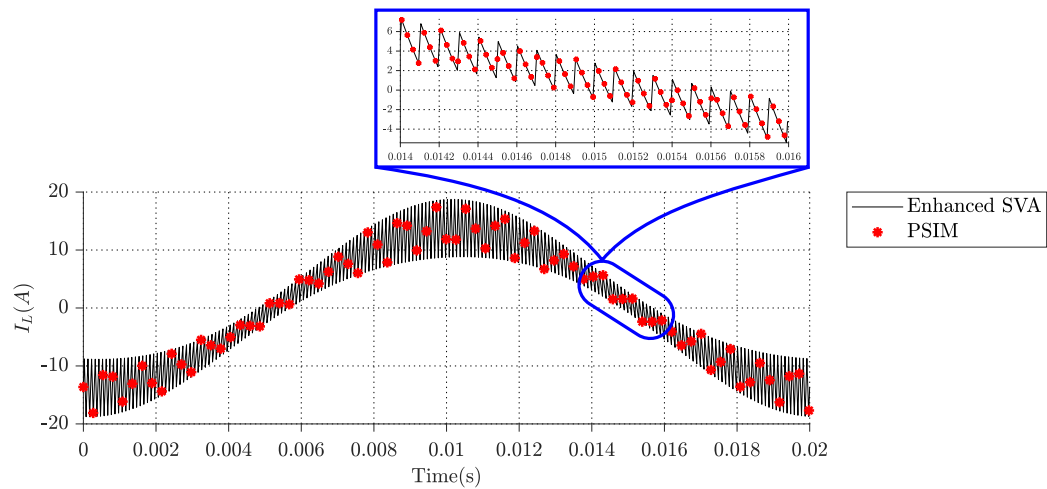


Figure 4.8: Inductor's current during the steady-state operation in the grid connected inverter.

Table. 4.4 shows the performance of the PLECS software and Enhanced SVA. Enhanced SVA can find the initial conditions in one iteration; however, the PLECS uses Newton Raphson methods, so it needs sixteen iterations to converge to the steady-state initial conditions.

Table 4.4: The number of iterations required to find the steady-state initial conditions of the grid connected inverter.

Method	Iteration
PLECS (NR)	16
Enhanced SVA	1

4.3 Study of Closed Loop Converters Using Enhanced SVA

To find the steady-state waveform of the power converters operating with the controller, it is necessary to find the steady-state initial conditions of the controller as well as the power converter. For instance, Fig. 4.9 shows the buck converter with the PI controller, and the output of the integrator is an additional state of the system. So the proper method must be able to find the steady-state value of this state at the start of the period as well as the steady-state initial conditions of the power circuit.

The control system and power circuit can be modeled using the state space representation as follows:

$$\begin{bmatrix} \dot{\mathbf{x}} \\ \dot{\mathbf{x}}_c \end{bmatrix} = A_s \begin{bmatrix} \mathbf{x} \\ \mathbf{x}_c \end{bmatrix} + B_s \mathbf{u} \quad (4.8)$$

where \mathbf{x}_c is the states of the controller, and \mathbf{x} is the states of the power circuit. Then the Enhanced SVA can use the system matrices (A_s and B_s) in its formulation (2.54)

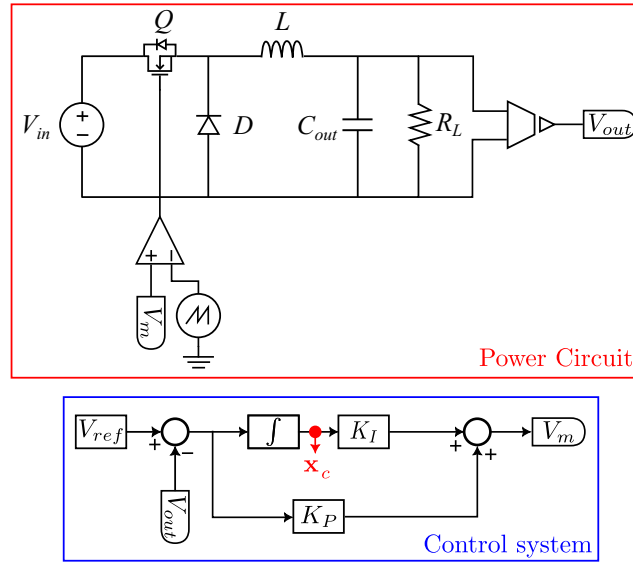


Figure 4.9: Circuit configuration of closed loop Buck converter.

to find the steady-state initial conditions of the controller and the power circuit. However, most systems with the controller cannot be modeled in the form of (4.8), and even if they can, the computer generation of the state space of the whole system can be challenging as there might be some nonlinear blocks in the loop. The STE mechanism proposed in the previous chapter is modified to address these issues and calculate the initial vector of the closed loop systems.

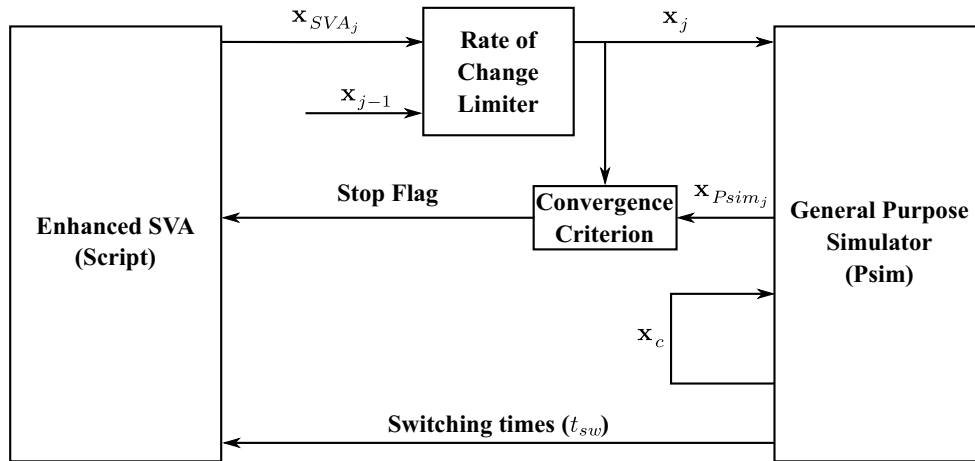


Figure 4.10: Block diagram of the modified STE method.

In this approach, first, the general-purpose simulator simulates the whole system for one period and returns the switching times (t_{sw}) and the states of the converter at the end of the period to the Enhanced SVA. The Enhanced SVA then uses this information to find the steady-state initial condition of the power circuit. Then the states of the power circuit will be updated, while the states of the control system will remain the same, and the system again will be simulated using the general purpose-simulator. The same procedure will be continued until the convergence to the steady-state initial conditions happens. In addition, this method uses the rate limiter block as shown in Fig. 4.10, which performs the same task as what is discussed and demonstrated in Fig. 3.7.

To indicate when the convergence happens, and the iteration should stop, the relative error will be defined as follows:

$$e_l = \frac{|\mathbf{x}_{Psim_j}[l] - \mathbf{x}_j[l]|}{\text{Max}\{|\mathbf{x}_j[l]|, x_{\min}\}} \quad l = 1, \dots, n \quad (4.9)$$

In addition, the convergence criterion is based on the requirement that the maximum relative error e in the state variables should be smaller than a predetermined limit η .

$$e = \text{Max}(e_l) \quad l = 1, \dots, n \quad (4.10)$$

$$e < \eta \quad (4.11)$$

where η is the specified error limit. Once this condition is met, the iteration should stop, and the steady-state initial conditions are found. Finally, the general-purpose simulator can simulate the circuit for one period starting from the calculated initial vector to draw the steady-state waveforms of the system.

4.4 Simulation of Closed Loop Phase-Shifted Full Bridge Converter

As an example of the closed loop power electronic system, Phase-Shifted full bridge converter with a PI controller is studied here to show the accuracy of the proposed approach in calculating the steady-state initial conditions of the closed loop power converter system. The schematic of this regulated converter is shown in Fig. 4.11. The parameters associated with this converter's power stage and controller are listed in Table. 4.5.

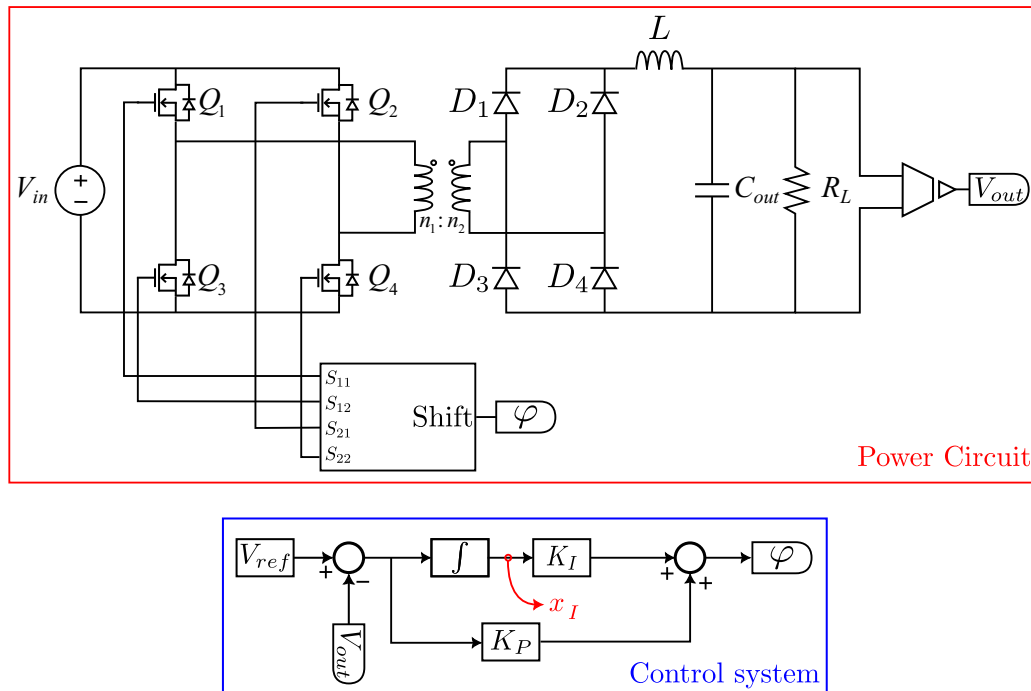


Figure 4.11: Circuit configuration of the phase-shifted full bridge converter with PI controller

This power converter topology is studied here because, in addition to the PI controller, it has uncontrolled switching events caused by the diode bridge. So it is a good benchmark to show the application of the modified STE method in finding the

steady-state initial condition of the closed loop power converter with uncontrolled events. In this circuit, in addition to the states of the power circuit, it is required to find the state of the controller, which is the output of the integral block (x_I). The steady-state initial conditions of the circuit can be calculated using the proposed method as follows:

$$\begin{bmatrix} I_L(0) \\ V_{C_{out}}(0) \\ x_I(0) \end{bmatrix} = \begin{bmatrix} 6.49530e - 06 \\ 13.8639 \\ 0.00373791 \end{bmatrix} \quad (4.12)$$

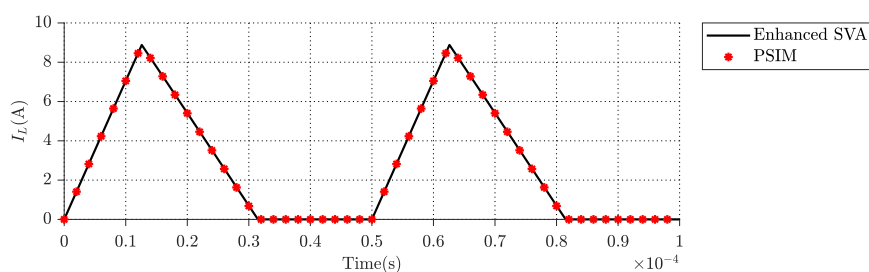
Table 4.5: System parameters of the Phase-shifted full bridge converter

	Parameter	Value
Input voltage	V_{in}	35v
Inductance	L	30 μ H
Output capacitance	C_{out}	200 μ F
Resistance	R	5 Ω
Transformer turn ratio	$n_1 : n_2$	1
Reference voltage	V_{ref}	14
Proportional gain	K_P	.01
Integral gain	K_I	100/3
Switching frequency	f_s	10kHz

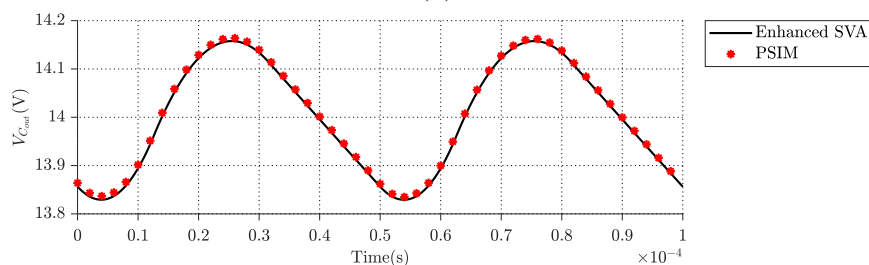
Using the calculated initial conditions the general-purpose simulator can simulate the circuit for one period to draw the steady-state waveforms. Fig. 4.12 compares the results of the proposed method with the PSIM generated waveform. In addition, since this closed loop circuit contains uncontrolled switches and operates in discontinuous conduction mode, the Newton Raphson based methods, such as PLECS's steady-state analysis tool, cannot find the steady-state solution, as shown in Table. 4.6.

Table 4.6: The number of iterations required to converge to a steady-state in the Phase-shifted full bridge converter with PI controller.

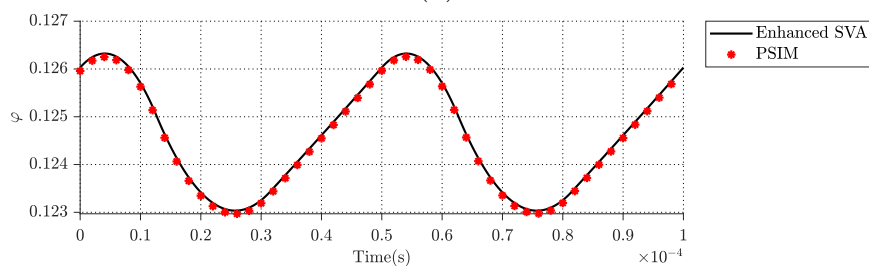
Method	Iteration
PLECS (NR)	—
Enhanced SVA	129



(a)



(b)



(c)

Figure 4.12: Steady-state waveforms of the Phase-shifted full bridge converter: (a) Inductor's current, (b) Output voltage, (c) Output of the controller (phase shift).

4.5 Summary

In this chapter, first, the estimation of steady-state initial conditions of the DC-AC and AC-DC converters using Enhanced SVA is discussed. For this purpose, it is shown that the period in which Enhanced SVA will be used should be considered as the largest existing period in the circuit, and if the circuit contains an AC source, the piecewise constant approximation of the source should be used in the calculation of the Γ_i . In the second part, the estimation of steady state initial conditions for closed loop power converters is provided by modifying the STE mechanism proposed in the previous chapter. In addition, several examples are provided to verify the effectiveness, speed, and accuracy of the methods. Moreover, in each example, the comparison between the proposed method and the steady-state analysis tool of the PLECS is provided, and the steady-state generated waveforms are compared to the PSIM generated waveforms.

Chapter 5

Summary and Future Work

5.1 Summary of Contributions

In this thesis, new approaches were proposed to calculate the steady-state initial conditions of the power converter systems. The main contributions and conclusions of this thesis are summarized below.

- (i) Improved Laplace Based Method (ILBT) is proposed to solve the problem of analyzing the interior switch-network converter using the LBT. In addition, the speed of initial vector calculation is increased using the state space model of the system in the ILBT formulation instead of the ODE representation, which was used in the LBT.
- (ii) Enhanced SVA is proposed, which uses the Taylor series and adaptive order selection to solve the problem of the singular characteristic matrix in conventional SVA and increase the method's speed. In addition, several simulation examples show that the Enhanced SVA is the fastest approach to analyze the

power converters compared to the other existing methods. Moreover, it does have the limitation of the existing methods, and can be used to analyse the wide range of converters.

- (iii) The bisection and STE method were proposed to calculate the initial vector of the converters with uncontrolled switching events, such as the converters operating in discontinuous conduction mode. The bisection approach was only able to analyze the converter with the monotonic function of the switching time. However, the STE method used the general-purpose simulator to find the uncontrolled event's switching time, so it did not face the limitation of the bisection method.
- (iv) The steady state initial conditions of the AC-DC and DC-AC converters are calculated by applying the Enhanced SVA to the largest existing period in the circuit and using the piecewise constant approximation of the AC sources in the calculation process.
- (v) The steady-state initial conditions of the closed loop power converters are calculated by modifying the STE method to update the states of the controller at each iteration.
- (vi) Steady-state waveforms are drawn using the proposed approaches for several examples, and a comparison with the PSIM generated steady-state waveforms are provided to show the accuracy of the methods.

5.2 Suggested Future Work

There are a number of directions that this research can be taken to; some of the most promising ones are suggested as follows:

- (i) This thesis presented a new mathematical method for finding the steady-state initial condition. In the next stage of the research, this approach can be used for the accurate analysis of complicated power converter topology to useful information, such as a plot of voltage gain or range of the ZVS, for designing the power converter.
- (ii) The proposed methods in this thesis considered all elements linear except the switches. As the next step, the application of the proposed methods to the converters with the nonlinear component can be investigated.
- (iii) The proposed method in chapter 4 for calculating the steady-state initial condition of the closed loop converters was only used to study the circuit with a simple controller. As the proposed method is general and could be used for more complicated control systems, the proposed method could be used to study the converter with a more complicated control structure in the next stage of the research.

Bibliography

- [1] J. Sun and H. Grotstollen, "Symbolic analysis methods for averaged modeling of switching power converters," *IEEE Trans. Power Electron.*, vol. 12, no. 3, pp. 537–546, May 1997.
- [2] R. Webster and K. D. T. Ngo, "Computer-based symbolic circuit analysis and simulation," in *Proc. IEEE Appl. Power Electron. Conf. Expo.*, Boston, MA, USA, Feb. 1992, pp. 772–779.
- [3] G. W. Wester and R. D. Middlebrook, "LowFrequency Characterization of Switched dc-dc Converters," *IEEE Transaction on Aerospace and Electronic Systems*, Vol. AES-9, No. 3, May 1973, pp. 376-385.
- [4] R. C. Wong, G. E. Rodriguez, H. A. Owen, Jr., and T. G. Wilson, "Application of Small-Signal Modeling and Measurement Techniques to the Stability Analysis of an Integrated SwitchingMode Power System," *IEEE Power Electronics Specialists Conference Record*, IEEE Publication No. 80CH1529-7, June 1980, pp. 104-118.
- [5] F. C. Lee and R. A. Carter, "Investigation of Stability and Dynamic Performances of Switching Regulators Employing Current-Injected Control," *IEEE Power Electronics Specialists Conference Record*, IEEE Publication No. 81CH1652-7, June 1981, pp. 3-16.

- [6] A. R. Brown and R. D. Middlebrook, "SampledData Modeling of Switching Regulators," IEEE Power Electronics Specialists Conference Record, IEEE Publication No. 81CH1652-7, June 1981, pp. 349-369.
- [7] C.-T. Chen, Linear system theory and design, 3rd ed. Oxford University Press, 1999.
- [8] N. Mohan, W. P. Robbins, T. M. Undeland, R. Nilssen, and O. Mo, "Simulation of power electronic and motion control systems-an overview," Proc. IEEE, vol. 82, no. 8, pp. 1287-1302, Aug. 1994.
- [9] D. Maksimovic, A. M. Stankovic, V. J. Thottuvelil, and G. C. Verghese, "Modeling and simulation of power electronic converters," Proc. IEEE, vol. 89, no. 6, pp. 898-912, Jun. 2001.
- [10] R. D. Middlebrook and S. Cuk, "A general unified approach to modelling switching-converter power stages," in 1976 IEEE Power Electronics Specialists Conference, Jun. 1976, pp. 18-34. doi: 10.1109/PESC.1976.7072895.
- [11] C. K. Tse and M. Di Bernardo, "Complex behavior in switching power converters," Proceedings of the IEEE, vol. 90, no. 5, pp. 768-781, May 2002, doi: 10.1109/JPROC.2002.1015006.
- [12] A. Davoudi, J. Jatskevich, and T. D. Rybel, "Numerical state-space average-value modeling of PWM DC-DC converters operating in DCM and CCM," IEEE Transactions on Power Electronics, vol. 21, no. 4, pp. 1003-1012, Jul. 2006, doi: 10.1109/TPEL.2006.876848.
- [13] R. J. King and T. A. Stuart, "Small-Signal Model for the Series Resonant Converter," IEEE Transactions on Aerospace and Electronic Systems, vol. AES-21, no. 3, pp. 301-319, May 1985, doi: 10.1109/TAES.1985.310560.

- [14] MathWorks Inc., Simulink user's guide R2020a, 2020. [Online]. Available: https://www.mathworks.com/help/pdf_doc/simulink
- [15] Plexim GmbH., PLECS User Manual, Version 4.3.6, 2020. [Online]. Available: <https://www.plexim.com/download/documentation>
- [16] C. Dufour, J. Mahseredjian, and J. Bélanger, "A combined state-space nodal method for the simulation of power system transients," *IEEE Trans. Power Del.*, vol. 26, no. 2, pp. 928–935, Apr. 2011.
- [17] Y. Zhu, Z. Zhao, B. Shi, and Z. Yu, "Discrete State Event-Driven Framework With a Flexible Adaptive Algorithm for Simulation of Power Electronic Systems," *IEEE Transactions on Power Electronics*, vol. 34, no. 12, pp. 11692–11705, Dec. 2019, doi: 10.1109/TPEL.2019.2907731.
- [18] B. Li, Z. Zhao, Y. Yang, Y. Zhu, and Z. Yu, "A novel simulation method for power electronics: discrete state event driven method," *CES Transactions on Electrical Machines and Systems*, vol. 1, no. 3, pp. 273–282, Sep. 2017, doi: 10.23919/TEMS.2017.8086106.
- [19] T. J. Aprille and T. N. Trick, "Steady-state analysis of nonlinear circuits with periodic inputs," *Proceedings of the IEEE*, vol. 60, no. 1, pp. 108–114, Jan. 1972, doi: 10.1109/PROC.1972.8563.
- [20] J. E. Dennis, R. B. Schnabel, *Numerical methods for unconstrained optimization and nonlinear equations*, SIAM Classics in applied mathematics 16, 1996.
- [21] D. L and R. Tymerski, "Comparison of simulation algorithms for accelerated determination of periodic steady state of switched networks," *IEEE Transactions on Industrial Electronics*, vol. 47, no. 6, pp. 1278–1285, Dec. 2000, doi: 10.1109/41.887956.

- [22] N. Femia, G. Spagnuolo, and M. Vitelli, “Steady-state analysis of hard and soft switching DC-to-DC regulators,” *IEEE Transactions on Power Electronics*, vol. 18, no. 1, pp. 51–64, Jan. 2003, doi: 10.1109/TPEL.2002.807086.
- [23] S. R. Naidu and D. A. Fernandes, “Technique for simulating the steady-state response of power electronic converters,” *IET Pwr. Electr.*, vol. 4, no. 3, p. 269, 2011, doi: 10.1049/iet-pel.2009.0321.
- [24] U. Ekambaram and R. A. Saleh, “An improved steady-state method applying Broyden’s technique to the shooting method [nonlinear circuits],” in *Proceedings of the 39th Midwest Symposium on Circuits and Systems*, Aug. 1996, vol. 3, pp. 1023–1026 vol.3. doi: 10.1109/MWSCAS.1996.592897.
- [25] M. Plesnik and M. Nakhla, “An efficient method for ripple analysis of networks with synchronized switching power converters,” in *2011 Twenty-Sixth Annual IEEE Applied Power Electronics Conference and Exposition (APEC)*, Mar. 2011, pp. 1111–1117. doi: 10.1109/APEC.2011.5744733.
- [26] Y. Kuroe, T. Maruhashi, N. Kanayama, “Computation of sensitivities with respect to conduction time of power semiconductors and quick determination of steady state for closed-loop power electronic systems,” *IEEE PESC*, 1988 Record, pp. 756764.
- [27] R. C. Wong, “Accelerated convergence to the steady-state solution of closed-loop regulated switching-mode systems as obtained through simulation,” in *1987 IEEE Power Electronics Specialists Conference*, Jun. 1987, pp. 682–692. doi: 10.1109/PESC.1987.7077242.
- [28] D. Maksimovic, “Automated steady-state analysis of switching power converters using a general-purpose simulation tool,” in *PESC97. Record 28th Annual IEEE*

- Power Electronics Specialists Conference. Formerly Power Conditioning Specialists Conference 1970-71. Power Processing and Electronic Specialists Conference 1972, Jun. 1997, vol. 2, pp. 1352–1358 vol.2. doi: 10.1109/PESC.1997.616944.
- [29] A. Brambilla and P. Maffezzoni, “Envelope-following method to compute steady-state solutions of electrical circuits,” *IEEE Transactions on Circuits and Systems I: Fundamental Theory and Applications*, vol. 50, no. 3, pp. 407–417, Mar. 2003, doi: 10.1109/TCSI.2003.808897.
- [30] B. K. H. Wong and H. S.-H. Chung, “Steady-state analysis of PWM DC/DC switching regulators using iterative cycle time-domain simulation,” *IEEE Transactions on Industrial Electronics*, vol. 45, no. 3, pp. 421–432, Jun. 1998, doi: 10.1109/41.679000.
- [31] G. De Luca, P. Bolcato, and W. H. A. Schilders, “Proper Initial Solution to Start Periodic Steady-State-Based Methods,” *IEEE Transactions on Circuits and Systems I: Regular Papers*, vol. 66, no. 3, pp. 1104–1115, Mar. 2019, doi: 10.1109/TCSI.2018.2874570.
- [32] M. Daryaei, M. Ebrahimi, and S. A. Khajehoddin, “Accurate parametric steady state analysis and design tool for DC-DC power converters,” in *2016 IEEE Applied Power Electronics Conference and Exposition (APEC)*, Mar. 2016, pp. 2579–2586. doi: 10.1109/APEC.2016.7468228.
- [33] M. Daryaei, M. Ebrahimi, and S. A. Khajehoddin, “Alternative Approach to Analysis and Design of Series Resonant Converter at Steady State,” *IEEE Transactions on Industrial Electronics*, vol. 66, no. 6, pp. 4424–4435, Jun. 2019, doi: 10.1109/TIE.2018.2860536.
- [34] M. Daryaei, S. A. Khajehoddin, J. Mashreghi, and K. K. Afridi, “A New Approach to Steady-State Modeling, Analysis, and Design of Power Converters,”

- IEEE Transactions on Power Electronics, vol. 36, no. 11, pp. 12746–12768, Nov. 2021, doi: 10.1109/TPEL.2021.3076745.
- [35] K. L. Lian and P. W. Lehn, “A generalized methodology for obtaining the steady-state solution of a closed-loop power converter,” in The 2010 International Power Electronics Conference - ECCE ASIA -, Jun. 2010, pp. 665–671. doi: 10.1109/IPEC.2010.5543351.
- [36] K. L. Lian and P. W. Lehn, “Steady-State Simulation Methods of Closed-Loop Power Converter Systems—A Systematic Solution Procedure,” IEEE Transactions on Circuits and Systems I: Regular Papers, vol. 59, no. 6, pp. 1299–1311, Jun. 2012, doi: 10.1109/TCSI.2011.2173397.
- [37] J. A. Baxter and D. J. Costinett, “Steady-State Convergence of Discrete Time State-Space Modeling with State-Dependent Switching,” in 2020 IEEE 21st Workshop on Control and Modeling for Power Electronics (COMPEL), Nov. 2020, pp. 1–8. doi: 10.1109/COMPEL49091.2020.9265734.
- [38] P. W. Lehn, “Exact modeling of the voltage source converter,” IEEE Transactions on Power Delivery, vol. 17, no. 1, pp. 217–222, Jan. 2002, doi: 10.1109/61.974210.
- [39] J. Celikovic, R. Das, H.-P. Le, and D. Maksimovic, “Modeling of Capacitor Voltage Imbalance in Flying Capacitor Multilevel DC-DC Converters,” in 2019 20th Workshop on Control and Modeling for Power Electronics (COMPEL), Jun. 2019, pp. 1–8. doi: 10.1109/COMPEL.2019.8769615.
- [40] M. Khatua et al., “High-Performance Megahertz-Frequency Resonant DC–DC Converter for Automotive LED Driver Applications,” IEEE Transactions on Power Electronics, vol. 35, no. 10, pp. 10396–10412, Oct. 2020, doi: 10.1109/TPEL.2020.2974970.

- [41] J. Zhu and D. Maksimović, “A Family of Transformerless Stacked Active Bridge Converters,” in 2019 IEEE Applied Power Electronics Conference and Exposition (APEC), Mar. 2019, pp. 19–24. doi: 10.1109/APEC.2019.8721857.
- [42] K. L. Lian and P. W. Lehn, “Harmonic Analysis of Single-Phase Full Bridge Rectifiers Based on Fast Time Domain Method,” in 2006 IEEE International Symposium on Industrial Electronics, Jul. 2006, vol. 4, pp. 2608–2613. doi: 10.1109/ISIE.2006.296023.
- [43] J. A. Baxter and D. J. Costinett, “Converter Analysis Using Discrete Time State-Space Modeling,” in 2020 IEEE 21st Workshop on Control and Modeling for Power Electronics (COMPEL), Nov. 2020, pp. 1–8. doi: 10.1109/COMPEL49091.2020.9265734.
- [44] J. A. Baxter and D. J. Costinett, “Converter Analysis Using Discrete Time State-Space Modeling,” in 2019 20th Workshop on Control and Modeling for Power Electronics (COMPEL), Jun. 2019, pp. 1–8. doi: 10.1109/COMPEL.2019.8769686.
- [45] A. Kumar, S. Sinha, and K. K. Afridi, “A high-frequency inverter architecture for providing variable compensation in wireless power transfer systems,” in 2018 IEEE Applied Power Electronics Conference and Exposition (APEC), Mar. 2018, pp. 3154–3159. doi: 10.1109/APEC.2018.8341552.
- [46] H. R. Visser and P. P. J. van den Bosch, “Modelling of periodically switching networks,” in PESC '91 Record 22nd Annual IEEE Power Electronics Specialists Conference, Jun. 1991, pp. 67–73. doi: 10.1109/PESC.1991.162655.
- [47] Z. Yu, Z. Zhao, B. Shi, Y. Zhu, and J. Ju, “An Automated Semi-symbolic State Equation Generation Method for Simulation of Power Electronic Systems,” *IEEE Transactions on Power Electronics*, vol. 36, no. 4, pp. 3946–3956, Apr. 2021, doi: 10.1109/TPEL.2020.3025785.
- [48] O. Wasynczuk and S. D. Sudhoff, “Automated state model generation algorithm

- for power circuits and systems,” IEEE Transactions on Power Systems, vol. 11, no. 4, pp. 1951–1956, Nov. 1996, doi: 10.1109/59.544669.
- [48] J. Jatskevich and T. Aboul-Seoud, “Automated state-variable formulation for power electronic circuits and systems,” in 2004 IEEE International Symposium on Circuits and Systems (IEEE Cat. No.04CH37512), May 2004, vol. 5, p. V–V. doi: 10.1109/ISCAS.2004.1329967.
- [49] R. J. Dirkman, “The simulation of general circuits containing ideal switches,” in 1987 IEEE Power Electronics Specialists Conference, Jun. 1987, pp. 185–194. doi: 10.1109/PESC.1987.7077181.
- [50] K. Altun, B. E. Platin, and T. Balkan, “Systematic State Equation Derivation for Linear Systems Using the Normal Tree Method,” in Dynamic Systems and Control, Volumes 1 and 2, Washington, DC, USA, Jan. 2003, pp. 869–877. doi: 10.1115/IMECE2003-41237.
- [51] J. Staudhammer, “Circuit Analysis by Digital Computer”, Prentice-Hall, Englewood Cliffs, N.J., 1975.
- [52] N. Balabanian and T. Bickart, “Linear Network Theory: Analysis, Properties, Design and Synthesis”, Matrix Publishers Inc., Beaverton, Oregon, 1981.
- [53] C. J. Hsiao, R. B. Ridley, H. Naitoh, and F. C. Lee, “Circuit-oriented discrete-time modeling and simulation for switching converters1,” in 1987 IEEE Power Electronics Specialists Conference, Jun. 1987, pp. 167–176. doi: 10.1109/PESC.1987.7077179.
- [54] L.O.Chua, Computer-Aided Analysis of Electronic Circuits: Algorithms and Computational Techniques. Englewood Cliffs, NJ, USA: PrenticeHall, 1975.

Appendix A

Computer Formulation of State Equations

ILBT and Enhanced SVA were proposed in chapter two to calculate the steady-state initial conditions of the power converter systems. These methods use the state space representation of the system in their formulation, so the state space derivation method is required to generate the system matrices A_i, B_i, C_i, D_i from the circuit's parameter and configuration [46]-[54]. Since power converter circuits contain switching actions that change the circuit configuration, an appropriate method must be able to find the state space matrices for each of these configurations. For instance, in the case of the buck converter, the circuit has two switching intervals (Fig. A.1), and the state space representation for these switching intervals is shown here.

$$A_1 = \begin{bmatrix} 0 & \frac{-1}{L} \\ \frac{1}{C_{out}} & \frac{-1}{R_L C_{out}} \end{bmatrix} \quad B_1 = \begin{bmatrix} \frac{1}{L} \\ 0 \end{bmatrix} \quad (\text{A.1})$$

$$A_2 = \begin{bmatrix} 0 & \frac{-1}{L} \\ \frac{1}{C_{out}} & \frac{-1}{R_L C_{out}} \end{bmatrix} \quad B_2 = \begin{bmatrix} 0 \\ 0 \end{bmatrix} \quad (\text{A.2})$$

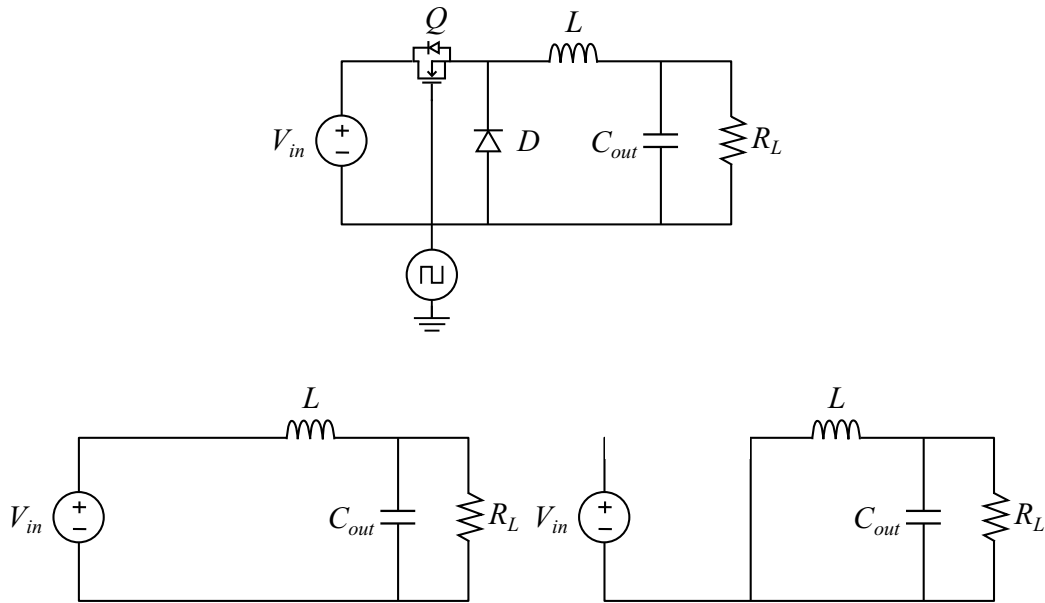


Figure A.1: The circuit configuration of the buck converter during each switching interval.

So two steps must be taken to find the state equations of the system. First, a change in circuit configuration must be detected, which can be done using the method proposed in chapter three to find the switching time of the power converters. Using that method, each switching time indicates the change in the circuit configuration, and the circuit's configuration can be determined based on the switches that turn off or on. In the second step, there is a need for an approach to generate the state equation of each configuration, which will be discussed in this section.

A.1 Circuit Identification

To find the state space model of a network, it is important to identify and store the network interconnections and parameters in the digital computer. So, in this section, first, the fundamentals of graph theory which are applicable to circuit analysis, are discussed.

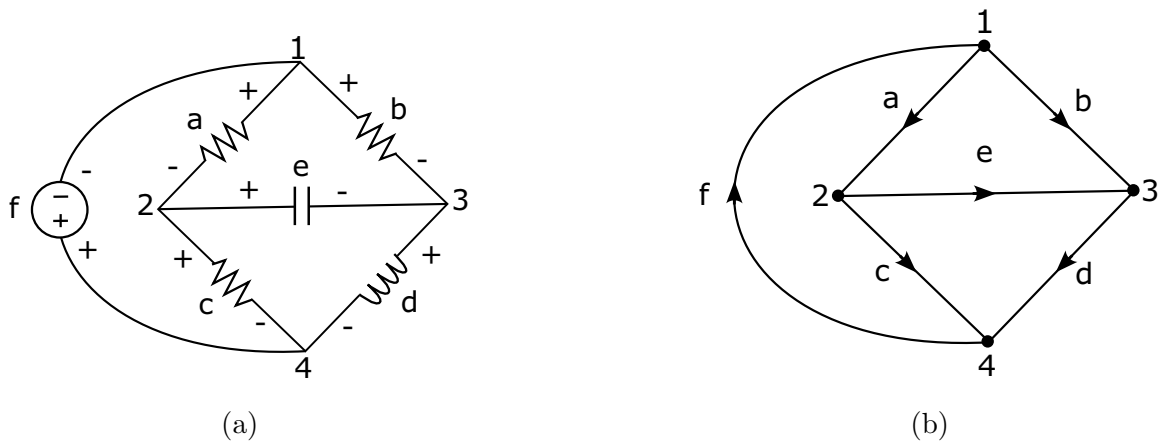


Figure A.2: Network and its associated graph.

Any network obeys three basic laws: the Kirchhoff voltage law (KVL), the Kirchhoff current law (KCL), and the elements' law (branch characteristics). The first two laws, KVL and KCL, are linear algebraic constraints on branch voltages and currents and are independent of the branch characteristics. So, a complete description of the network model must then contain the following information:

1. How the branches are connected.
2. The reference directions for branch currents and voltages.
3. The branch characteristics.

A.1.1 Network Graph

One natural and simple way to depict items 1 and 2 is to draw a directed graph G_d associated with the given network N , according to the following rule: replace each two-terminal element with a line segment called a branch, with an arrow in the same direction as the assumed positive current through that branch. Thus, the directed

graph G_d gives complete information for items 1 and 2. For example, Fig. A.2a shows a network N , and Fig. A.2b shows the directed graph G_d associated with N . Based on this directed graph following basic concepts can be defined in the network topology.

(A) **Path:** A set of branches (b_1, b_2, \dots, b_n) in G_d is called a path between two nodes V_j and V_k if the branches can be labeled such that

- Consecutive branches b_i and b_{i+1} always have a common endpoint.
- No node of G_d is the endpoint of more than two branches in the set.
- V_j is the endpoint of exactly one branch in the set, and so is V_k .

For example, in Fig. A.3, branches $(d \ h \ i \ b)$ form a path between nodes 1 and 2.

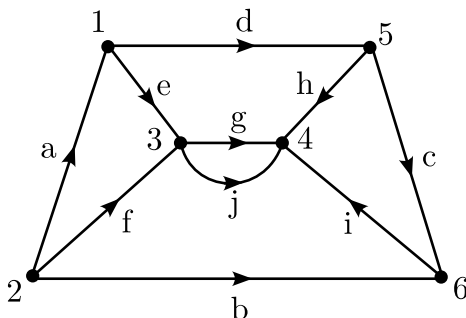


Figure A.3: Sample of graph.

(B) **Connected Graph:** A graph G_d is said to be connected if a path exists between any two nodes of the graph.

(C) **Loop (Circuit):** A subgraph G_s of a graph G_d is called a loop if

- G_s is connected.
- Every node of G_s has precisely two branches of G_s incident at it.

For example, in Fig. A.3, the branches $(a \ b \ c \ d)$ form a loop.

(D) **Tree:** A subgraph G_s of a connected graph G_d is called a tree if

- G_s is connected.
- G_s , contains all nodes of G_d .
- G_s has no loops.

For example, in Fig. A.3, the branches $(a \ e \ d \ g \ i)$ form a tree. Moreover, the branches that belong to a tree T are called tree branches, and those which do not belong to a tree T are called links (chords). All the links of a given tree T form what is called a cotree T_c with respect to the tree T .

(E) **Cutset:** A set of branches of a connected graph G_d is said to be a cutset if

- The removal of the set of branches (but not their endpoints) results in a graph that is not connected.
- After the removal of the set of branches, the restoration of any one branch from the set will result in a connected graph again.

For example, in Fig. A.3, branches $(a \ e \ d)$ form a cutset.

A.1.2 Incidence Matrix

Although the graph G_d defined here completely describes the interconnection and the reference directions of the branches of a network, it is not in a form suitable for storing in a digital computer. To solve this issue, the information contained in a directed graph G_d can be completely stored in a matrix called an incidence matrix (A_a). For a directed graph G_d with n nodes and b branches, the incidence matrix defined to be an $n \times b$ matrix:

$$A_a = [a_{ij}] \tag{A.3}$$

where

$a_{ij} = 1$ if branch j is incident at node i , and the arrow is pointing away from node i .

$a_{ij} = -1$ if branch j is incident at node i , and the arrow is pointing toward node i .

$a_{ij} = 0$ if branch j is not incident at node i .

For example, for the directed graph of Fig. A.2b

$$A_a = \begin{array}{c} \text{node} \\ 1 \\ 2 \\ 3 \\ 4 \end{array} \begin{array}{cccccc} & a & b & c & d & e & f \\ \left[\begin{array}{cccccc} 1 & 0 & 1 & 0 & 0 & -1 \\ -1 & 1 & 0 & 0 & 1 & 0 \\ 0 & 0 & -1 & 1 & -1 & 0 \\ 0 & -1 & 0 & -1 & 0 & 1 \end{array} \right] \end{array} \begin{array}{l} \text{incident branche} \\ (acf) \\ (abe) \\ (cde) \\ (bdf) \end{array} \quad (\text{A.4})$$

Since every branch is connected to two distinct nodes, every column of A_a has exactly two nonzero elements, a 1 and a -1 , with the rest being zeros. Any one row of A_a can be deleted without losing information because this deleted row may be restored correctly whenever necessary by observing the rule that every column of A_a must add up to zero. A matrix obtained from A_a by deleting any one row is called a reduced incidence matrix and is denoted by A , which can be partitioned as:

$$A = [A_T \mid A_L] \quad (\text{A.5})$$

where the columns of A_T correspond to the tree branches of a chosen tree T , and the columns of A_L correspond to the links.

Let the branch currents of the network N be represented by a column vector $i(t)$ of order $b \times 1$. Let the columns of A and the rows of i be arranged in the same branch order, that is, the k th column of A and k^{th} row of i correspond to the same branch

of G_d . Then KCL, when applied to all nodes, can be expressed very compactly as one matrix equation:

$$Ai = 0 \tag{A.6}$$

A.1.3 Cutset Matrix

A general form of the KCL states that the algebraic sum of all currents through a cutset, from one part to the other, is zero at all times. For example, applying the generalized KCL to Fig. A.2b, we can write:

$$\begin{aligned} i_a + i_c - i_f &= 0 \\ i_c + i_e + i_b - i_f &= 0 \\ &etc. \end{aligned}$$

A cutset matrix is introduced to express the generalized KCL equations compactly as a single matrix. For a directed graph G_d with b branches and n_e oriented cutsets, we define the cutset matrix to be an $n_e \times b$ matrix:

$$D_a = [d_{ij}]$$

where

$d_{ij} = 1$ if branch j is in cutset i , and their directions agree.

$d_{ij} = -1$ if branch j is in cutset i , and their directions oppose.

$d_{ij} = 0$ if branch j is not in cutset i .

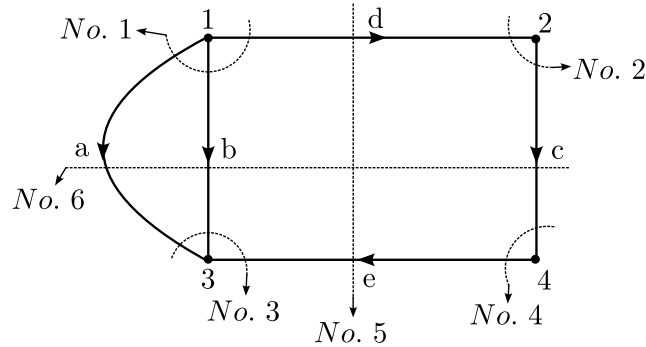


Figure A.4: Construction of the cutset matrix for a directed graph.

For example, there are six cutsets in Fig. A.4, and the cutset matrix is:

$$D_a = \begin{array}{c} \text{Cutset} \\ 1 \\ 2 \\ 3 \\ 4 \\ 5 \\ 6 \end{array} \begin{array}{ccccc} a & b & c & d & e \\ \left[\begin{array}{ccccc} 1 & 1 & 0 & 1 & 0 \\ 0 & 0 & -1 & 1 & 0 \\ 1 & 1 & 0 & 0 & 1 \\ 0 & 0 & 1 & 0 & -1 \\ 0 & 0 & 0 & 1 & -1 \\ -1 & -1 & -1 & 0 & 0 \end{array} \right] \end{array} \begin{array}{l} \text{branches in the cutset} \\ (abc) \\ (cd) \\ (de) \\ (abd) \\ (abe) \\ (ce) \end{array} \quad (\text{A.7})$$

This matrix is comprised of a set of n_c rows that are not linearly independent. Any submatrix of D_a that consists of the maximum number of independent rows of D_a is called a basic cutset matrix and is denoted by D_b , which has $n - 1$ rows. A systematic method of constructing a basic cutset matrix is through the aid of a tree T . Each tree branch of T together with some links in the associated cotree T_c forms a cutset, the fundamental cutset for that tree branch. For a connected graph with n nodes, there are $n - 1$ tree branches, and hence $n - 1$ fundamental cutsets for each chosen tree. A submatrix of D_a constructed with the $n - 1$ fundamental cutsets is called a fundamental cutset matrix, and is denoted by D .

For example, in Fig. A.4, if T is chosen to consist of branches aec , then the fundamental cutset matrix is:

$$D = \begin{array}{ccccc} & a & c & e & b & d \\ \left[\begin{array}{ccccc} 1 & 0 & 0 & 1 & 1 \\ 0 & 1 & 0 & 0 & -1 \\ 0 & 0 & 1 & 0 & -1 \end{array} \right] \end{array} \quad (\text{A.8})$$

From the way the D matrix is defined, any D matrix can be partitioned as:

$$D = \left[1 \mid D_L \right] \quad (\text{A.9})$$

where the columns of $\mathbf{1}$ correspond to tree branches and the columns of D_L correspond to links. Using D generalized KCL can be expressed compactly as:

$$D\mathbf{i} = 0 \tag{A.10}$$

A.2 Computer Generation of Topological Matrices

So far, A and D matrices have been defined, and it has been discussed how to find them from the graph of the network. This section shows how a digital computer may generate these matrices.

The generation of A is extremely simple. First, all elements of the matrix A are set to zero. Then, consecutive integers are assigned to the branches and nodes of a network graph. Finally, if branch k is connected between nodes i and j , with the reference arrow pointing toward node j , two nonzero elements of A_a are then generated: $a_{ik} = 1$ and $a_{jk} = -1$.

To generate D , the computer must first choose a tree T . Very often, T must be chosen with some preference as to the order of the different types of network elements included in the tree. For example, the particular tree used in formulating the state equations is required to have the following preferred order of element types: independent voltage sources, controlled voltage sources, capacitances, resistances, and inductances. Therefore, we have two problems to consider:

1. Find a tree T with a given preference of network element types for inclusion in the tree.
2. Find the fundamental cutset matrix D relative to the chosen tree T .

To solve these problems, elementary row operations on A are used in the following sections.

A.2.1 Finding a Tree

For finding a tree, first, columns of A must be arranged from left to right in the order corresponding to the desired preference of element types. Then, since any $n - 1$ linearly independent columns of A form a tree, the problem is simply to pick an independent set of $n - 1$ columns, starting from the leftmost column and moving successively to the right.

The recognition of a set of linearly independent columns is made easier by reducing A to the echelon form through a series of elementary row operations as follows:

Type 1. Interchange of two rows.

Type 2. Multiplication of any row by a nonzero scalar constant.

Type 3. Replacement of the j^{th} row by the sum of the j^{th} row and α times the k^{th} row, where $k \neq j$ and α is any scalar constant.

Here is an example of an echelon matrix.

$$\left[\begin{array}{cccccc} \textcircled{1} & 1 & -1 & 0 & 0 & 1 & -1 \\ 0 & \textcircled{1} & 2 & 1 & 3 & 1 & 0 \\ 0 & 0 & \textcircled{1} & 0 & 2 & 0 & 2 \\ 0 & 0 & 0 & 0 & \textcircled{1} & -1 & 1 \\ 0 & 0 & 0 & 0 & 0 & \textcircled{1} & 1 \\ 0 & 0 & 0 & 0 & 0 & 0 & 0 \end{array} \right]$$

Note that the dashed line has the form of a stair. Below the stair, all elements are zero. Each element above the stair and immediately to the right of the vertical dashed lines is always a +1.

For the present case, the matrix A is $(n - 1) \times b$ and has $n - 1$ independent columns. A may be reduced to the following typical echelon form:

$$\begin{bmatrix} \textcircled{1} & \times & \dots & \dots & \dots & \dots & \times \\ 0 & \textcircled{1} & \times & \times & \dots & \dots & \times \\ 0 & 0 & \textcircled{1} & \times & \dots & \dots & \times \\ 0 & 0 & 0 & 0 & \textcircled{1} & \times & \dots & \times \\ 0 & 0 & 0 & 0 & 0 & \textcircled{1} & \times & \dots & \times \\ 0 & 0 & 0 & 0 & 0 & 0 & \textcircled{1} & \dots & \times \end{bmatrix}$$

where each \times indicates a $+1$, -1 , or 0 . Here, $n - 1$ rows in the A_{ech} starts with 1. The $n - 1$ columns of A_{ech} corresponding to these 1's form an upper triangular matrix and therefore are linearly independent. Since elementary row operations do not affect the linear independence or dependence of a set of columns, the corresponding $n - 1$ columns of A are also linearly independent, and the corresponding $n - 1$ branches form a tree. In choosing the $n - 1$ columns from A_{ech} , columns have been favored to the left. Thus, the specified element-type preference requirement has been taken care of automatically.

A.2.2 Generation of D

Assume that a tree T has been chosen and that the matrices A and D are partitioned as

$$\begin{aligned} A &= [A_T \mid A_L] \\ D &= [1_\rho \mid D_L] \end{aligned} \tag{A.11}$$

Then as proven in [54], D can be found using the following equations:

$$D = [1_\rho \mid D_L] = A_T^{-1} [A_T \mid A_L] = A_T^{-1} A \tag{A.12}$$

(A.12) is the key to the matrix method of generating D . It says that if first A_T^{-1} is found, and then premultiply A by A_T^{-1} , the result is D . However, it is an inefficient approach because it should calculate the A_T^{-1} . To solve this issue, elementary row operations will be used. For performing an elementary row operation on a matrix Q , the product εQ can be calculated [54]. Where ε is the elementary matrix obtained by performing the intended row operation on the identity matrix. In addition, if Q is a nonsingular square matrix, we can always find a sequence of m elementary row operations that reduce Q to an identity matrix.

$$\varepsilon_m \dots \varepsilon_3 \varepsilon_2 \varepsilon_1 Q = 1 \quad (\text{A.13})$$

where ε_k indicates a type of elementary row operation ($k = 1, 2, \text{ or } 3$). From (A.13) the following equation can be written:

$$Q^{-1} = \varepsilon_m \dots \varepsilon_3 \varepsilon_2 \varepsilon_1 \quad (\text{A.14})$$

and

$$Q = \varepsilon_1^{-1} \varepsilon_1^{-1} \varepsilon_3^{-1} \dots \varepsilon_m^{-1} \quad (\text{A.15})$$

(A.15) shows that any nonsingular matrix is expressible as the product of some elementary matrices. Now the A_T^{-1} in (A.12) can be written as follows:

$$A_T^{-1} = \varepsilon_m \dots \varepsilon_3 \varepsilon_2 \varepsilon_1 \quad (\text{A.16})$$

So D is equal to:

$$D = A_T^{-1} A = (\varepsilon_m \dots \varepsilon_3 \varepsilon_2 \varepsilon_1) A \quad (\text{A.17})$$

This equation means that D may be obtained from A by performing a sequence of elementary row operations on A . In addition, the following equation shows that the

required sequence of row operations is just those operations which, when performed on A_T will result in an identity matrix.

$$A_T^{-1}A_T = \left(\begin{array}{ccc} \varepsilon_m & \dots & \varepsilon_3\varepsilon_2\varepsilon_1 \end{array} \right) A_T = \mathbf{1} \quad (\text{A.18})$$

Putting these two facts together, following an alternative method of generating D from A is possible. Perform elementary row operations on A to reduce A_T to an identity matrix. The resulting matrix is D when this state is attained.

A.3 State Space Derivation

This section discusses an algorithm to find the state space of the network. The algorithm uses the incidence matrix and circuit parameters (capacitance, inductance, resistance, and admittance matrices) as input. The circuit parameters obey the following equations:

$$\begin{aligned} v_{R_J} &= R_J i_{R_J} & i_{R_J} &= G_J v_{R_J} \\ i_{R_L} &= G_L v_{R_L} & v_{R_L} &= R_L i_{R_L} \end{aligned} \quad (\text{A.19})$$

$$C : \begin{bmatrix} i_{C_J} \\ i_{C_L} \end{bmatrix} = \begin{bmatrix} C_J & 0 \\ 0 & C_L \end{bmatrix} \frac{d}{dt} \begin{bmatrix} v_{C_J} \\ v_{C_L} \end{bmatrix} \quad (\text{A.20})$$

$$L : \begin{bmatrix} v_{L_J} \\ v_{L_L} \end{bmatrix} = \begin{bmatrix} L_{JJ} & L_{JL} \\ L_{LJ} & L_{LL} \end{bmatrix} \frac{d}{dt} \begin{bmatrix} i_{L_J} \\ i_{L_L} \end{bmatrix} \quad (\text{A.21})$$

Using these inputs, the algorithm will take the following steps to generate the state space equations:

1. Selection of a tree j that contains the following:
 - (a) All independent voltage sources.

- (b) No independent current sources.
- (c) As many capacitors as possible.
- (d) As few inductors as possible.

Such a tree, called a normal tree, can always be constructed using the matrix procedure described in Section A.2.1. The subscript \mathcal{J} for the normal tree and \mathcal{L} for the links (cotree) is used to indicate the branches of the circuits. In addition, after finding this tree a suitable choice for the state variables is $v_{C_{\mathcal{J}}}$ and $i_{L_{\mathcal{L}}}$ [54].

2. Calculate the cutset matrix (D) using the method proposed in section A.2.2, and write the fundamental cutset (KCL) equations for the network as follows:

$$Di = \begin{bmatrix} E_{\mathcal{J}} & C_{\mathcal{J}} & R_{\mathcal{J}} & L_{\mathcal{J}} & J_{\mathcal{L}} & L_{\mathcal{L}} & R_{\mathcal{L}} & C_{\mathcal{L}} \\ 1_{E_{\mathcal{J}}} & 0 & 0 & 0 & F_{11} & F_{12} & F_{13} & F_{14} \\ 0 & 1_{C_{\mathcal{J}}} & 0 & 0 & F_{21} & F_{22} & F_{23} & F_{24} \\ 0 & 0 & 1_{R_{\mathcal{J}}} & 0 & F_{31} & F_{32} & F_{33} & 0 \\ 0 & 0 & 0 & 1_{L_{\mathcal{J}}} & F_{41} & F_{42} & 0 & 0 \end{bmatrix} i = 0 \quad (\text{A.22})$$

using this equation, the submatrices F_{11} to F_{44} can be found.

3. Calculation of R and G matrices using the following equations:

$$\begin{aligned} G &= G_{\mathcal{J}} + F_{33}G_{\mathcal{L}}F_{33}^t \\ R &= R_{\mathcal{L}} + F_{33}^tR_{\mathcal{J}}F_{33} \end{aligned} \quad (\text{A.23})$$

4. Find the state space equations of the network using the following equations [54]:

$$M^{(0)} \frac{d}{dt} \begin{bmatrix} v_{C_{\mathcal{J}}} \\ i_{L_{\mathcal{L}}} \end{bmatrix} = A^{(0)} \begin{bmatrix} v_{C_{\mathcal{J}}} \\ i_{L_{\mathcal{L}}} \end{bmatrix} + B^{(0)} \begin{bmatrix} v_{E_{\mathcal{J}}} \\ i_{J_{\mathcal{L}}} \end{bmatrix} + B_1^{(0)} \frac{d}{dt} \begin{bmatrix} v_{E_{\mathcal{J}}} \\ i_{L_{\mathcal{L}}} \end{bmatrix} \quad (\text{A.24})$$

$$M^{(0)} = \begin{bmatrix} C_{\mathcal{J}} + F_{24}C_{\mathcal{L}}F_{24}^t & 0 \\ 0 & (L_{\mathcal{L}\mathcal{L}} - F_{42}^tL_{\mathcal{J}\mathcal{L}} - L_{\mathcal{L}\mathcal{J}}F_{42} + F_{42}^tL_{\mathcal{J}\mathcal{J}}F_{42}) \end{bmatrix} \quad (\text{A.25})$$

$$A^{(0)} = \begin{bmatrix} -F_{23}R^{-1}F_{23}^t & (-F_{22} + F_{23}R^{-1}F_{33}^tR_{\mathcal{J}}F_{32}) \\ (F_{22}^t - F_{32}^tG^{-1}F_{33}G_{\mathcal{L}}F_{23}^t) & -F_{32}^tG^{-1}F_{32} \end{bmatrix} \quad (\text{A.26})$$

$$B^{(0)} = \begin{bmatrix} -F_{23}R^{-1}F_{13} & (-F_{21} + F_{23}R^{-1}F_{33}^tR_{\mathcal{J}}F_{31}) \\ (F_{12}^t - F_{32}^tG^{-1}F_{33}G_{\mathcal{L}}F_{13}^t) & -F_{32}^tG^{-1}F_{31} \end{bmatrix} \quad (\text{A.27})$$

$$B_1^{(0)} = \begin{bmatrix} -F_{24}C_{\mathcal{L}}F_{14}^t & 0 \\ 0 & -F_{42}^tL_{\mathcal{J}\mathcal{J}}F_{41} + L_{\mathcal{L}\mathcal{J}}F_{41} \end{bmatrix} \quad (\text{A.28})$$

Then, premultiplying both sides of (A.24) by $[M^{(0)}]^{-1}$, results in the following equation:

$$\dot{\hat{\mathbf{x}}} = A\hat{\mathbf{x}} + B\mathbf{u} + B_1\dot{\mathbf{u}} \quad (\text{A.29})$$

where

$$\begin{aligned} A &= [M^{(0)}]^{-1} A^{(0)} \\ B &= [M^{(0)}]^{-1} B^{(0)} \\ B_1 &= [M^{(0)}]^{-1} B_1^{(0)} \end{aligned} \quad (\text{A.30})$$

The derivative of the input vector u appears in (A.29), which can be removed by a simple change of variables:

$$\mathbf{x} = \hat{\mathbf{x}} - B_1\mathbf{u} \quad (\text{A.31})$$

Putting (A.31) into (A.29) results in:

$$\dot{\mathbf{x}} = A\mathbf{x} + (B + AB_1)\mathbf{u} \quad (\text{A.32})$$

which is the state space equation of the network.

To illustrate the procedure of generating the state space equations of the network, a circuit of Fig. A.5 is discussed here. This circuit has mutual inductances, and the

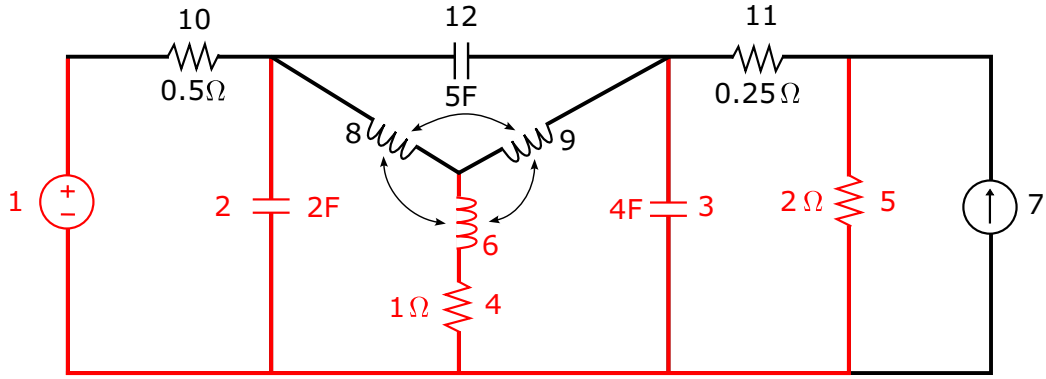


Figure A.5: A typical network.

inductance matrix is:

$$\begin{bmatrix} v_6 \\ v_8 \\ v_9 \end{bmatrix} = \begin{bmatrix} 4 & -1 & -1 \\ -1 & 2 & -1 \\ -1 & -1 & 2 \end{bmatrix} \frac{d}{dt} \begin{bmatrix} i_6 \\ i_8 \\ i_9 \end{bmatrix} \quad (\text{A.33})$$

To find the state space matrices of this circuit, the following steps must be taken:

Step 1: A proper tree consisting of branches 1, 2, 3, 4, 5, and 6 is chosen, as shown in Fig. A.5. Moreover, the states of the circuit are v_2 , v_3 , i_8 , and i_9 based on this choice of proper tree.

Step 2: The cutset matrix with respect to the proper tree is found to be:

$$D = \begin{bmatrix} 1 & 0 & 0 & 0 & 0 & 0 & 0 & 0 & 0 & 1 & 0 & 0 \\ 0 & 1 & 0 & 0 & 0 & 0 & 0 & -1 & 0 & -1 & 0 & 1 \\ 0 & 0 & 1 & 0 & 0 & 0 & 0 & 0 & -1 & 0 & 1 & -1 \\ 0 & 0 & 0 & 1 & 0 & 0 & 0 & 1 & 1 & 0 & 0 & 0 \\ 0 & 0 & 0 & 0 & 1 & 0 & -1 & 0 & 0 & 0 & -1 & 0 \\ 0 & 0 & 0 & 0 & 0 & 1 & 0 & 1 & 1 & 0 & 0 & 0 \end{bmatrix} \quad (\text{A.34})$$

from which F_{11} to F_{44} is identified as follows:

$$F_{11} = 0, \quad F_{12} = \begin{bmatrix} 0 & 0 \end{bmatrix}, \quad F_{13} = \begin{bmatrix} 1 & 0 \end{bmatrix} \quad F_{14} = 0$$

$$\begin{aligned}
 F_{21} &= \begin{bmatrix} 0 \\ 0 \end{bmatrix}, & F_{22} &= \begin{bmatrix} -1 & 0 \\ 0 & -1 \end{bmatrix}, & F_{23} &= \begin{bmatrix} -1 & 0 \\ 0 & 1 \end{bmatrix}, & F_{24} &= \begin{bmatrix} 1 \\ -1 \end{bmatrix} \\
 F_{31} &= \begin{bmatrix} 0 \\ -1 \end{bmatrix}, & F_{32} &= \begin{bmatrix} 1 & 1 \\ 0 & 0 \end{bmatrix}, & F_{33} &= \begin{bmatrix} 0 & 0 \\ 0 & -1 \end{bmatrix} \\
 F_{41} &= 0, & F_{42} &= \begin{bmatrix} 1 & 1 \end{bmatrix}
 \end{aligned}$$

Step 3: R and G matrices are calculated:

$$\begin{aligned}
 G &= \begin{bmatrix} 1 & 0 \\ 0 & 0.5 \end{bmatrix} + \begin{bmatrix} 0 & 0 \\ 0 & -1 \end{bmatrix} \begin{bmatrix} 2 & 0 \\ 0 & 4 \end{bmatrix} \begin{bmatrix} 0 & 0 \\ 0 & -1 \end{bmatrix} = \begin{bmatrix} 1 & 0 \\ 0 & 4.5 \end{bmatrix} \\
 R &= \begin{bmatrix} 0.5 & 0 \\ 0 & 0.25 \end{bmatrix} + \begin{bmatrix} 0 & 0 \\ 0 & -1 \end{bmatrix} \begin{bmatrix} 1 & 0 \\ 0 & 2 \end{bmatrix} \begin{bmatrix} 0 & 0 \\ 0 & -1 \end{bmatrix} = \begin{bmatrix} 0.5 & 0 \\ 0 & 2.25 \end{bmatrix}
 \end{aligned} \tag{A.35}$$

Step 4: Finally, $M^{(0)}$, $A^{(0)}$, $B^{(0)}$, and $M_1^{(0)}$ can be calculated using the matrices found in the previous steps:

$$\mathbf{M}^{(0)} = \begin{bmatrix} 7 & -5 & 0 & 0 \\ -5 & 9 & 0 & 0 \\ 0 & 0 & 8 & 5 \\ 0 & 0 & 5 & 8 \end{bmatrix} \tag{A.36}$$

$$\mathbf{A}^{(0)} = \begin{bmatrix} -2 & 0 & 1 & 0 \\ 0 & -\frac{4}{9} & 0 & 1 \\ -1 & 0 & -1 & -1 \\ 0 & -1 & -1 & -1 \end{bmatrix} \tag{A.37}$$

$$\mathbf{B}^{(0)} = \begin{bmatrix} 2 & 0 \\ 0 & \frac{8}{9} \\ 0 & 0 \\ 0 & 0 \end{bmatrix} \tag{A.38}$$

$$\mathbf{B}_1^{(0)} = \mathbf{0} \quad (\text{A.39})$$

By substituting (A.36)-(A.39) into (A.29), the state space equation of the network of Fig. A.5 can be written as follows:

$$\begin{aligned} \frac{d}{dt} \begin{bmatrix} v_2 \\ v_3 \\ i_8 \\ i_9 \end{bmatrix} &= \begin{bmatrix} -\frac{9}{19} & -\frac{10}{171} & \frac{9}{38} & \frac{5}{38} \\ -\frac{5}{19} & -\frac{14}{171} & \frac{5}{38} & \frac{7}{38} \\ -\frac{8}{39} & \frac{5}{39} & -\frac{1}{13} & -\frac{1}{13} \\ \frac{5}{39} & -\frac{8}{39} & -\frac{1}{13} & -\frac{1}{13} \end{bmatrix} \begin{bmatrix} v_2 \\ v_3 \\ i_8 \\ i_9 \end{bmatrix} \\ &+ \begin{bmatrix} \frac{9}{19} & \frac{20}{171} \\ \frac{5}{19} & \frac{28}{171} \\ 0 & 0 \\ 0 & 0 \end{bmatrix} \begin{bmatrix} v_1 \\ i_7 \end{bmatrix} \end{aligned} \quad (\text{A.40})$$